Optimierung von Kieferperiostzellen für das Knochen-Tissue Engineering: Herstellung von iPS-Zellen und Analyse von Progenitor-Oberflächenmarkern

Dissertation

der Mathematisch-Naturwissenschaftlichen Fakultät

der Eberhard Karls Universität Tübingen

zur Erlangung des Grades eines

Doktors der Naturwissenschaften

(Dr. rer. nat.)

vorgelegt von

M.Sc. Felix Umrath

aus

Tübingen

Tübingen

2019

Gedruckt mit Genehmigung der Mathematisch-Naturwissenschaftlichen Fakultät der Eberhard Karls Universität Tübingen.

Tag der mündlichen Qualifikation:	09.03.2020
Dekan:	Prof. Dr. Wolfgang Rosenstiel
1. Berichterstatter:	Prof. Dr. Stefan Stevanović
2. Berichterstatter:	Prof. Dr. Dorothea Alexander-Friedrich

Inhalt

I Abkürzungen

ALP	alkalische Phosphatase
AM	adipogenes Medium
ATMPs	Advanced Therapy Medicinal Products
BcM	B18R-konditioniertes Medium
BMMSCs	Knochenmark-MSC
BMP-2	bone morphogenic protein 2
BMP-4	bone morphogenic protein 4
BTE	Bone Tissue Engineering
CAM	Chorioallantoismembran
CM	chondrogenes Medium
CO	Kontrolle
COL2A1	Collagen2α1
COMP	cartilage oligomeric matrix protein
Dexa	Dexamethason
E8	Essential 8 Medium
EB	Embryoidbody
EPC	endothelial progenitor cell
ESC	embryonale Stammzelle
FACS	fluorescence-activated cell sorting
FBS	Fetal Bovine Serum
GAGs	Glykosaminoglykane
GAPDH	Glycerinaldehyd-3-phosphat-Dehydrogenase
GCP	Good Clinical Practice
GFP	grün fluoreszierendes Protein
GMP	Good Manufacturing Practice
hPL	humanes Plättchenlysat
HUVECs	Human Umbilical Vein Endothelial Cells
IBMX	3-Isobutyl-1-methylxanthin
iMSC	MSC-ähnliche Zelle
Indo	Indomethacin
iPSCs	induzierte pluripotente Stammzellen
ISCT	International Society for Cellular Therapy
JPCs	jaw periosteal cells
KLF4	Kruppel-Like Factor 4
KO	Kontrolle
MACS	magnetic-activated cell sorting
MCAM	Melanoma Cell Adhesion Molecule
MFI	Median-Fluoreszenzindex
MKGC	Mund-, Kiefer- und Gesichtschirurgie
MSCA-1	Mesenchymal Stromal Cell Antigen-1
MSC	mesenchymale Stamm-/Stromazelle
NaB	Natriumbutyrat

OCN	Osteocalcin
OCT4	Octamer Binding Transcription Factor 4
PRP	plättchenreiches Plasma
$Puro^r$	Puromycin-Resistenzgen
ROCK	Rho-associated protein kinase
RUNX2	runt-related transcription factor 2
SA-β-Gal	Seneszenz-assoziierte Beta-Galactosidase
SDF-1	stromal cell-derived factor 1
SOX2	Sex Determining Region Y-Box 2
SOX9	Sex Determining Region Y-Box 9
srRNA	selbstreplizierende RNA
SSEA-3	Stage-Specific Embryonic Antigen-3
SSEA-4	Stage-Specific Embryonic Antigen-4
t_d	Verdopplungszeit
TERT	telomerase reverse transcriptase
TNAP	Tissue non-specific Alkaline Phosphatase
VEE	Venezuelan equine encephalitis
VEGF	vascular endothelial growth factor
Vit. C	Ascorbinsäure/Vitamin C
VTN	Vitronectin
β-Gly	β-Glycerophosphat
μ	Wachstumsrate

II Zusammenfassung

Die Knochengewebezüchtung im Labor (engl.: Bone Tissue Engineering, BTE) könnte in Zukunft autologe Knochentransplantate in der Mund-, Kiefer- und Gesichtschirurgie (MKGC) ersetzen. Für die Herstellung klinisch anwendbarer BTE-Produkte sind die Qualität und die Verfügbarkeit der dabei eingesetzten Stammzellen entscheidende Faktoren.

Die Verfügbarkeit von Stammzellen ist einerseits durch die Größe der Gewebebiopsie, andererseits durch die Abnahme der Vitalität und des osteogenen Potenzials im Laufe der *in vitro* Kultivierung limitiert. Da für die Herstellung von BTE-Konstrukten zur Regeneration größerer Knochendefekte, z.B. nach Tumorresektionen, große Mengen osteogener Vorläuferzellen benötigt werden, sollten in der vorliegenden Arbeit induzierte pluripotente Stammzellen (iPSCs) aus Kieferperiostzellen (JPCs) generiert, und als Zellquelle für das BTE etabliert werden. iPSCs besitzen die Fähigkeit zur Selbsterneuerung und sind daher in großen Mengen verfügbar. Im Hinblick auf zukünftige klinische Anwendungen der Zellen, wurde zur Generierung von iPSCs eine besonders sichere xenogen-freie RNA-basierte Reprogrammierungstechnik entwickelt.

Durch die Differenzierung von iPSCs zu MSC-ähnlichen Zellen (iMSCs) ist es möglich osteogene Vorläuferzellen herzustellen, welche analog zu normalen MSCs (mesenchymale Stamm-/Stromazellen) eingesetzt werden können. In der vorliegenden Arbeit wurden daher aus JPCs generierte iPSCs zu iMSCs differenziert, und ihre Eignung für Anwendungen im BTE anhand der osteogenen Differenzierung *in vitro* getestet.

Neben der Verfügbarkeit von Stammzellen ist auch die Qualität des zur Verfügung stehenden Zellmaterials ein entscheidender Faktor. Die Gewinnung von Stammzellen aus Gewebebiopsien führt jedoch meistens zur Isolation von heterogenen Zellpopulationen aus verschiedenen Zelltypen, wodurch die Qualität sowie das Stammzellpotenzial der für das BTE benötigten Zellkulturen beeinträchtigt werden kann. Zur Qualitätskontrolle und zur Isolation osteogener Vorläuferzellen aus solchen Mischpopulationen werden Oberflächenmarker benötigt, mit denen sich osteogene Vorläuferzellen in heterogenen Zellpopulationen identifizieren und ggf. mithilfe von Fluorescence-activated Cell Sorting (FACS) isolieren lassen.

In der vorliegenden Arbeit wurden die Oberflächenmarker MSCA-1 (Mesenchymal Stromal Cell Antigen-1) und CD146 (Melanoma Cell Adhesion Molecule (MCAM)) auf ihre Eignung für die Separation osteogener Vorläuferzellen aus der Periostzelllinie TAg58 getestet. Dabei zeigte sich, dass obwohl beide Marker in der Literatur als osteogene Marker beschrieben waren, sich nur MSCA-1 zur Identifikation und Sortierung osteogener Vorläuferzellen in der verwendeten Zelllinie als geeignet erwies.

Zur Herstellung von BTE-Produkten unter GMP-gerechten Bedingungen sollte bei der Zellkultur auf xenogene Bestandteile verzichtet werden. Daher wurde im Zuge dieser Arbeit die Kultivierung von JPCs von FBS- (fötales Kälberserum) auf hPL- (humanes Plättchenlysat) supplementiertes Medium umgestellt. Dabei zeigte sich, dass sich hPL wesentlich besser für die Kultivierung von JPCs eignete und Proliferation sowie Differenzierungspotenzial deutlich verbessert wurden. Zudem konnte für die osteogene Induktion von Periostzellen auf die Zugabe von Dexamethason unter hPL-Supplementierung verzichtet werden.

III Summary

Bone tissue engineering (BTE) has the potential to replace autologous bone grafts in the future. For the production of clinically applicable bone tissue engineering products, the quality and availability of the cell material are crucial factors.

However, the supply of stem cells is limited on the one hand by the size of the tissue biopsy and on the other hand by decreasing cell vitality and osteogenic potential during *in vitro* cell passaging. Since high numbers of osteogenic progenitor cells are required for the regeneration of large bone defects, e.g. after tumor resections, this work aimed to produce induced pluripotent stem cells (iPSCs) from jaw periosteal cells (JPCs) to use them as a cell source for the BTE.

iPSCs have similar properties to embryonic stem cells. They can differentiate into any cell type of the body and are available in large quantities due to their ability to self-renew. By differentiating iPSCs into MSC-like cells (iMSCs), osteogenic progenitor cells similar to MSCs (mesenchymal stem/stromal cells) can be produced. The aim of this work was to generate iPSCs from jaw periosteal cells (JPCs) and subsequently differentiate them to iMSCs. The stem cell potential of iMSCs was tested *in vitro*. With regard to future clinical applications of these cells, a particularly safe and xeno-free RNA-based reprogramming technique was used to generate iPSCs.

In addition to the stem cell supply, the quality of the available cell material is another crucial factor, but the isolation of stem cells from tissue biopsies leads to the generation of heterogeneous cell populations consisting of different cell types, considerably compromising quality and osteogenic potential of obtained cell cultures and their availability for BTE.

For quality assessment and isolation of osteogenic progenitors from mixed cell populations, appropriate surface markers need to be identified and used for fluorescence-activated cell sorting (FACS).

In the present work, the surface markers MSCA-1 (mesenchymal stromal cell antigen-1) and CD146 (melanoma cell adhesion molecule (MCAM)) were tested for their suitability for separation of osteoprogenitors from the periosteal cell line TAg58. Although both markers have been described as osteogenic markers, this study showed that only MSCA-1 was suitable for the identification and sorting of osteogenic progenitor cells in the cell line used.

For the production of BTE products under GMP-compliant conditions, xenogenic components should be avoided in cell culture. Therefore, the cultivation of JPCs and iMSCs was changed from FBS- (fetal bovine serum) to hPL- (human platelet lysate) supplemented medium. In this process, it could be shown that hPL was much better suited for the proliferation of JPCs and that the differentiation potential was clearly improved. Further, the addition of dexamethasone for the osteogenic induction of JPCs is no longer necessary under hPL supplementation.

IV Publikationen

Veröffentlichte Publikationen

1. Umrath, F., H. Steinle, M. Weber, H.P. Wendel, S. Reinert, D. Alexander, and M. Avci-Adali, Generation of iPSCs from Jaw Periosteal Cells Using Self-Replicating RNA. Int. J. Mol. Sci., 2019. 20(7): p. 1648.
2. Umrath, F., C. Thomalla, S. Pöschel, K. Schenke-Layland, S. Reinert, and D. Alexander, Comparative Study of MSCA-1 and CD146 Isolated Periosteal Cell Subpopulations. Cell. Physiol. Biochem., 2018. 51(3): p. 1193-1206.
3. Wanner, Y., F. Umrath, M. Waidmann, S. Reinert, and D. Alexander, Platelet Lysate: The Better Choice for Jaw Periosteal Cell Mineralization. Stem Cells Int., 2017. 2017: p. 8303959.
4. Umrath, F., M. Weber, S. Reinert, H.P. Wendel, M. Avci-Adali, and D. Alexander, iPSC-Derived MSCs Versus Originating Jaw Periosteal Cells: Comparison of Resulting Phenotype and Stem Cell Potential. Int. J. Mol. Sci., 2020. 21(2).

Eigenanteil

- Publikation 1: Isolation und Expansion von JPCs. Transfektion und Reprogrammierung von JPCs mit VEE-OKSM-GFP RNA welche von Heidrun Steinle aus der Arbeitsgruppe von Prof. Dr. Meltem Avci-Adali (AG Prof. Dr. Hans-Peter Wendel) hergestellt wurde. Charakterisierung der generierten iPSCs mittels qPCR und Durchflusszytometrie. Differenzierung von iPSCs zu iMSCs und Charakterisierung sowie osteogene Differenzierung der iMSCs. Verfassen des Manuskripts.
- Publikation 2: Kultivierung und Expansion von TAg58 Zellen. FACS-Separation der TAg58 Zellen in 4 Subpopulationen. Durchführung und Auswertung der osteogenen Differenzierung der 4 Subpopulationen. Analyse der Subpopulationen mittels multispektraler bildgebender Durchflusszytometrie und qPCR. Verfassen des Manuskripts.
- Publikation 3: Umstellung der Kultivierung von JPCs von FBS- auf hPL-Medium. Vorversuche zur Ermittlung der optimalen hPL-Konzentration für

Wachstum und Differenzierung von JPCs. Betreuung von Yvonne Wanner bei der Durchführung der Versuche.

- Publikation 4: Durchführung aller Experimente mit Ausnahme der Bestimmung der Telomerlängen. Verfassen des Manuskripts.

Kongressbeiträge

Vorträge:

1. Analysis of MSCA-1 and CD146 Subpopulations from Cranial Periosteal Tissue, F. Umrath, C. Thomalla, S. Pöschel, K. Schenke-Layland, S. Reinert, D. Alexander, International Bone-Tissue-Engineering Conference, München, 12.-14.10.2017
2. Verwendung von MSCA-1 und CD146 als Marker zur Identifikation von osteogenen Vorläuferzellen aus Schädelperiost, F. Umrath, C. Thomalla, S. Pöschel, K. Schenke-Layland, S. Reinert, D. Alexander, 68. Kongress & Praxisführungsseminar der Deutschen Gesellschaft für Mund., Kiefer- und Gesichtschirurgie, Dresden, 06.-09.06.2018
3. Generierung von induzierten pluripotenten Stammzellen aus Kieferperiostzellen, F. Umrath, H. Steinle, M. Weber, M. Avci-Adali, S. Reinert, D. Alexander, 69. Kongress & Praxisführungsseminar der Deutschen Gesellschaft für Mund., Kiefer- und Gesichtschirurgie, Frankfurt, 26.-29.06.2019

Poster:

1. Reprogramming of human jaw periosteal cells using self-replicating RNA, F. Umrath, H. Steinle, M. Weber, M. Avci-Adali, S. Reinert, D. Alexander, International Osteology Symposium, Barcelona, 25.-27.04.2019

1. Einleitung

1.1 Knochentransplantationen in der Mund-, Kiefer- und Gesichtschirurgie (MKGC)

Knochentransplantationen werden in der plastischen und wiederherstellenden MKGC aufgrund vielfältiger Indikationen durchgeführt. Einsatzgebiete sind unter anderem Kieferspaltplastiken, Kieferaugmentationen, Zystenoperationen, Traumata des Gesichtsschädels und Tumoroperationen [1]. 2017 zählten Knochentransplantationen und -transpositionen deutschlandweit mit 87.114 Fällen zu den 45 am häufigsten durchgeführten Operationen [2]. Dabei handelte es sich in 97,8% (total 85.190) der Fälle um orthopädische Operationen und in 2,2 % (total 1.924) der Fälle um Operationen an Kiefer- und Gesichtsschädelknochen [2]. Im Zeitraum zwischen 2006 und 2017 verzeichneten die Fallzahlen von Knochentransplantationen und -transpositionen in der Orthopädie einen moderaten Anstieg um 7,9 % (Abbildung 1a), die Fallzahlen in der MKGC zeigten einen starken Anstieg um 91,3 % (Abbildung 1b) [2]. Im selben Zeitraum stiegen auch die Fallzahlen der Hauptursachen von Knochentransplantationen in der MKGC, partielle und totale Resektionen eines Gesichtsschädelknochens und partielle und totale Resektionen der Mandibula, um 137,3 % bzw. um 58,6 % (Abbildung 1b) [2].

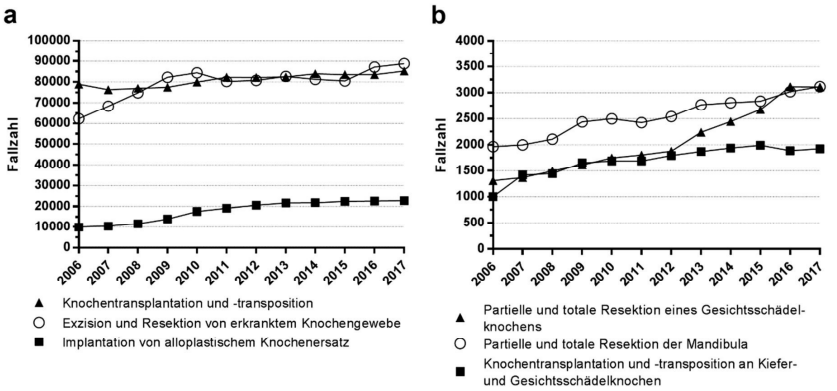

Abbildung 1: Fallzahlen von Knochentransplantationen in der Orthopädie und der MKG-Chirurgie. a) Fallzahlen von Knochentransplantationen und -transpositionen (▲), Exzisionen und Resektionen von erkranktem Knochengewebe (○) und Implantationen von alloplastischem Knochenersatz (■) bei orthopädischen Operationen in Deutschland zwischen 2006 und 2017. b) Fallzahlen von partiellen und totalen Resektionen eines Gesichtsschädelknochens (▲), partiellen und totalen Resektionen der Mandibula (○) und Knochentransplantationen und -transpositionen an Kiefer- und Gesichtsschädelknochen (■) in Deutschland zwischen 2006 und 2017.[2]

Diese Zahlen verdeutlichen den steigenden Bedarf an Knochentransplantaten und die damit einhergehende Relevanz der Entwicklung alternativer Transplantatmaterialien, insbesondere in der MGKC.

Zur Behandlung von Knochendefekten werden als Knochenersatzmaterial alloplastische Implantate (z.B. aus Titan, Hydroxylapatit, Polyethylen), xenogene Transplantate (dezellularisiertes bovines oder porcines Knochengerüst), sowie allogene und autologe Transplantate verwendet [1, 3].

Da es sich bei alloplastischen Implantaten und xenogenen Transplantaten um nicht-vitale Knochenersatzmaterialien handelt, eignen sich diese weniger zur Behandlung größerer Knochendefekte, sondern werden hauptsächlich zur Füllung kleinerer Defekte, z.B. nach Entfernung von Zysten, oder bei Kieferaugmentationen eingesetzt.

Allogene Transplantate haben den Vorteil, dass sie in größeren Mengen verfügbar sind als autologe Transplantate und keine weitere Operationsstelle eröffnet werden muss. Durch den Verarbeitungsprozess (Sterilisation, Gefriertrocknung, etc.) geht die Osteoinduktivität der Transplantate, d.h. die Fähigkeit die Knochenbildung zu stimulieren, verloren, oder ist wie im Fall von demineralisierter Knochenmatrix nur noch in geringem Maße vorhanden [3-5]. Zudem besteht ein Risiko durch übertragbare Infektionskrankheiten und Abstoßungsreaktionen [6, 7].

Der Goldstandard der Transplantatmaterialien ist noch immer das autologe Knochentransplantat [8]. Als Entnahmestellen eigenen sich, insbesondere für die Versorgung großer Knochendefekte, der Beckenkamm, sowie Scapula und Fibula, aber auch Schädelkalotte, Rippen und Tibia werden verwendet [4, 9-11]. Da keine Abstoßungsreaktionen auftreten, haben autogene Transplantate die besten Einheilungschancen und sind, v.a. bei mikrochirurgischer Versorgung, resistenter gegenüber Wundinfektionen und Knochenresorption [1]. Der Nachteil autologer Transplantate ist die Eröffnung einer weiteren Operationsstelle mit dem Risiko von Nachblutungen, Schwellungen, Schmerzen, Wundheilungsstörungen, Infektionen, Nervenschädigungen, Narbenbildung und anderer Komplikationen [12]. Zudem ist die Verfügbarkeit von autologem Knochen begrenzt und kommt bei manchen Patienten, z.B. Säuglingen, immundefizienten Patienten, oder Patienten mit Osteoporose nicht infrage.

1.2 Knochen-Tissue-Engineering/Knochengewebezüchtung

Die grundlegenden Elemente des Knochen-Tissue Engineerings sind Stammzellen, Scaffolds (Gerüstmaterialien) und Wachstumsfaktoren [13]. Mithilfe dieser Elemente, und durch ihre Kombination, werden alternative Knochenimplantate hergestellt, und versucht die Nachteile der bisher eingesetzten Implantatmaterialien (limitierte Verfügbarkeit, Eröffnung einer weiteren Operationsstelle, Abstoßungsreaktionen, mangelnde Osteogenese (Knochendifferenzierung), etc.) zu überwinden.

Osteokonduktive Scaffolds aus biokompatiblen Materialien dienen als dreidimensionale Matrix, ermöglichen die Adhäsion und Invasion von knochenbildenden Zellen und sorgen dabei für die nötige Stabilität des Implantats [13]. Forschungsschwerpunkte im Bereich der Biomaterialien sind die Verbesserung von mechanischen (z.B. Stabilität, Elastizität, Oberflächenbeschaffenheit) und biologischen Eigenschaften (z.B. Osteoinduktivität, Osteointegration, Resorbierbarkeit) [14]. Zudem werden neue Materialien für „Rapid Prototyping" Verfahren wie CAD/CAM oder 3D-Druck entwickelt, um patientenspezifisch passgenaue Implantate herstellen zu können [15].

Biomaterialien können mit Zytokinen kombiniert werden, um einerseits die Vaskularisierung des Konstrukts zu fördern (z.B. durch VEGF) [16], und andererseits osteoinduktiv wirken und das „Homing" (z.B. durch SDF-1) und die Differenzierung (z.B. durch BMP-2) von Knochenstammzellen induzieren zu können [17-19]. Alternativ kann auch autologes plättchenreiches Plasma (PRP) als Quelle natürlicher Zytokine eingesetzt werden [20].

Die Besiedelung von Scaffolds mit Stammzellen führt idealerweise zur Neubildung von Knochen und unterstützt die Integration des Konstrukts in den Knochendefekt. Die Stammzellen bilden dabei einerseits selbst Knochenmatrix, fördern aber auch durch die Ausschüttung von Zytokinen die Rekrutierung körpereigener osteogener und vaskulogener Zellen [13]. Geeignete Stammzellen können aus einer Vielzahl von Spendergeweben isoliert werden. Dabei handelt es sich in der Regel um mesenchymale Stamm-/ oder Stromazellen (engl. Mesenchymal stem/stromal cells, MSCs). Klinisch relevant sind jedoch hauptsächlich MSCs aus dem Knochenmark und Fettgewebe [13]. Aufgrund ihres starken osteogenen Potenzials und ihrer wichtigen Rolle bei der Knochenregenerierung werden auch zunehmend periostale Stammzellen im BTE eingesetzt [21]. Daher liegt in der Klinik und Poliklinik für Mund-, Kiefer- und Gesichtschirurgie des Universitätsklinikums Tübingen der Fokus

auf der Erforschung und der zukünftigen klinischen Anwendung von Kieferperiostzellen (engl. jaw periosteal cells, JPCs) in der MKG-Chierurgie [22-24]. Aufgrund ihrer guten Verfügbarkeit und ihres regenerativen Potenzials wird, so wie in dieser Arbeit, zudem an der Verwendung induzierter pluripotenter Stammzellen (engl. induced pluripotent stem cells, iPSCs) geforscht [25].

1.3 Stammzellen

1.3.1 Mesenchymale Stammzellen

Aus Knochenmark isolierte mesenchymale Stamm-, oder Stromazellen (MSCs) wurden in den 1970er Jahren erstmals von A. J. Friedenstein beschrieben [26]. MSCs können ebenso aus zahlreichen anderen Geweben wie z.B. Periost, Pulpa oder Fettgewebe isoliert werden [23, 27, 28]. Sie werden charakterisiert durch die Dominici Kriterien, einschließlich einer spindelförmigen Morphologie, des adhärenten Wachstums auf Plastikkulturschalen, der Expression der Oberflächenantigene CD73, CD90, CD105, sowie des Fehlens der Oberflächenantigene CD11b, CD19, CD34, CD45 und HLA-DR [29]. Zudem sind MSCs multipotente adulte Stammzellen, die das Potenzial besitzen *in vitro* unter anderem zu Adipozyten, Chondrozyten und Osteoblasten zu differenzieren.

Neben diesen „Minimalkriterien“ besitzen MSCs weitere Eigenschaften, wie die Fähigkeit in verletztes oder entzündetes Gewebe zu wandern („Homing“) [30], die Sekretion von parakrinen Faktoren [31], sowie immunmodulatorische Funktionen [32]. Aufgrund dieser Eigenschaften eignen sich MSCs für die Behandlung einer Vielzahl von Erkrankungen und werden bereits in zahlreichen klinischen Studien eingesetzt. Eine aktuelle Suche in der größten Datenbank für klinische Studien ClinicalTrials.gov ergab 965 Treffer für Studien mit MSCs [33].

Trotz vielversprechender Ergebnisse klinischer Studien, welche die Sicherheit autologer und allogener MSCs sowie die Wirksamkeit, z.B. bei der Behandlung von GvHD (graft-versus-host-disease) belegen [34], gibt es weiterhin Hindernisse für die Anwendung von MSCs in der klinischen Routine. Neben den komplizierten Zulassungsverfahren für zellbasierte Therapeutika, bereiten vor allem die begrenzte Verfügbarkeit von autogenen MSCs und die noch nicht standardisierte Qualität der isolierten Zellkulturen Probleme.

Die Qualität, bzw. das Differenzierungspotenzial von MSC-Kulturen, wird durch mehrere Faktoren beeinflusst. Dazu zählen die Entnahmestelle, das Patientenalter,

sowie die Heterogenität der Zellkultur [35-37]. Um die Qualität der MSC-Kulturen zu verbessern, wird daher nach Oberflächenmarken gesucht mit welchen osteogene Vorläuferzellen identifiziert und isoliert werden können [38]. Zu diesem Zweck wurden in der vorliegenden Arbeit die Oberflächenantigene MSCA-1 und CD146 verwendet, um osteogene Vorläuferzellen aus dem Periostzellkulturen zu isolieren bzw. die erhaltenen Subpopulationen auf ihr Stammzellpotenzial zu untersuchen [23, 39, 40].

Für die Regenerierung großer Knochendefekte werden entsprechend große Zellmengen benötigt. Aufgrund der geringen Anzahl von MSCs in einigen Donorgeweben können teilweise nicht ausreichend Zellen isoliert werden. Zudem ist die *in vitro* Expansion der Zellen nur begrenzt möglich, da die Vitalität und das Differenzierungspotenzial der Zellen nach einigen Passagen nachlassen [41]. Weiterhin besteht eine negative Korrelation zwischen dem Alter des Donors und der MSC-Konzentration im Gewebe, der Vitalität der Zellen, sowie ihres Differenzierungspotenzials [36]. Daher wird an Alternativen zu autologen MSCs, z.B. allogenen MSCs oder iPSCs, geforscht.

1.3.2 Induzierte pluripotente Stammzellen

Humane induzierte pluripotente Stammzellen (iPSCs) entsprechen in allen ihren Eigenschaften weitestgehend humanen embryonalen Stammzellen (ESCs) [42]. Im Gegensatz zu ESCs, welche nur in einem sehr kurzen Zeitraum im Blastozystenstadium am 4.-5. Tag der Embryonalentwicklung existieren, können iPSCs durch die Reprogrammierung somatischer Zellen hergestellt werden [43]. Wie embryonale Stammzellen besitzen iPSCs die Fähigkeit zur Selbsterneuerung, was sie zu einer theoretisch unerschöpflichen Stammzellquelle macht [42]. Ihre Pluripotenz erlaubt die Differenzierung in verschiedenste Zelltypen und bietet großes Potenzial für die Herstellung klinisch relevanter autologer Zelltypen und deren zukünftige Anwendung in der regenerativen Medizin [42].

iPSCs weisen die für ESCs typische Morphologie mit kleinen, in dichten Kolonien mit scharf abgegrenzten Rändern wachsenden Zellen auf (Abbildung 2). Zudem exprimieren sie große Mengen des Enzyms Tissue non-specific Alkaline Phosphatase (TNAP), wodurch sich iPSC-Kolonien durch die Umsetzung chromogener Substrate durch TNAP anfärben und identifizieren lassen [44, 45].

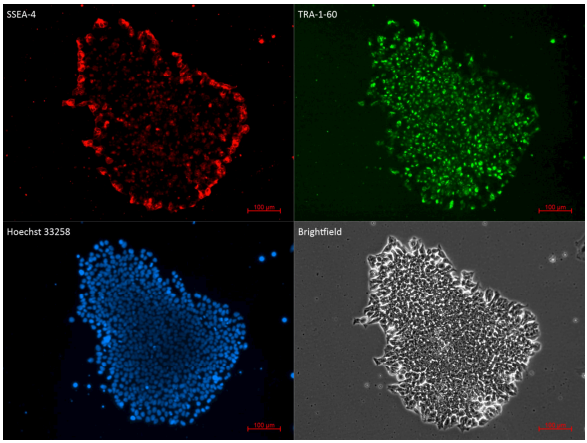

Abbildung 2: Fluoreszenzmikroskopische Aufnahme einer aus JPCs generierten iPSC-Kolonie. Immunfärbung mit anti-SSEA-4-DyLight550 und anti-TRA-1-60-DyLight488 Antikörpern, sowie Hoechst33258 Kernfärbung und Hellfeldaufnahme (Maßstabsbalken = 100 µm).

Humane pluripotente Stammzellen werden durch die Expression der Oberflächenantigene SSEA-3 (Stage-Specific Embryonic Antigen-3), SSEA-4 (Stage-Specific Embryonic Antigen-4), TRA-1-60 (Podocalyxin) und TRA-1-81 (Podocalyxin), sowie der Pluripotenzgene OCT4 (Octamer Binding Transcription Factor 4), SOX2 (Sex Determining Region Y-Box 2) und NANOG charakterisiert [46]. Zum Nachweis der Pluripotenz werden die Zellen entweder gezielt, mit speziellen Differenzierungsprotokollen, oder spontan, *in vitro* durch die Bildung von sog. Embryoidbodies (EBs), oder *in vivo* durch die Bildung von Teratomen nach Injektion in immundefiziente Mäuse, in Zellen der drei Keimblätter differenziert [46].

iPSCs können aus somatischen Zellen durch die erzwungene Expression der Transkriptionsfaktoren OCT4, SOX2, KLF4 (Kruppel-Like Factor 4) und c-MYC (OSKM oder Yamanaka Faktoren) generiert werden [43, 47]. OCT4, SOX2 und KLF4 sind sog. Pioniertranskriptionsfaktoren, welche in der Lage sind, an inaktives Heterochromatin zu binden und dieses für andere Transkriptionsfaktoren zugänglich zu machen [48]. c-MYC ist nicht essenziell, erhöht die Reprogrammierungseffizienz jedoch erheblich, wobei die unterliegenden Mechanismen bisher noch unklar sind [49-51].

Die Reprogrammierungs- oder Yamanaka-Faktoren bewirken eine globale Umwandlung und Löschung von epigenetischen Markierungen der somatischen Zelle, induzieren die Expression Pluripotenz-assoziierter Gene und die

Herunterregulierung somatischer Gene, sowie morphologische und metabolische Veränderungen, zurück zur embryonalen Stammzelle [48, 52].

Durch die Reprogrammierung somatischer Zellen können ethische und rechtliche Probleme bei der Gewinnung von ESCs umgangen werden. Daher werden iPSCs mittlerweile in vielen Bereichen der medizinischen Forschung eingesetzt. Zudem ermöglicht die Reprogrammierung von Patientenzellen die Erforschung von Krankheitsursachen und –mechanismen, sowie die Entwicklung potentieller Therapien [53].

2014 wurden zum ersten Mal iPSCs in einer klinischen Studie an einem Patienten mit altersbedingter Makuladegeneration angewendet [54]. Derzeit laufen weitere klinische Studien zum Einsatz von iPSCs u.a. bei Parkinson, Diabetes, Herzinfarkt und Knochenmarksverletzungen [55].

Für eine spätere klinische Verwendung von iPSCs ist eine sichere Reprogrammierung der Zellen entscheidend. Dabei müssen vor allem genetische Veränderungen der Zellen durch einen Reprogrammierungsvektor verhindert werden. Yamanaka und Ko-Autoren (2007) führten die erste Reprogrammierung humaner Zellen mithilfe retroviraler Vektoren durch [43]. Durch die zufällige Integration der Vektoren in das Genom der Wirtszellen kann es bei dieser Methode zu ungewollten Mutationen kommen die, z.B. durch die Deletion von Tumorsuppressorgenen oder die Aktivierung von Onkogenen, zur Transformation der Zellen führen können. Auch bei der Verwendung nicht-integrierender DNA-Vektoren wie Adenoviren, episomalen Plasmiden oder Minicircles, besteht die Gefahr von Mutationen durch eine Integration der Vektor-DNA bei der Reparatur von Doppelstrangbrüchen der genomischen DNA der Zellen [56-61]. Um auch diese Gefahr auszuschließen wurden nicht integrierende, DNA-freie Reprogrammierungsmethoden entwickelt (siehe Abbildung 3).

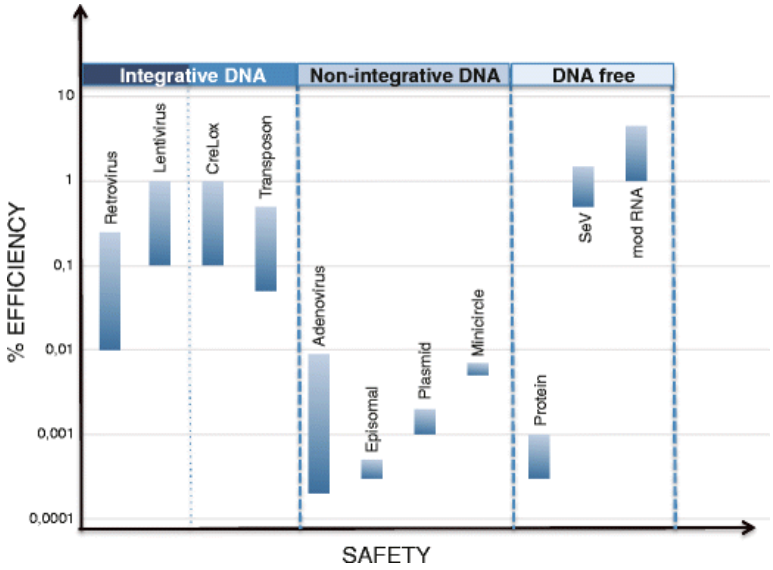

Abbildung 3: Vergleich verschiedener integrativer, nicht-integrativer und DNA-freier Reprogrammierungsvektoren unter den Gesichtspunkten Effizienz und Sicherheit (SeV: Sendai Virus, mod RNA: modifizierte RNA). Nach Bernal, J.A., 2013 [62].

Diese Methoden basieren, bis auf die Reprogrammierung mittels OSKM-Proteinen, auf der Verwendung von RNA [63-65]. Die heute am häufigstem eingesetzten Methoden zur sicheren Herstellung integrationsfreier iPSCs sind die Verwendung von Sendaiviren (RNA-Viren) oder von mRNA [66, 67].

Die Reprogrammierung mit Sendaiviren funktioniert einfach und effizient, setzt aber ein Labor der gentechnischen Sicherheitsstufe 2 voraus, da mit infektiösen Viruspartikeln gearbeitet wird. Dem Reprogrammierungsvektor wurde das Gen zur Fusion der Hüllproteine entfernt [66]. Dadurch entstehen nach der Transduktion keine infektiösen Viruspartikel, die Virus-RNA wird jedoch weiterhin in den Zellen repliziert. Sie kann nach einigen Passagen durch Verdünnung aus der Zelle verschwinden, oft sind vektorfreie iPSC-Klone aber nur durch manuelle Selektion zu erhalten [66].

Die Reprogrammierung mittels synthetischer mRNA wurde von Warren et al. (2010) entwickelt [67]. Die Vorteile von mRNA sind, dass sie nicht in das Wirtsgenom integrieren kann und, dass sie schnell abgebaut und aus der Zelle entfernt wird, sodass keine Spuren der RNA in den iPSCs verbleiben. Dies ist jedoch zugleich der größte Nachteil von mRNA, da durch die Instabilität tägliche Transfektionen über

einen Zeitraum von bis zu 3 Wochen nötig sind. Zudem löst die Transfektion einzelsträngiger RNA eine antivirale Immunantwort der Zelle aus, wodurch die Apoptose der Zellen induziert und häufig eine effiziente Reprogrammierung verhindert wird [68].

Yoshioka et al. (2013) veröffentlichten die Reprogrammierung mittels eines synthetischen RNA-Replicons, welches die Vorteile der beiden Methoden vereint [69]. Dieser Vektor basiert auf dem venezolanischen Pferdeenzephalomyelitisvirus (engl. Venezuelan Equine Encephalitis, VEE), welchem die Gene der Hüllproteine entfernt, und die OSKM-Gene sowie ein Resistenzgen für ein Selektionsantibiotikum eingefügt wurden. Dieses Replicon wird wie mRNA durch *in vitro* Transkription synthetisiert und in Zellen transfiziert, wo es in der Lage ist sich wie virale RNA zu replizieren. Die Replikation der RNA funktioniert jedoch nur, solange die antivirale Immunantwort der Zellen unterdrückt wird. Durch Beendigung der Immunsuppression nach der Reprogrammierung wird die RNA effizient aus den Zellen entfernt, sodass Rückstandsfreie iPSCs generiert werden können.

1.3.3 Aus iPSCs generierte MSC-ähnliche Zellen (iMSCs)

Aufgrund ihrer Tumorigenität sind iPSCs nicht für eine direkte Anwendung am Patienten geeignet. Stattdessen können sie zu MSC-ähnlichen Zellen (iMSCs) differenziert werden, welche dann ohne das Risiko einer Teratombildung als osteogene Vorläuferzellen eingesetzt werden können [70]. Diese Vorgehensweise hat zudem den Vorteil, dass iMSCs mit etablierten Protokollen analog zu MSCs behandelt werden können.

Die genauen Mechanismen der Differenzierung von iPSCs zu iMSCs sind bisher noch weitgehend unbekannt. Aus diesem Grund gibt es eine Vielzahl von Differenzierungsprotokollen, deren Wirkungsweise jedoch immer auf der Kombination von ungezielter Differenzierung der iPSCs und anschließender Selektion MSC-ähnlicher Zellen beruht.

Eine gängige Differenzierungsmethode funktioniert durch die Herstellung von Sphäroiden, sog. Embryoidbodies (EBs), in welchen die iPSCs spontan differenzieren [70, 71]. Alternativ können iPSCs als Kolonien oder vereinzelt in serumhaltigem Medium inkubiert werden, was ebenfalls zur spontanen Differenzierung der iPSCs führt [72-74]. In beiden Fällen werden anschließend MSC-ähnliche Zellen anhand ihrer Plastikadhärenz und durch die Kultivierung in MSC-

Medium über mehrere Passagen selektiert. In vielen Publikationen werden zudem Wachstumsfaktoren oder andere Wirkstoffe während der Differenzierung hinzugegeben [75, 76].
Während der Differenzierung werden Pluripotenzgene wie OCT4, NANOG und TERT herunterreguliert, während MSC-marker wie CD44, CD73, oder CD105 verstärkt exprimiert werden. Die so generierten iMSCs weisen mit MSCs vergleichbare Eigenschaften bezüglich Oberflächenmarkerexpression, Morphologie, Differenzierungspotenzial und immunmodulatorischer Eigenschaften auf und erfüllen die Minimalkriterien für MSCs der ISCT (International Society for Cellular Therapy), die bereits unter Kapitel 1.3.1 erwähnt wurden [77, 78].
Einige Publikationen berichten zudem von Anzeichen von Verjüngung in Zellen, welche aus iPSCs differenziert wurden. So wurden z.B. verlängerte Telomere, eine beschleunigte Proliferation und eine mit zellulärer Verjüngung assoziierte Genexpressionssignatur, sowie die Entfernung von seneszenz-, und altersassoziierten DNA-Methylierungen beobachtet [31, 32]. Ob sich aus diesen Verjüngungszeichen möglicherweise positive Effekte auf Anwendungen in der regenerativen Medizin ergeben wird Gegenstand zukünftiger Forschungsprojekte sein.

1.3.4 Klinische Anwendung von Stammzellen

Obwohl die Forschung an zellbasierten Therapien in den letzten Jahren große Fortschritte gemacht hat, findet kaum eine Translation der Forschung in die Klinik statt. Das liegt hauptsächlich an den schwierigen Zulassungsverfahren für derartige Therapien.
Während die Entnahme von Zellen und ihre Rückführung in den Patienten während der Behandlung ohne „substantielle“ Bearbeitung, wie z.B. bei der direkten Verwendung von Knochenmarkaspirat [21], nicht unter das Arzneimittelgesetz fällt (§ 4a Satz 1 AMG), gelten BTE-Produkte, zu deren Herstellung Zellen *in vitro* kultiviert wurden, als „neuartige Therapien“, deren Zulassungsvoraussetzungen in der EU-Verordnung 1394/2007/EG über die „Advanced Therapy Medicinal Products“ (ATMPs) zusammengefasst sind. Werden Stammzellen und Medizinprodukte im Sinne des Artikels 1 Absatz 2 Buchstabe a der Richtlinie 93/42/EWG kombiniert, wie z.B. bei der Besiedelung von Scaffolds mit MSCs, handelt es sich um ein „kombiniertes ATMP“, für dessen Zulassung der Medizinproduktbestandteil zudem

bereits eine CE-Kennzeichnung besitzen sollte. Zum Nachweis von Qualität, Unbedenklichkeit und Wirksamkeit von ATMPs müssen klinische Studien unter “Good Clinical Practice” (GCP) Richtlinien (EU Directive 2001/20/CE und 2005/28/CE) durchgeführt werden und in Deutschland durch eine Ethikkommission und das Paul-Ehrlich-Institut genehmigt werden.

Nationale Ausnahmen von der ATMP Verordnung können genehmigt werden und unterliegen in Deutschland § 4b Abs. 3 Satz 1 AMG, wenn das ATMP „nicht-routinemäßig“, „als individuelle Zubereitung für einen einzelnen Patienten“ in einer „spezialisierten Einrichtung der Krankenversorgung“ hergestellt wird.

Voraussetzung dafür ist zudem, dass das ATMP unter „spezifischen Qualitätsnormen“ hergestellt wird, was in erster Linie die Herstellung unter Richtlinien der „guten Herstellungspraxis“ (engl. good manufacturing practice, GMP) bedeutet.

Um eine zukünftige klinische Anwendung der in der vorliegenden Arbeit generierten iMSCs zu erleichtern, wurde versucht diesen Richtlinien bestmöglich zu entsprechen. Dazu wurde zum einen ein besonders sicherer RNA-basierter Reprogrammierungsvektor zur Herstellung von iPSCs eingesetzt. Zum anderen wurde in der Zellkultur auf tierische Zusätze, insbesondere fötales Kälberserum (fetal bovine serum, FBS) verzichtet, da mögliche Immunreaktionen und die Übertragung von Krankheiten wie BSE nicht ausgeschlossen werden können. Alternativ wurde humanes Thrombozytenlysat (human platelet lysate, hPL) als Zellkultursupplement eingesetzt, welches die GMP-Standards erfüllt und als „Ausgangsstoff zur Herstellung von Zelltherapeutika“ zugelassen ist, und das Wachstum und die Differenzierung von MSCs und iMSCs unterstützt [74, 79, 80].

2. Zielsetzung

Ziel dieser Arbeit war es die Qualität und Verfügbarkeit von osteogenen Vorläuferzellen für das BTE zu verbessern. Dazu wurden unterschiedliche Ansätze verfolgt.

Zur Verbesserung der Verfügbarkeit geeigneter Stammzellen sollten in dieser Arbeit iPSCs aus Kieferperiostzellen hergestellt, und Protokolle für die Verwendung von iPSCs im BTE entwickelt werden. Um zukünftige klinische Anwendungen zu erleichtern sollte die Herstellung von iPSCs mit Hilfe eines nicht integrierenden, selbst-replizierenden RNA-Vektors, sowie ohne xenogene Medienzusätze durchgeführt werden. Aus Kieferperiostzellen hergestellte iPSCs sollten expandiert und charakterisiert werden und anschließend, ebenfalls ohne xenogene Medienbestandteile, zu osteogenen Vorläuferzellen (iMSCs) differenziert werden. Diese Zellen sollten die minimalen Kriterien für MSCs erfüllen und ein möglichst großes osteogenes Differenzierungspotenzial besitzen um für das BTE eingesetzt werden zu können.

Zur Verbesserung der Qualität osteogener Vorläuferzellen, welche aus patienteneigenem Kieferperiost isoliert werden, sollten Oberflächenmarker untersucht werden, die die Identifikation und Isolation osteogener Vorläuferzellen in heterogenen Zellpopulationen ermöglichen. Aufgrund von eigenen Vorarbeiten sowie Publikationen anderer Arbeitsgruppen lag dabei der Fokus auf den Oberflächenantigenen MSCA-1 und CD146. Zudem fiel bei der Charakterisierung der cranialen Periostzelllinie TAg58 (TAg-Zellen) eine erhöhte Expression der beiden Marker sowie ein erhöhtes Mineralisierungspotenzial der Zellen auf. Um die Eignung von MSCA-1 und CD146 zur Identifikation osteogener Vorläuferzellen, sowie einen möglichen Synergismus der Marker bei der osteogenen Differenzierung zu untersuchen sollten TAg-Zellen mittels FACS anhand der beiden Oberflächenantigene in 4 Subpopulationen (MSCA-$1^{+/-}$/$CD146^{+/-}$) separiert, und anschließend die osteogene Differenzierung der Subpopulationen anhand der Mineralisierung der Zellen analysiert werden.

3. Ergebnisse und Diskussion

3.1 Generierung und Charakterisierung von iPSCs aus JPCs

Zur Generierung von iPSCs aus JPCs wurden in dieser Arbeit Zellen von 3 Patienten der MKGC in Übereinstimmung mit der lokalen Ethikkommission (Ethikvotum 074/2016BO2, 17.05.2016) und nach Aufklärung und schriftlicher Zustimmung in diese Studie aufgenommen.

3.1.1 Reprogrammierung von JPC mittels VEE-OKSM-GFP RNA

Die Reprogrammierung mithilfe von selbstreplizierender RNA (srRNA) wurde 2013 von Yoshioka et al. entwickelt [69]. Wie in vielen publizierten Reprogrammierungsprotokollen wurden dabei Fibroblasten, meist sehr junger Spender, verwendet, welche sich durch eine gute Vitalität und hohe Proliferationsraten auszeichnen [67, 69]. Zudem wurden FBS-haltige Medien und Feeder-Zellen eingesetzt. Ziel der vorliegenden Arbeit war auch das Reprogrammierungsprotokoll zunächst für die Transfektion von JPCs in xenogen-freiem Medium ohne Feeder-Zellen anzupassen. Weiterhin wurde dem ursprünglichen VEE-OKSM-Puro^r Reprogrammierungsvektor ein GFP-Gen (grün fluoreszierendes Protein) hinzugefügt, welches es ermöglichte, die Expression der srRNA mittels Fluoreszenzmikroskopie zu detektieren und die Transfektionseffizienz mittels Durchflusszytometrie zu bestimmen (Abbildung 4). So konnte mit dem hierfür entwickelten Protokoll 24h nach der Transfektion eine durchschnittliche Effizienz von 32,48 % ± 2,0 % detektiert werden (Abbildung 4d) [25].

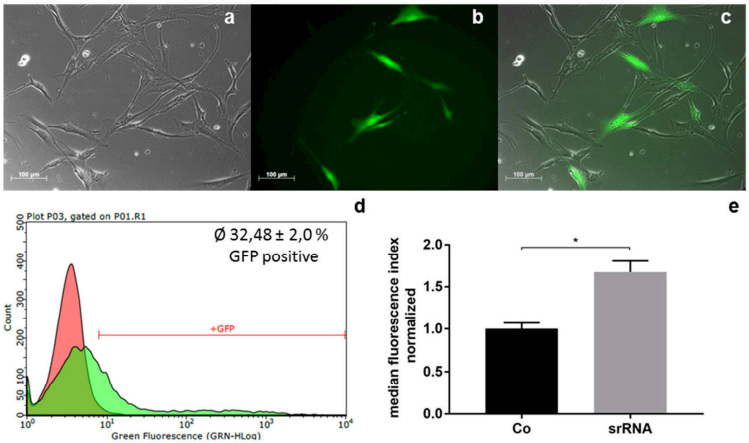

Abbildung 4: Transfektion von JPCs mit srRNA. a-c) Repräsentative a) Hellfeld-, b) GFP- und c) kombinierte Mikroskopaufnahmen von JPCs 24 h nach srRNA-Transfektion. d) Repräsentatives Histogramm von Durchflusszytometriemessungen nicht-transfizierter (rot) und srRNA-transfizierter (grün) JPCs 24 h nach Transfektion. e) MFI (Median Fluoreszenzindex) Mittelwerte ± SD von srRNA-transfizierten und nicht-transfizierten (Co) JPCs in Relation zu MFI Werten von nicht-transfizierten (Co) Proben wurden berechnet und mit dem Student's t-Test verglichen (n = 3 Patienten, * $p < 0,05$). Nach Umrath, F. et al., 2019 [25].

Die Reprogrammierung der JPCs erfolgte wie in Schema Abbildung 5a dargestellt. JPCs wurden in hPL5-Medium (5% hPL) transfiziert. Dem Medium wurde während der Reprogrammierung B18R, bzw. B18R-konditioniertes Medium (BcM) zugesetzt, um eine Immunreaktion der Zellen auf die srRNA zu inhibieren. Zusätzlich wurde ab Tag 3 der Histondeacetylaseinhibitor Natriumbutyrat (NaB) zugegeben, um die Reprogrammierungseffizienz zu erhöhen [81]. Von Tag 1-5 wurde dem Medium Puromycin zugesetzt um nicht-transfizierte Zellen abzutöten. An Tag 5 wurden die Zellen passagiert und ab Tag 7 auf iPSC-Medium (Essential 8, E8) umgestellt.

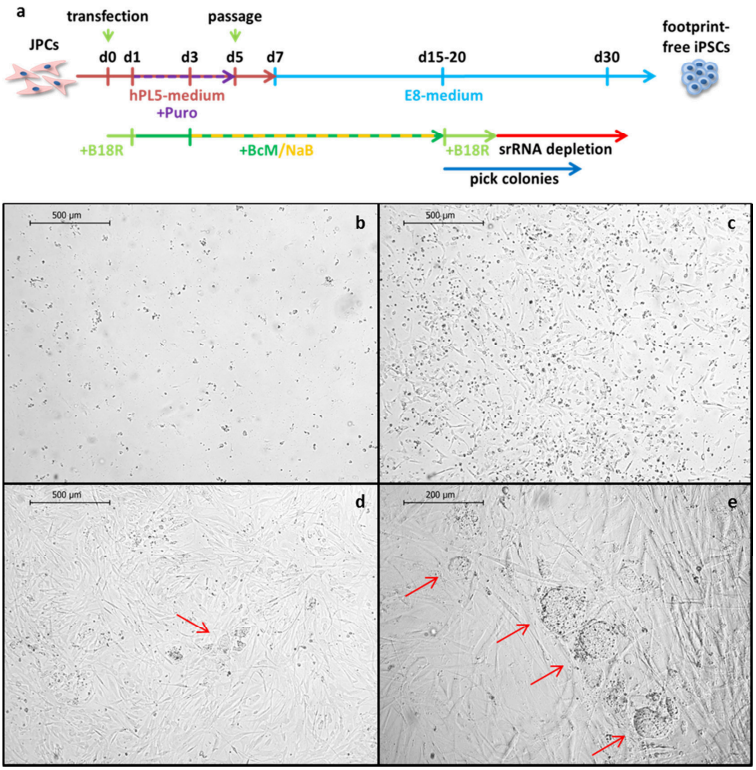

Abbildung 5: Reprogrammierung von JPCs. a) Zeitachse der JPC-Reprogrammierung. JPCs wurden in hPL5-Medium mit 0,2 µg/ml B18R-Protein transfiziert (d0). An Tag 1 wurde das Medium auf hPL5 mit 25% B18R-konditioniertes Medium (BcM) und 1,0 µg/ml Puromycin (Puro) umgestellt. Die Puromycin-Selektion wurde bis zum Tag 5 fortgesetzt (violetter Pfeil). Die Zellen wurden an Tag 5 passagiert, und an Tag 7 wurde das Medium auf Essential 8 (E8) mit 25% BcM umgestellt. Natriumbutyrat (NaB) wurde dem Medium von Tag 3 bis 15 zugesetzt. Als die ersten iPSC-Kolonien entstanden, wurde das Medium auf E8 mit 0,2 µg/ml B18R-Protein umgestellt. iPSC-Kolonien wurden ab Tag 15 gepickt. b-e) Repräsentative Hellfeldbilder von JPCs während der srRNA-Reprogrammierung. b) Nicht transfizierte JPCs an Tag 5, die mit Puromycin behandelt wurden. c) srRNA-transfizierte JPCs an Tag 5, die mit Puromycin behandelt wurden. d) srRNA-transfizierte JPCs an Tag 12 mit ersten iPSC-Kolonien (mit einem roten Pfeil gekennzeichnet). e) srRNA-transfizierte JPCs an Tag 15 mit iPSC-Kolonien (durch rote Pfeile gekennzeichnet). Nach Umrath, F. et al., 2019 [25].

An Tag 12 entstanden erste iPSC-Kolonien, die mithilfe einer Pipettenspitze gepickt und in Vitronectin(VTN)-beschichteten Zellkulturplatten in iPSC-Medium expandiert wurden.

3.1.2 Charakterisierung generierter JPC-iPSCs

In den aus JPCs generierten iPSCs konnte die Expression von Pluripotenzmarkern, sowohl mittels Immunzytochemie als auch mittels Durchflusszytometrie und quantitativer PCR (qPCR) nachgewiesen werden (Abbildung 6).

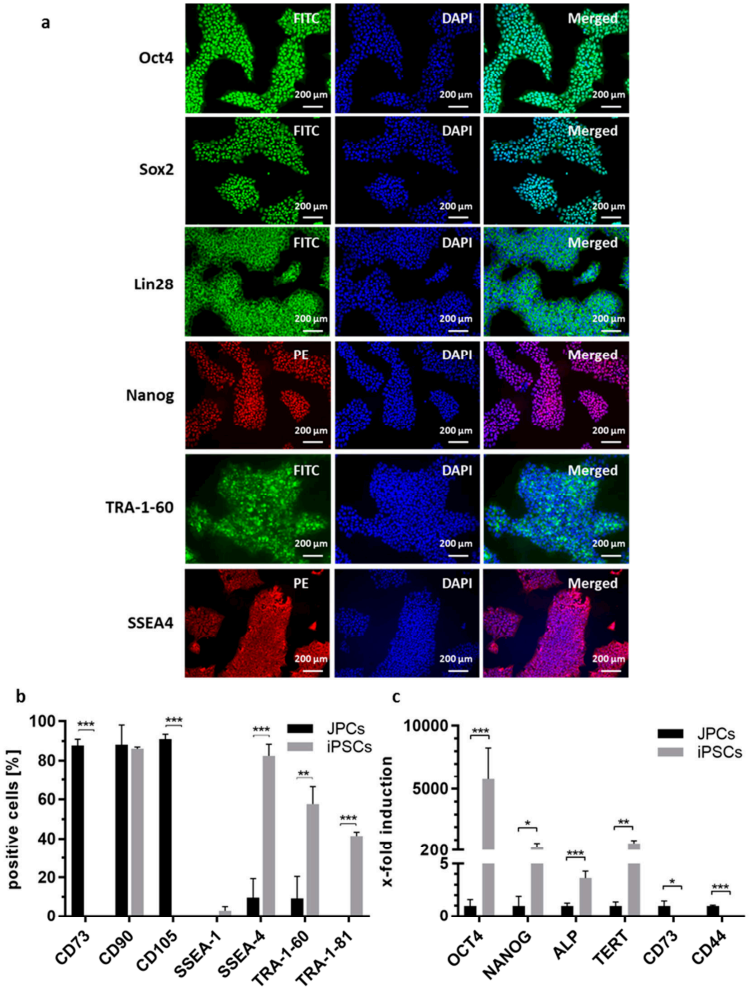

Abbildung 6: Markerexpression von JPCs und iPSCs. a) Oct4, Sox2, Lin28, Nanog, TRA-1-60 und SSEA4 Immunfärbung von iPSCs. b) Oberflächenmarkerexpression von JPCs und JPC-basierten iPSCs, die mittels Durchflusszytometrie analysiert und mit dem Student's t-Test auf Signifikanz geprüft wurden (n = 3, p* < 0,05, p** < 0,01, p*** < 0,001). c) Genexpressionsanalyse von JPCs und JPC-basierten iPSCs durch quantitative PCR. Die Genexpressionswerte wurden auf die Werte von GAPDH normalisiert. Die Mittelwerte ± SD der iPSC- und JPC-Genexpression werden relativ zu denen der JPCs dargestellt. Die statistische Signifikanz wurde mit Student's t-Test berechnet. (n = 3 Patienten, * p < 0,05, ** p < 0,01, *** p < 0,001). Nach Umrath, F. et al., 2019 [25].

Die Pluripotenz der Zellen wurde durch gezielte mesodermale, endodermale und ektodermale Differenzierung *in vitro*, sowie durch spontane Teratombildung nach Injektion in die Chorioallantoismembran (CAM) von Hühnereiern nachgewiesen [25]. Somit konnte der Nachweis erbracht werden, dass es sich bei den generierten Zellen um vollständig reprogrammierte iPSCs handelt.

Durch qPCR konnte mittels spezifischer Primer für die zur Replikation der RNA wichtigen nsP-Gene („nonstructural Proteins“) gezeigt werden, dass die srRNA nach der Reprogrammierung aus den Zellen entfernt wurde (Abbildung 7a). Nach 3 Passagen war kein Unterschied zwischen iPSCs und untransfizierten JPCs mehr zu detektieren, wohingegen in JPCs 48 h nach Transfektion mit srRNA (JPCs+) sehr hohe RNA-Mengen nachgewiesen werden konnten.

Anhand von Karyotypisierungen konnten keine chromosomalen Veränderungen durch die Reprogrammierung festgestellt werden, und die genetische Stabilität der Zellen bestätigt werden (Abbildung 7b). Die Zellen konnten somit für die Herstellung von iMSCs eingesetzt werden.

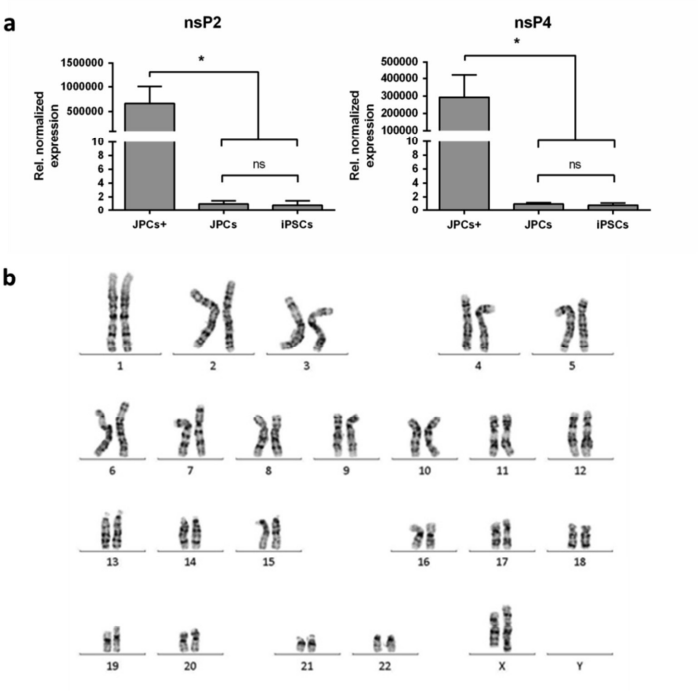

Abbildung 7: Eliminierung von srRNA nach der iPSC-Generierung und Karyotypisierung von iPSCs. a) qRT-PCR-Analyse von nsP2- und nsP4-Transkripten in iPSCs (Passage 3), unbehandelten JPCs und srRNA enthaltenden JPCs (JPCs+) 48 h nach der Transfektion. Die Daten werden als Mittelwerte + SEM dargestellt. Die Unterschiede wurden anhand einer einseitigen ANOVA (n = 3, p* < 0,05, ns. = nicht signifikant) verglichen. b) Repräsentatives Karyogramm von aus JPCs hergestellten iPSCs mit einem normalen Karyotyp (46, XX). Nach Umrath, F. et al., 2019 [25].

In diesem Projekt gelang erstmalig die Reprogrammierung von Kieferperiostzellen zu iPSCs mit der VEE-OKSM-Puro^{r}-GFP RNA unter xenogen-freien Bedingungen. Die

Expression von Pluripotenzmarkern sowie die Fähigkeit in die drei Keimblätter zu differenzieren zeigen, dass es sich bei den generierten Zellen um iPSCs handelt. Die Karyotypisierung und der schnelle Abbau der srRNA nach der Reprogrammierung demonstrieren die genomische Integrität der Zellen und die hohe Sicherheit der srRNA-basierten Reprogrammierung. Der Verzicht auf xenogene Medienzusätze vereinfacht die Translation dieser Methode in eine spätere klinische Anwendung.

3.2 Differenzierung von JPC-basierten iPSCs zu iMSCs

iPSCs sind aufgrund ihrer Tumorigenität und ihrer Neigung spontan zu differenzieren nicht für eine direkte klinische Anwendung geeignet. Daher war ein weiteres Ziel dieser Arbeit die aus JPCs generierten iPSCs zu MSC-ähnlichen Zellen (iMSCs) zu differenzieren.

3.2.1 iMSC Differenzierung

Um die Differenzierung von iPSCs zu iMSCs zu induzieren, werden iPSCs häufig mit FBS haltigem Medium inkubiert [72, 73]. Da in dieser Arbeit auf xenogene Medienzusätze verzichtet werden sollte, wurde stattdessen humanes Plättchenlysat (hPL) als Mediumsupplement verwendet.

In Vorversuchen zeigte sich, dass die Effizienz der iMSC-Differenzierung durch eine 10-tägige Kultivierung der iPSCs ohne weitere Passagierung gesteigert werden konnte. Vermutlich wird dabei die Differenzierung der iPSCs durch die hohe Zelldichte induziert. Nach diesem Schritt wurden die Zellen vereinzelt und in MSC-Medium mit 5% hPL (hPL5 Medium) + 150 µM Ascorbinsäure (Vit. C) ausplattiert (Abbildung 8a,c). Ascorbinsäure stimuliert die Proliferation von MSCs und wird auch für die Differenzierung von iPSCs zu Kardiomyozyten eingesetzt [82, 83]. Um das Absterben der Zellen durch die Vereinzelung zu verhindern wurde dem Medium in den ersten 24 h Rho-associated protein kinase (ROCK)-Inhibitor (Y27632) zugegeben. Die Zellen wurden anschließend über mehrere Passagen in hPL5 Medium + Vit. C kultiviert, bis die Zellen eine einheitliche MSC-artige Morphologie entwickelten (Abbildung 8b-e).

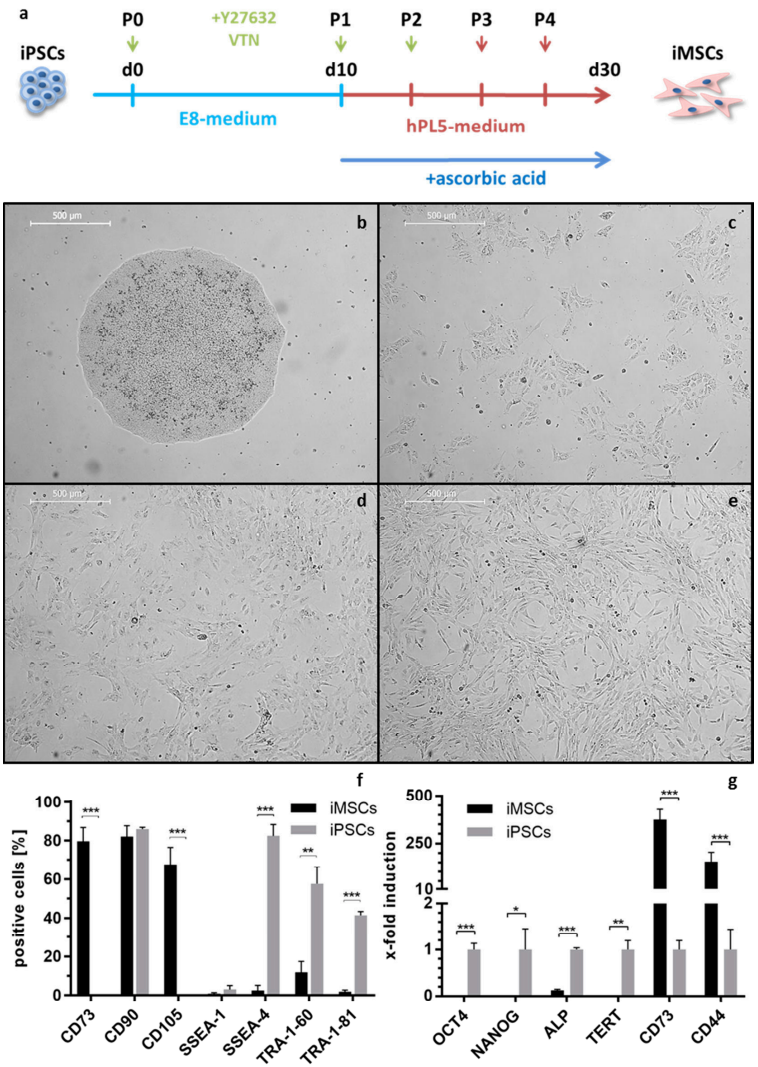

Abbildung 8: Differenzierung von iPSCs zu iMSCs. a) Zeitachse: iPSCs wurden in Gegenwart des ROCK-Inhibitors Y27632 auf Vitronectin beschichtete Platten gesät und 10 Tage lang in E8 medium (hellblaue Linie) kultiviert. Danach wurde den Zellen hPL5-Medium mit 150 µM Ascorbinsäure zugesetzt (rote Linie). Die Zellen wurden 3-5 mal passagiert, bis sie nach ca. 30 Tagen eine homogene MSC-ähnliche Morphologie zeigten. b-e) Änderung der Morphologie bei der Differenzierung von iPSCs in iMSCs. b) iPSC-Kolonie vor der Differenzierung. c) iMSCs nach der Einzelzellplattierung in Passage 0. d) Differenzierung von iMSCs in Passage 2. e) Zellmorphologie von iMSCs in Passage 4 (Maßstabsbalken entsprechen 500 µm). f) Mittels Durchflusszytometrie nachgewiesene Oberflächenmarkerexpression von iMSCs im Vergleich zu iPSCs. g) Genexpressionswerte von iMSCs wurden auf Werte des Housekeeping-Gens GAPDH normiert und als x-fache Induktion im Vergleich zu iPSCs dargestellt (Normierung auf 1). Unterschiede in Oberflächenmarker- und Genexpression wurden mit dem Student's t-Test verglichen. (n = 3, *p < 0,05, **p < 0,01, ***p < 0,001). Nach Umrath, F. et al., 2019 [25].

Nach Abschluss der iMSC Differenzierung zeigte die Analyse der Genexpression die Induktion der MSC-Markergene CD73 und CD44, sowie die drastische Herunterregulierung der Pluripotenzgene OCT4, NANOG, ALP und TERT (Abbildung 8g). Die durchflusszytometrische Analyse zeigte, dass 79,6% bzw. 67,6% der Zellen die MSC-typischen Oberflächenmarker CD73 und CD105 exprimierten und nur noch jeweils 2,6%, 11,8% und 2,0% der Zellen die Pluripotenzmarker SSEA-4, TRA-1-60 und TRA-1-81 exprimierten (Abbildung 8f). Diese Daten zeigen, dass zwar der Großteil der Zellen in Richtung MSCs differenzierte, ideal wäre jedoch die Expression von MSC-Markern in über 95% der Zellen, bzw. die Expression von Pluripotenzmarkern in weniger als 5% der Zellen. Die Expression von TRA-1-60 in 11,8% der Zellen deutet auf eine unvollständige Differenzierung hin, sodass sich noch undifferenzierte Zellen in den iMSC-Populationen befinden können. Vor einer klinischen Anwendung müsste daher die Fähigkeit der Zellen Teratome zu bilden überprüft werden. Auch der Anteil an MSC-Marker exprimierenden Zellen ist noch nicht optimal, und deutet auf eine spontane Differenzierung zu anderen Zelltypen hin. Eine Verlängerung der Differenzierungsdauer über eine oder mehrere zusätzliche Passagen könnte den Anteil TRA-1-60-negativer und CD73- und CD105-positiver Zellen weiter erhöhen. Zudem könnte die Effizienz der Differenzierung durch die Zugabe von stimulierenden Faktoren, wie z.B. Dexamethason, BMP-4 oder SB-431542 erhöht werden [73, 75, 76]. Alternativ könnten unerwünschte Zellen mittels FACS entfernt werden [84, 85].

3.2.2 Charakterisierung von iMSCs

Zum Nachweis des Differenzierungspotenzials wurden die iMSCs durch Inkubation in entsprechenden Differenzierungsmedien zur adipogenen, chondrogenen und osteogenen Differenzierung stimuliert und die Expression spezifischer Markergene, sowie die Bildung von Fettvakuolen (adipogene Differenzierung), Glykosaminoglykanen (GAGs, chondrogene Differenzierung) und Kalziumphosphatpräzipitaten (osteogene Differenzierung) anhand spezifischer Färbungen nachgewiesen (Abbildung 9).

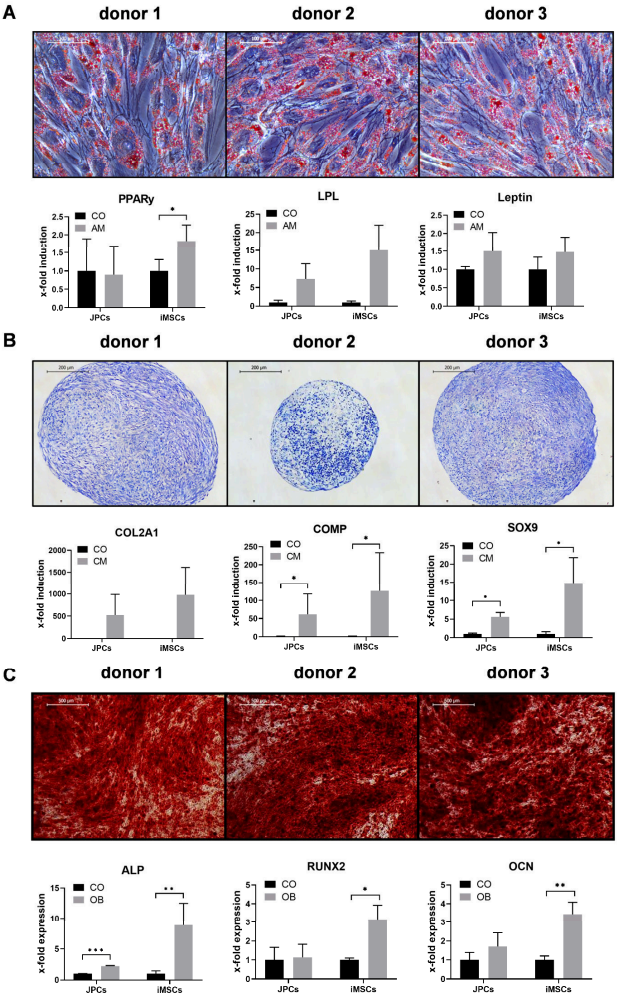

Abbildung 9: Adipogene, chondrogene und osteogene Differenzierung von iMSCs. A) Adipogene Differenzierung. Oben: Mikroskopische Aufnahmen (20-fache Vergrößerung, Maßstabsbalken = 100 µm) von Oil Red gefärbten iMSCs nach 15 Tagen adipogener Differenzierung. Unten: Expression der adipogenen Markergene PPRγ, LPL und Leptin von JPCs und iMSCs nach 10 tägiger Inkubation in Kontroll- (CO) und adipogenem Medium (AM). B) Chondrogene Differenzierung von iMSCs. Oben: Toluidinblau-Färbung von iMSCs, die 25 Tage lang mit chondrogenem Medium behandelt wurden (4-fache Vergrößerung, Maßstabsbalken = 500 µm). Unten: Expression der chondrogenen Markergene COL2A1, SOX9 und COMP von JPCs und iMSCs nach 20 Tagen Inkubation in Kontroll- (CO) und chondrogenem Medium (CM). C) Osteogene Differenzierung von iMSCs. Oben: Alizarin Red Färbung von iMSCs, die 15 Tage lang mit osteogenem Medium behandelt wurden (donor1, 20 Tage) (4-fache Vergrößerung, Maßstab = 500 µm). Unten: Expression der osteogenen Markergene ALP, RUNX2 udn OCN von JPCs und iMSCs nach 15 Tagen Inkubation in Kontroll- (CO) und osteogenem Medium (OB). Die Genexpressionsdaten von JPC- und iMSC-Proben wurden auf die entsprechende Expression des Housekeeping-Gens GAPDH normiert. Genexpressionsmittelwerte ± SD von behandelten (AM, CM, OB) und Kontrollproben (CO) wurden als x-fache Induktionswerte relativ zu den CO-Proben dargestellt. Die statistische Signifikanz wurde mit dem Student's t-Test berechnet. (n = 3 Patienten, * $p < 0,05$, ** $p < 0,01$, *** $p < 0,001$). Nach Umrath, F. et al., 2019 [86].

Die spezifischen Färbungen sowie die Expression der jeweiligen Markergene zeigen, dass die generierten iMSCs multipotente Stammzellen sind und ein hohes Differenzierungspotenzial besitzen. Somit erfüllen sie größtenteils (bis auf die Expression von MSC-Marken in >95% der Zellpopulation, siehe Abbildung 8f) die Minimalkriterien für MSCs der International Society for Cellular Therapy (ISCT) [29]. Insbesondere die starke Mineralisierung der Zellen während der osteogenen Differenzierung zeigt, dass die Zellen prinzipiell für eine Anwendung im Knochen-Tissue-Engineering geeignet sind.

3.2.3 Seneszenz und Verjüngung

Mehrere Publikationen beschreiben eine biologische Verjüngung von iPSCs und den aus ihnen differenzierten Zellen [87-89]. Daher wurden die in der vorliegenden Arbeit hergestellten Zellen ebenfalls auf Merkmale einer Verjüngung hin untersucht. Ein wichtiger Marker für das biologische Alter einer Zelle ist die Telomerlänge. Diese nimmt in somatischen Zellen mit jeder Zellteilung ab, was letztendlich zur replikativen Seneszenz der Zellen führt [90]. Daraus ergibt sich eine maximale Anzahl an Zellteilungen, auch bekannt als „Hayflick Limit“ [91]. Durch die Aktivierung des Enzyms Telomerase können die Telomerenden wieder verlängert, und so das „Hayflick Limit“ überschritten werden [92].
Bei der Reprogrammierung wird die Telomerase in somatischen Zellen reaktiviert und bleibt in iPSCs aktiv, sodass die Telomere verlängert werden und denen embryonaler Stammzellen gleichen [93]. Die Analyse der in dieser Arbeit generierten iPSCs und iMSCs zeigte, dass diese Zellen deutlich verlängerte Telomere im Vergleich zu den ursprünglichen JPCs aufwiesen, wobei die Telomere der iMSCs bereits wieder etwas kürzer waren als die der iPSCs (Abbildung 10). Diese Daten korrelieren mit der Expression des Telomerase-Reverse-Transkriptase-Gens (TERT) in den iPSCs und der erneuten Herunterregulierung in den iMSCs (Abbildung 8g).

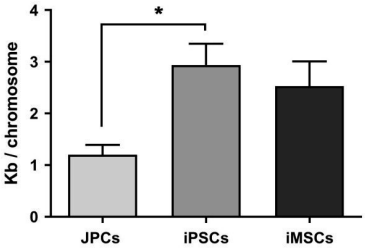

Abbildung 10: Telomerlängenquantifizierung durch qRT-PCR-Analyse von JPCs, JPC-iPSCs und iMSCs (n = 3 Patienten, Mittelwerte ± SEM, einfache ANOVA, * = p < 0,05). Nach Umrath, F. et al., 2019 [86].

Da die Elongation der Telomere auf eine Verjüngung der iMSCs gegenüber den ursprünglichen JPCs hindeutet, wurden weitere Merkmale zellulärer Seneszenz analysiert. Dazu zählen unter anderem Proliferation, metabolische Aktivität, Seneszenz-assoziierte β-Galactosidase (SA-β-Gal) Aktivität, sowie die Expression seneszenzassoziierter Gene [94].

Überraschenderweise zeigte der Vergleich der Proliferation und der metabolischen Aktivität von JPCs und iMSCs eine signifikant niedrigere Proliferation und metabolische Aktivität von iMSCs gegenüber JPCs (Abbildung 11).

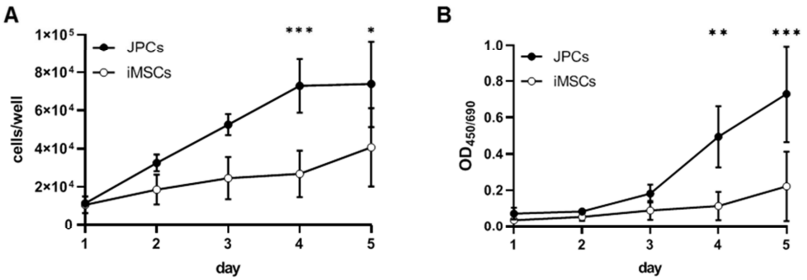

Abbildung 11: Proliferation und metabolische Aktivität von JPCs und iMSCs. Quantifizierung von A) Zellproliferation durch Zellzählung und B) Stoffwechselaktivität durch kolorimetrische Messung von Formazan, welches durch Reduktion von Tetrazoliumsalz in den Mitochondrien von JPCs und iMSCs gebildet wird (EZ4U). Zellzahlen und metabolische Aktivität von JPCs und iMSCs wurden mittels zweiweg ANOVA verglichen (n = 3, * = p > 0.05, ** = p > 0.01, *** = p > 0.001). Nach Umrath, F. et al., 2019 [86].

Die Untersuchung der Seneszenz-assoziierten Beta-Galactosidase ergab eine deutlich höhere SA-β-Gal-Aktivität in den iMSCs verglichen zu den ursprünglichen JPCs und iPSCs (Abbildung 12A-E).

Zudem wurde eine höhere Expression der Seneszenzmarkergene $P16^{INK4a}$ und $P21^{Cip1}$ in den iMSCs verglichen zu JPCs detektiert, jedoch ohne statistische

Signifikanz (Abbildung 12F, G). Eine signifikant niedrigere Expression von $P16^{INK4a}$ und $P21^{Cip1}$ wurde in iPSCs nachgewiesen.

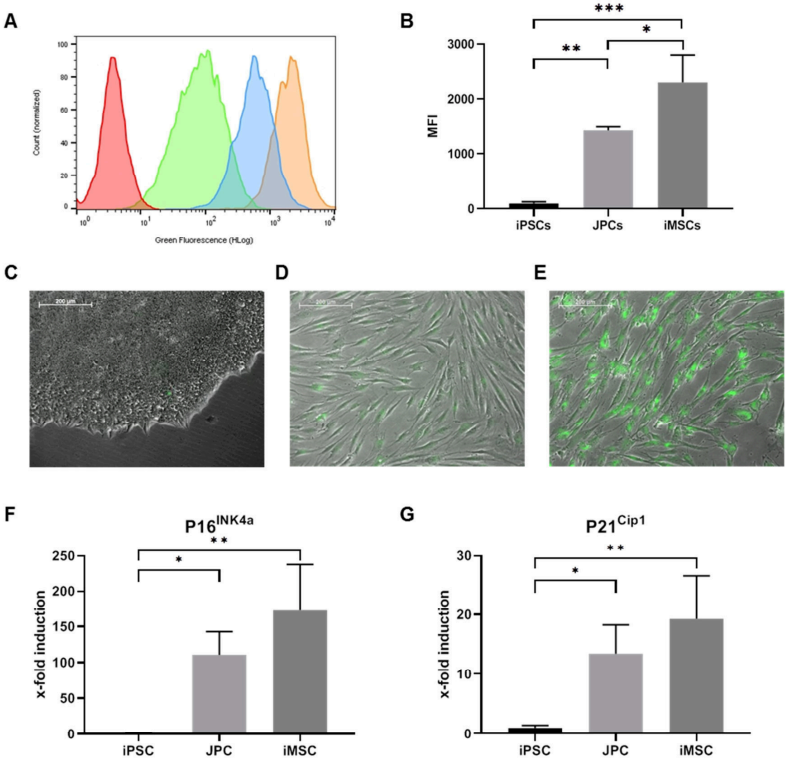

Abbildung 12: SA-β-Gal Aktivität und Expression von Seneszenzmarkergenen. A) Repräsentatives Histogramm der SA-β-Gal Aktivität in iPSCs (grün), JPCs (blau) und iMSCs (orange) sowie ungefärbter Kontrolle (rot). B) MFI-Werte der SA-β-Gal Expression in iPSCs, JPCs und iMSCs (* = p > 0.05, ** = p > 0.01, *** = p > 0.001). C-E) Fluoreszenzmikroskopische Aufnahme von C) iPSCs, D) JPCs und E) iMSCs (10-fache Vergrößerung, Maßstabsbalken = 200 µm). Nach Umrath, F. et al., 2019 [86].

Die erhobenen Daten deuten auf eine frühe Seneszenz der iMSCs hin und stehen damit im Widerspruch zu den Publikationen über eine Verjüngung von aus iPSCs differenzierten Zellen [87, 88].

Feng et al. beobachteten ebenfalls seneszente Zellen bei der Differenzierung von iPSCs zu Hämangioblasten und erklärten diese mit der retroviralen Vektorinsertion und einer Reaktivierung von Reprogrammierungsgenen bei der Differenzierung [95]. Gokoh et al. zeigten jedoch, dass ein effizienteres Protokoll zur Hämangioblastendifferenzierung, sowie die Vermeidung von Stressfaktoren die

Entstehung seneszenter Zellen verhinderte [96]. Ebenso ist auch in der vorliegenden Arbeit anzunehmen, dass die Ursachen der frühen Seneszenz von iMSCs, der Stress durch den Differenzierungsprozess, sowie die unzureichende Effizienz der Differenzierungsmethode, und eine damit einhergehende exzessive Expansion von wenigen differenzierten Zellen, sind. Für diese Theorie spricht, dass durch die anfängliche Einzelzellplattierung der iPSCs und die spätere Passagierung auf unbeschichtete Zellkulturschalen während der Differenzierung zu iMSCs ein großer Teil der Zellen abstirbt. Dabei findet vermutlich eine Selektion von bereits differenzierten, oder zur Differenzierung stimulierten Zellen statt. Diese Hypothese wird durch die Beobachtung gestützt, dass iPSCs welche über 10 Tage ohne Passagierung kultiviert wurden, was vermutlich die Differenzierung induzierte, effizienter zu iMSCs differenzierten. Somit könnte dieses Problem durch die Optimierung des Differenzierungsprotokolls gelöst werden. Dazu könnten Stressfaktoren wie z.B. das Vereinzeln von iPSCs vermieden werden. Zudem könnten während der Differenzierung stimulierenden Faktoren, wie z.B. Dexamethason, BMP4 oder SB-431542 zugegeben werden um die Differenzierungseffizienz zu verbessern [73, 75, 76].

3.3 Verwendung von humanem Thrombozytenlysat für die Kultivierung und Differenzierung von JPCs und iMSCs

3.3.1 Proliferation und Differenzierungspotenzial

Um den theoretischen Anforderungen für die klinische Anwendung von iPSCs und den daraus differenzierten iMSCs zu entsprechen, wurde für dieses Projekt die gesamte Zellkultur, von der Isolation der JPCs bis zur osteogenen Differenzierung der iMSCs, in xenogen-freien Medien etabliert. Da genau definierte, kommerzielle Medien das Wachstum, die Differenzierung und besonders die Reprogrammierung von JPCs nicht in ausreichendem Maße unterstützten (wie die Ergebnisse von Vorversuchen zeigten), wurde hPL als Zellkultursupplement eingesetzt. In vorläufigen Arbeiten wurde das Wachstum und das Differenzierungspotenzial von JPCs mit FBS und hPL-Supplementierung verglichen und die optimale hPL Konzentration für das Wachstum und die Differenzierung von JPCs bestimmt (Abbildung 13 und Abbildung 14). Dabei zeigte sich, dass die hPL-Supplementierung zu einer deutlichen Verbesserung der genannten Zellfunktionen führte.

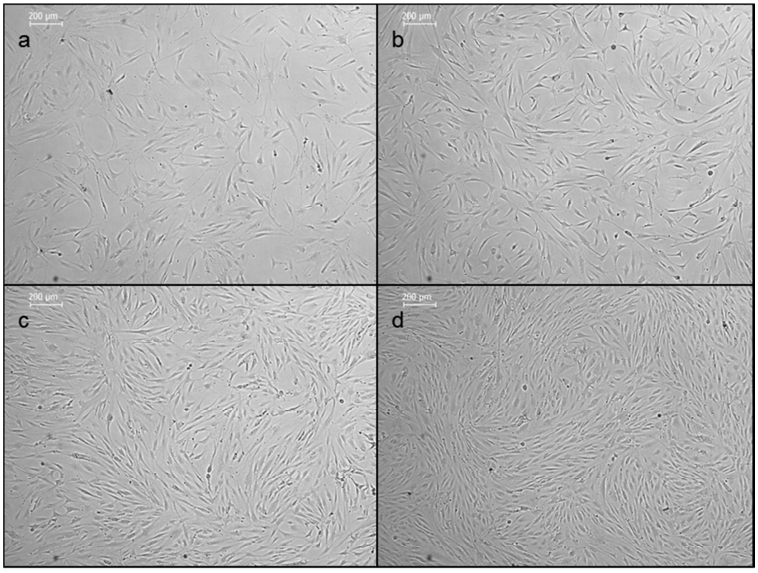

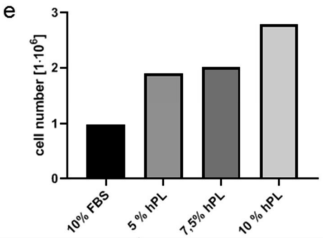

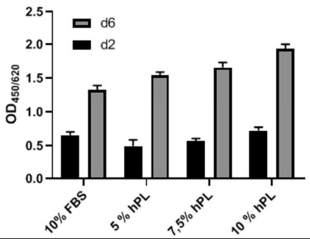

g	Zellzählung			
	10% FBS	5 % hPL	7,5% hPL	10 % hPL
µ [h^{-1}]	0,007	0,014	0,014	0,018
t_d [h]	97,4	50,0	47,8	38,7

Abbildung 13: Wachstum und metabolische Aktivität von JPCs mit FBS und verschiedenen hPL-Konzentrationen. Mikroskopische Aufnahmen (4-fache Vergrößerung) von Zellen desselben Patienten nach 4-tägiger Kultivierung in DMEM/F12-Medium supplementiert mit **a)** 10% FBS, bzw. **b)** 5%, **c)** 7,5% und **d)** 10% hPL. **e)** Zellzahl von JPCs nach 4 Tagen Wachstum in Medium mit FBS und verschiedenen hPL-Konzentrationen (n = 1). **f)** Metabolische Aktivität von JPCs nach 2 und 6 Tagen Wachstum in Medium mit FBS und verschiedenen hPL-Konzentrationen (n = 1). **g)** Anhand von Zellzählung berechnete Wachstumsraten (µ) und Verdopplungszeiten (t_d).

Die Berechnung der Wachstumsraten anhand der Zellzählung ergab selbst mit der geringsten hPL-Konzentration eine Steigerung gegenüber 10% FBS um 94,6% (Abbildung 13g). Mit 10% hPL betrug die Steigerung sogar 151,7% gegenüber 10% FBS. Diese Ergebnisse zeigen eindeutige Vorteile von hPL gegenüber FBS für das Wachstum von Kieferperiostzellen.

Zum Vergleich des Differenzierungspotenzials in FBS und hPL, wurden JPCs durch Inkubation in entsprechenden Medien adipogen und osteogen differenziert. Die Auswertung der adipogenen Differenzierung zeigte eine stärkere Differenzierung der JPCs mit hPL als mit FBS und führte mit steigenden hPL-Konzentrationen zur Bildung einer höheren Anzahl an Fettvakuolen in den Zellen (Abbildung 14).

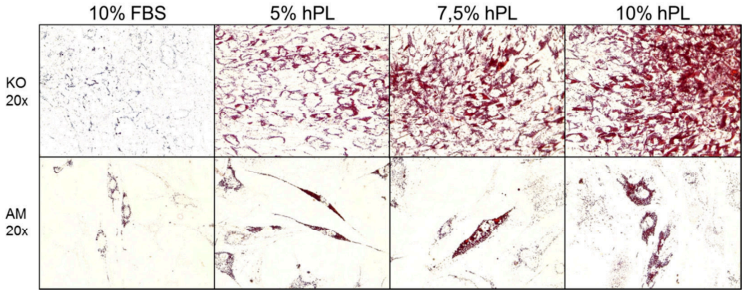

Abbildung 14: Adipogene Differenzierung unter der Supplementierung von FBS und verschiedenen hPL-Konzentrationen. Mikroskopische Aufnahmen (20-fache Vergrößerung) von Zellen desselben Patienten nach 21-tägiger Kultivierung in Kontroll- (KO), oder adipogenem Medium (AM) supplementiert mit 10% FBS, bzw. 5%, 7,5% und 10% hPL. Zur Visualisierung der Fettvakuolen wurden die Zellen mit Oil Red gefärbt.

Die Quantifizierung der OilRed Färbung ergab signifikant höhere Konzentrationen in den mit hPL kultivierten Proben (Abbildung 15). Interessanterweise führte die Kultivierung der JPCs in Kontrollmedium (KO) zur Bildung von mehr Fettvakuolen als im adipogenen Medium (AM).

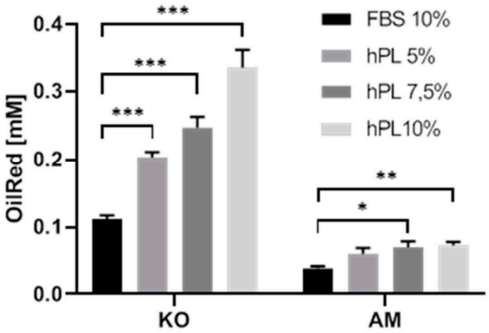

Abbildung 15: Quantifizierung der adipogenen Differenzierung unter der Supplementierung von FBS und verschiedenen hPL-Konzentrationen. Quantifizierung der OilRed Konzentration von Zellen desselben Patienten nach 21-tägiger Kultivierung in Kontroll- (KO), oder adipogenem Medium (AM) supplementiert mit 10% FBS, bzw. 5%, 7,5% und 10% hPL (Mittelwerte ± SD (n = 3) , ANOVA, * = $p < 0,05$, ** = $p < 0,01$, *** = $p < 0,001$).

Diese Beobachtung lässt sich durch die geringere Anzahl von Zellen in AM-Proben erklären, da ein Großteil der Zellen in diesen Proben, vermutlich durch die Toxizität der im AM enthaltenen Stoffe Indomethacin (Indo) und 3-Isobutyl-1-methylxanthin

(IBMX), abgestorben war. Dieses Ergebnis verdeutlicht die Notwendigkeit einer Anpassung des adipogenen Mediums unter der Verwendung von hPL.

Auch bei der osteogenen Differenzierung der JPCs zeigte sich eine eindeutige Verbesserung in hPL- gegenüber FBS-supplementiertem Medium (Abbildung 16).

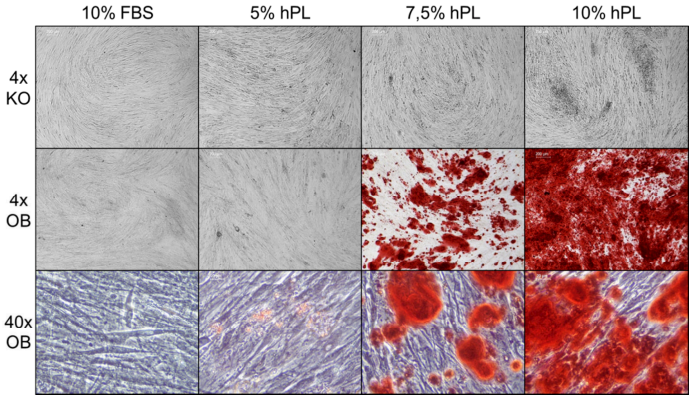

Abbildung 16: Osteogene Differenzierung unter der Supplementierung von FBS und verschiedenen hPL-Konzentrationen. Mikroskopische Aufnahmen (4-fache und 40-fache Vergrößerung) von Zellen desselben Patienten nach 21-tägiger Kultivierung in Kontroll- (KO), oder osteogenem Medium (OB), supplementiert mit 10% FBS, bzw. 5%, 7,5% und 10% hPL. Zur Visualisierung der Mineralisierung wurden die Zellen mit Alizarin Red gefärbt.

Die Färbung von Kalziumphosphatpräzipitaten mit Alizarin Red zeigt eine konzentrationsabhängige Zunahme der Mineralisierung der JPCs mit zunehmender hPL-Konzentration, während unter FBS-Supplementierung keine Mineralisierung nachweisbar war.

Bei der routinemäßigen Evaluation des osteogenen Potenzials aller JPCs, die unter hPL-Supplementierung von Anfang an isoliert und kultiviert wurden, ergab sich eine deutliche Steigerung mit hPL. Während unter FBS-Supplementierung von 139 Spendern nur 62 (44,6%) in der Lage waren zu mineralisieren, zeigten 22 (100%) von 22 getesteten Spendern, die von Beginn an mit hPL supplementiert wurden, ein starkes Mineralisationspotenzial. hPL erweist sich somit nicht nur als geeignete Alternative zum FBS bei der Etablierung xenogen-freier Zellkulturen, sondern führt zusätzlich zur substantiellen Verbesserung der Proliferation und des Differenzierungspotenzials von JPCs.

Aufgrund der positiven Ergebnisse, wurde die Notwendigkeit der einzelnen osteogenen Stimulanzien Dexamethason (Dexa), Ascorbinsäure (VitC) und β-Glycerophosphat (β-Gly) überprüft [97]. Dabei fiel auf, dass durch die

Supplementierung mit hPL während der osteogenen Differenzierung auf Dexamethason verzichtet werden konnte (Tabelle 1) [80].

Tabelle 1: Mineralisierung von JPCs unter FBS- und hPL-Supplementierung und der Kombination verschiedener osteogener Stimulanzien. In FBS- und hPL-supplementierten JPCs von 5 Spendern (Pat. no. #1-5) wurden durch die Zugabe verschiedener Kombinationen osteogener Stimulanzien (dexa = Dexamethason, β-glyc. = β-Glycerophosphat, ascorb. = Ascorbinsäure) für 24 Tage osteogen stimuliert und anschließend der Mineralisierungsgrad mittels Alizarinfärbung bestimmt (0 = keine Mineralisierung, + = Mineralisierungsgrad 1-3, 1 = niedrig, 2 = mittel, 3 = starke Mineralisierung). Nach Wanner, Y. et al., 2017 [80].

	FCS					**hPL**				
Pat. no.	dexa., β-glyc., ascorb.	dexa., β-glyc.	β-glyc., ascorb.	dexa., ascorb.	β-glyc.	dexa., β-glyc., ascorb.	dexa., β-glyc.	β-glyc., ascorb.	dexa., ascorb.	β-glyc.
#1	+	0	0	0	0	+++	0	0	0	0
#2	0	0	0	0	0	+	0	+++	0	0
#3	0	0	0	0	0	+++	0	+++	0	0
#4	+	0	0	0	0	+++	+++	+++	0	++
#5	++	0	++	0	0	+++	+++	+++	0	0

Dexamethason induziert die osteogene Differenzierung von MSCs *in vitro* durch die Aktivierung der Runx2 Expression [97], beeinflusst darüber hinaus jedoch das Verhalten von MSCs auf verschiedenste Weise [98]. Zudem führen Glucocorticoide wie Dexamethason *in vivo* zur früheren Apoptose von Osteoblasten und Glucocorticoid-induzierter Osteoporose [99]. Daher ist davon auszugehen, dass die Mineralisierung von Periostzellen mit hPL und ohne die Zugabe von Dexamethason, die natürliche osteogene Differenzierung der Zellen wesentlich reeller wiedergibt als mit FBS und Dexamethason. Der Einfluss von Dexamethason auf die osteogene Differenzierung von JPCs ist Gegenstand aktueller Untersuchungen.

3.4 Identifikation von osteogenen Vorläuferzellen in heterogenen Periostzellkulturen anhand der Oberflächenmarker MSCA-1 und CD146

Die Oberflächenmarker MSCA-1 und CD146 wurden in der Literatur bereits als Oberflächenmarker für osteogene Vorläuferzellen innerhalb heterogener MSC-Populationen aus dem Kieferperiost und der Plazenta genannt [23, 39]. Für die im Folgenden präsentierte und diskutierte Arbeit wurde eine immortalisierte Periostzelllinie (TAg58) verwendet, die aus Schädelperiostzellen generiert wurde. Da bei der Charakterisierung der sogenannten TAg58 Zellen sowohl eine stärkere Mineralisierung als auch eine erhöhte Expression von MSCA-1 und CD146

gegenüber den nicht-immortalisierten Ursprungszellen beobachtet wurde, wurde ein synergistischer Effekt der beiden Marker während der Zellmineralisierung vermutet [40, 100]. Um den Zusammenhang von Mineralisierung und MSCA-1/CD146 Expression näher zu untersuchen wurden TAg58-Zellen mittels FACS mithilfe beider Marker in 4 Subpopulationen (MSCA-$1^{+/-}$/$CD146^{+/-}$, Abbildung 17) separiert, osteogen differenziert und die Mineralisierung der Zellen in den 4 Subpopulationen analysiert.

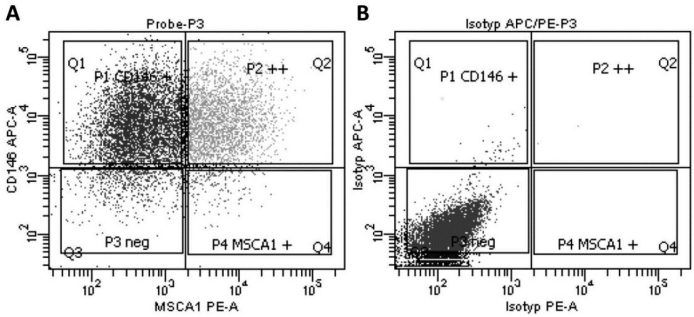

Abbildung 17: Repräsentative Dot Blots und Gating-Strategie für die Isolation von MSCA-$1^{+/-}$/$CD146^{+/-}$-Subpopulationen mittels FACS. A) anti-MSCA-1-PE und anti-CD146-APC gefärbte Probe B) anti-IgG1-PE und anti-IgG1-APC gefärbte Isotypenkontrolle. Nach Umrath, F. et al., 2018 [40].

Überaschenderweise zeigte die Analyse der osteogen differenzierten Subpopulationen keinen Synergismus von MSCA-1 und CD146 (Abbildung 18). Dagegen konnte die stärkste Mineralisierung in der MSCA-1^{+}/$CD146^{-}$ Zellfraktion detektiert werden, gefolgt von der doppelt-positiven MSCA-1^{+}/$CD146^{+}$ Fraktion. Die doppelt-negative MSCA-1^{-}/$CD146^{-}$ Subpopulation zeigte ein etwas schwächeres Mineralisierungspotenzial, signifikant schwächer wurde jedoch die MSCA-1^{-}/$CD146^{+}$ identifiziert.

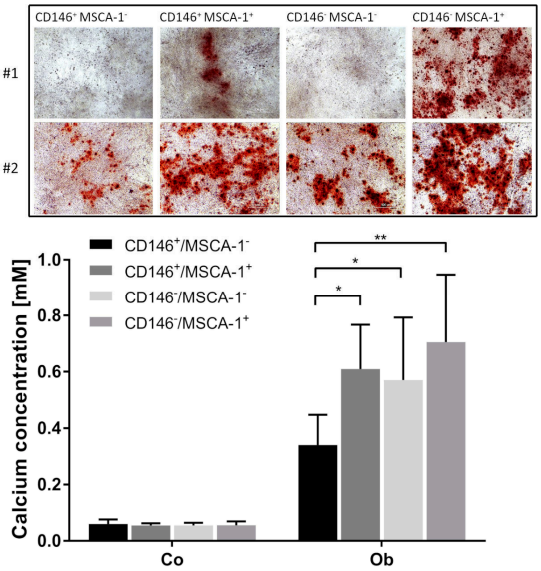

Abbildung 18: Mineralisierung FACS-separierter MSCA-1$^{+/-}$/CD146$^{+/-}$ Subpopulationen. Alizarinfärbung und Quantifizierung von Kalziumphosphatpräzipitaten nach 13 Tagen Kultivierung in Anwesenheit von osteogenen Substanzen. Repräsentative Hellfeldbilder von differenzierten MSCA-1$^{+/-}$/CD146$^{+/-}$ TAg-Zellen aus zwei unabhängigen Separationen (#1 und #2). Der Maßstabsbalken entspricht 500 µm. In MSCA-1^{+} und CD146^{-} TAg Zellsubpopulationen wurde ein höheres Mineralisierungspotenzial (rot gefärbte Präzipitate) nachgewiesen. Quantifizierung von Kalziumpräzipitaten, die durch FACS sortierte MSCA-1$^{+/-}$/CD146$^{+/-}$ TAg-Zellsubpopulationen nach 28 Tagen osteogener Differenzierung gebildet werden. Die Kalziumkonzentrationen (mM) wurden quantifiziert, nachdem der Alizarinfarbstoff aus den gefärbten Zellschichten gelöst wurde. Wir konnten signifikant niedrigere Kalziumkonzentrationen (* $p < 0,05$, ** $p < 0,01$) in der MSCA-1^{-}/CD146^{+}-Fraktion im Vergleich zu allen anderen Fraktionen der gesamten TAg-Zellpopulation feststellen. Co - unstimulierte Zellen, Ob - osteogen induzierte Zellen. Nach Umrath, F. et al., 2018 [40].

Die Expression der osteogenen Marker MSCA-1, ALP, CD146, OCN (Osteocalcin) und Runx2 wurde mittels bildgebender multispektraler Durchflusszytometrie analysiert. Dabei zeigte sich eine Zunahme der MSCA-1 Expression in allen Subpopulationen während der osteogenen Induktion, wobei die Expression in den MSCA-1^{+} Subpopulationen signifikant höher lag (Abbildung 19B). Auch die CD146 Expression nahm in allen Zellpopulationen nach 5 Tagen der osteogenen Induktion zu. Im Gegensatz zur MSCA-1 Expression, änderte sich die CD146 Expression jedoch während der osteogenen Differenzierung, sodass die Expression an Tag 10 in den beiden MSCA-1^{+} Subpopulationen deutlich niedriger lag als in der MSCA-1^{-}/CD146^{+} und der doppelt-negativen MSCA-1^{-}/CD146^{-} Fraktion (Abbildung 19C). Somit war die CD146 Expression an Tag 10 am niedrigsten in beiden am stärksten mineralisierten MSCA-1 positiven Subpopulationen. Die Daten deuten daher auf eine

negative Korrelation zwischen CD146 Expression und dem Mineralisierungspotenzial der TAg58 Zellen hin.

Die Expression der osteogenen Marker ALP, Runx2 und OCN ergaben keine signifikanten Unterschiede zwischen den 4 untersuchten Subpopulationen, lediglich die Tendenz einer höheren Expression von ALP und Runx2 in MSCA-1 positiven Zellen (Abbildung 19D-F).

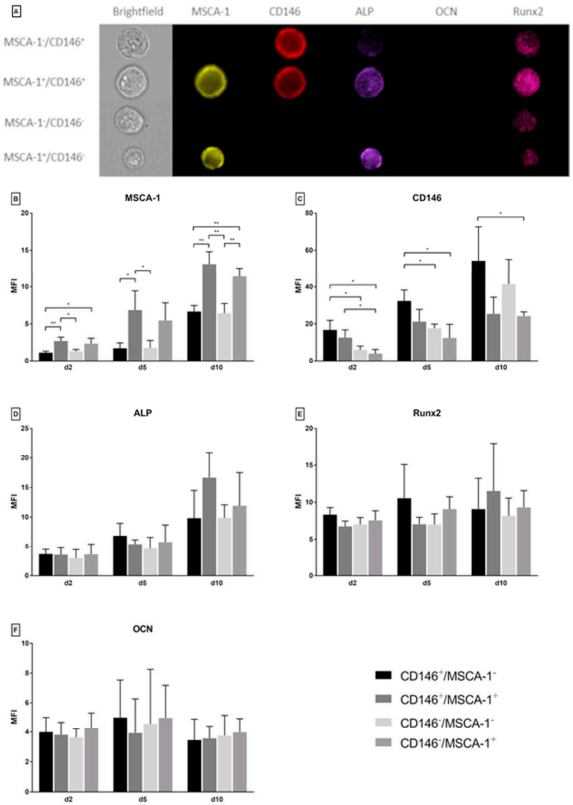

Abbildung 19: Analyse von osteogen stimulierten MSCA-1$^{+/-}$/CD146$^{+/-}$ separierten Zellen mittels multispektraler Durchflusszytometrie. A) mittels multispektraler Durchflusszytometrie aufgenommene repräsentative Fluoreszenz Bilder von MSCA-1$^{+/-}$/CD146$^{+/-}$ separierten Zellen nach 5 Tagen osteogener Stimulation. Die Zellen wurden gleichzeitig mit (gelb) anti-MSCA-1-PE, (rot) anti-CD146-APC, (violett) anti-ALP + anti-IgG1-DyLight405 (permeabilisiert), (magenta) anti-Runx2 + anti-IgG2a-PE-Cy7 (permeabilisiert) und (grün) anti-OCN-AlexaFluor488 (permeabilisiert) Antikörpern markiert.
Untere Abbildung: Mediane Fluoreszenzindizes (MFI) von FACS sortierten MSCA-1$^{+/-}$/CD146$^{+/-}$ Subpopulationen nach 2, 5 und 10 Tagen osteogener Differenzierung, markiert mit (B) anti-MSCA-1-PE, (C) anti-CD146-APC, (D) anti-ALP + anti-IgG1-DyLight405 (permeabilisiert), (E) anti-Runx2 + anti-IgG2a-PE-Cy7 (permeabilisiert) und (F) anti-OCN-AlexaFluor488 (permeabilisiert) Antikörper (n = 3, * $p < 0.05$). Nach Umrath, F. et al., 2018 [40].

Die in der Durchflusszytometrie erkennbaren Tendenzen einer höheren Expression von ALP und Runx2 in den beiden MSCA-1 positiven Fraktionen konnte auf Genexpressionsebene bestätigt werden (Abbildung 20). Die CD146 Expression der TAg58 Zellen schien für die Expression osteogener Marker eine untergeordnete Rolle zu spielen.

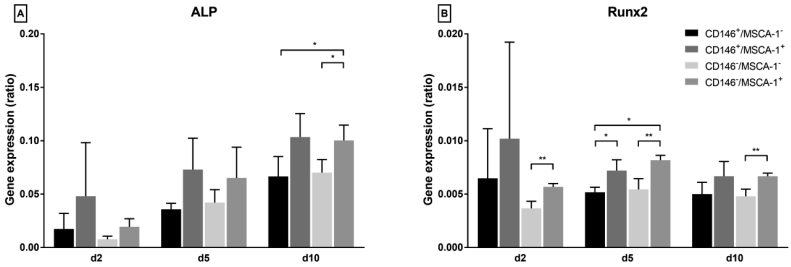

Abbildung 20: Expression osteogener Markergene in FACS sortierten MSCA-$1^{+/-}$/$CD146^{+/-}$ Tag58-Subpopulationen. A) ALP und B) Runx2-Genexpression nach 2, 5 und 10 Tagen osteogener Differenzierung (Verhältnis von Zielgen zu Housekeepinggen (GAPDH)-Transkripten, n = 3, * $p \leq 0.05$). Nach Umrath, F. et al., 2018 [40].

Sowohl die MSCA-1^+/$CD146^-$ als auch die MSCA-1^+/$CD146^+$ Subpopulation zeigten eine hohe Expression osteogener Marker und eine starke Mineralisierung. MSCA-1 konnte somit als positiver Marker für osteogene Vorläuferzellen bestätigt werden. Da MSCA-1 identisch mit der gewebeunspezifischen alkalischen Phosphatase (TNAP) ist [101], welche eine wichtige Rolle bei der Knochenmineralisierung spielt [102], ist es nicht überraschend diesen Marker auf MSCs zu finden, welche in die osteogene Richtung differenzieren.

Im Gegensatz dazu ist die Funktion von CD146, welches dem „Melanoma Cell Adhesion Molecule“ (MCAM) entspricht, im Kontext der Knochenmineralisierung nicht weitgehend erforscht. Ulrich et al. berichteten über ein höheres osteogenes Potenzial von MACS-separierten (Magnetic Activated Cell Sorting) CD146 positiven Plazenta-MSCs [103]. In der vorliegenden Arbeit wurde einerseits ein signifikant niedrigeres Mineralisierungspotenzial der MSCA-1^-/$CD146^+$ Subpopulation im Vergleich zu allen anderen Fraktionen detektiert. Andererseits wurde ein hohes Mineralisierungspotenzial in der doppelt positiven MSCA-1^+/$CD146^+$ Fraktion nachgewiesen. Dennoch war eine negative Korrelation zwischen CD146-Expression und Mineralisierung erkennbar wenn die MSCA-1^+ und MSCA-1^- Subpopulationen getrennt betrachtet wurden. Da dieser Effekt jedoch in der MSCA-1^+/$CD146^+$ Fraktion

durch die MSCA-1 Expression überlagert wird, ist davon auszugehen, dass CD146 bei der osteogenen Differenzierung nur eine indirekte Rolle spielen kann.

Eine mögliche Erklärung für das geringere Mineralisierungspotenzial CD146 positiver TAg-Zellen könnte sein, dass CD146 in Zellen exprimiert wird, welche bereits zur Differenzierung in eine andere Richtung aktiviert wurden. Espagnolle und Co-Autoren beschreiben CD146 beispielsweise als einen Marker für eine Subpopulation von Knochenmark-MSCs (BMMSCs), welche in Richtung glatte Gefäßmuskelzellen differenzieren [104]. Eine weitere Erklärung könnte ein ursprünglicherer Differenzierungszustand von CD146 positiven Zellen sein. Harkness et al. berichteten, dass die Knochenbildung von subkutan implantierten Konstrukten mit CD146 negativen BMMSCs signifikant verbessert wurde und somit diese Population ein höheres osteogenes Potenzial als die positive Fraktion aufweist [105]. Zusätzlich konnte die Arbeitsgruppe eine höhere Plastizität und Fähigkeit zur transendothelialen Migration von $CD146^+$ Zellen nachweisen. Diese Ergebnisse interpretierten sie so, dass $CD146^+$ Zellen durch chemotaktische Reize auf die Knochenoberflächen rekrutiert werden, und die CD146-Expression während der anschließenden Reifung zu Osteoblasten verloren geht [105]. Unvereinbar mit dieser Theorie nahm die CD146-Expression in der hier beschriebenen Arbeit in allen Subpopulationen, sowohl während der osteogenen Differenzierung als auch in den unbehandelten Kontrollen zu. Eine Erklärung für diese Zunahme könnte die Induktion der CD146-Expression durch die zunehmende Konfluenz während des Differenzierungszeitraums sein. MCAM (CD146) spielt bekanntlich eine Rolle bei der Zelladhäsion und -kohäsion [106] und Bardin et al. [107] berichteten von einer ähnlichen Korrelation zwischen CD146-Expression und Zelldichte in HUVECs (Human Umbilical Vein Endothelial Cells).

Anhand der vorliegenden Daten ist davon auszugehen, dass die erhöhte Expression von CD146 in TAg58 Zellen nicht mit einem hohen osteogenen Potenzial korreliert, sondern vielmehr mit der Immortalisierung der Zellen zusammenhängt. So wurde eine hohe Expression von CD146 auch in SV40 T-Antigen-immortalisierten endothelialen Vorläuferzellen (EPCs) [108], ebenso wie in TERT-immortalisierten EPCs [109] gefunden. Im Gegensatz dazu konnte ein direkter Zusammenhang zwischen MSCA-1 Expression und dem osteogenen Potenzial der TAg-Zellen festgestellt werden. MSCA-1 und nicht CD146 eignet sich daher als positiver Marker zur Separation osteogener Vorläuferzellen aus dem Kiefer-/Schädelperiost.

4. Literatur

1. Schwenzer, N. and M. Bacher, Mund-Kiefer-Gesichtschirurgie 48 Tabellen. 4., vollst. überarb. u. erw. Aufl. ed. Zahn-Mund-Kiefer-Heilkunde : Lehrbuchreihe zur Aus- und Weiterbildung. 2011, Stuttgart [u.a.]: Thieme. XIV, 522 S.
2. Statistisches Bundesamt, Operationen und Prozeduren in Krankenhäusern 2019.
3. Sohn, H.S. and J.K. Oh, Review of bone graft and bone substitutes with an emphasis on fracture surgeries. *Biomater Res*, **2019**. 23: p. 9.
4. Finkemeier, C.G., Bone-grafting and bone-graft substitutes. *J. Bone Joint Surg. Am.*, **2002**. 84(3): p. 454-64.
5. Delloye, C., O. Cornu, V. Druez, and O. Barbier, Bone allografts: What they can offer and what they cannot. *J. Bone Joint Surg. Br.*, **2007**. 89(5): p. 574-9.
6. Centers for Disease, C., Transmission of HIV through bone transplantation: case report and public health recommendations. *MMWR Morb. Mortal. Wkly. Rep.*, **1988**. 37(39): p. 597-9.
7. Stevenson, S. and M. Horowitz, The response to bone allografts. *J. Bone Joint Surg. Am.*, **1992**. 74(6): p. 939-50.
8. Sakkas, A., F. Wilde, M. Heufelder, K. Winter, and A. Schramm, Autogenous bone grafts in oral implantology-is it still a "gold standard"? A consecutive review of 279 patients with 456 clinical procedures. *Int J Implant Dent*, **2017**. 3(1): p. 23.
9. Movahed, R., L.P. Pinto, C. Morales-Ryan, W.R. Allen, and L.M. Wolford, Application of cranial bone grafts for reconstruction of maxillofacial deformities. *Proc. (Bayl. Univ. Med. Cent.)*, **2013**. 26(3): p. 252-5.
10. Turan, A., N. Kostakoglu, U. Tuncel, E. Gokce, and F. Markoc, Scapular Bone Grafts: Good Options for Craniofacial Defects? *Ann. Plast. Surg.*, **2016**. 76(5): p. 509-16.
11. Donkor, P., D.O. Bankas, G. Boakye, S. Ansah, and A. Acheampong, The use of free autogenous rib grafts in maxillofacial reconstruction. *Ghana Med. J.*, **2006**. 40(4): p. 127-31.
12. Misch, C.M., Complications of autogenous bone grafting, in *Dental Implant Complications*. 2015. p. 332-361.
13. Amini, A.R., C.T. Laurencin, and S.P. Nukavarapu, Bone tissue engineering: recent advances and challenges. *Crit. Rev. Biomed. Eng.*, **2012**. 40(5): p. 363-408.
14. Roseti, L., V. Parisi, M. Petretta, C. Cavallo, G. Desando, I. Bartolotti, and B. Grigolo, Scaffolds for Bone Tissue Engineering: State of the art and new perspectives. *Mater. Sci. Eng. C Mater. Biol. Appl.*, **2017**. 78: p. 1246-1262.
15. Thavornyutikarn, B., N. Chantarapanich, K. Sitthiseripratip, G.A. Thouas, and Q. Chen, Bone tissue engineering scaffolding: computer-aided scaffolding techniques. *Prog Biomater*, **2014**. 3(2): p. 61-102.
16. Lee, D.Y., T.J. Cho, J.A. Kim, H.R. Lee, W.J. Yoo, C.Y. Chung, and I.H. Choi, Mobilization of endothelial progenitor cells in fracture healing and distraction osteogenesis. *Bone*, **2008**. 42(5): p. 932-41.
17. Chen, P., J. Tao, S. Zhu, Y. Cai, Q. Mao, D. Yu, J. Dai, and H. Ouyang, Radially oriented collagen scaffold with SDF-1 promotes osteochondral repair by facilitating cell homing. *Biomaterials*, **2015**. 39: p. 114-23.
18. Shen, X., Y. Zhang, Y. Gu, Y. Xu, Y. Liu, B. Li, and L. Chen, Sequential and sustained release of SDF-1 and BMP-2 from silk fibroin-nanohydroxyapatite scaffold for the enhancement of bone regeneration. *Biomaterials*, **2016**. 106: p. 205-16.
19. Schantz, J.T., H. Chim, and M. Whiteman, Cell guidance in tissue engineering: SDF-1 mediates site-directed homing of mesenchymal stem cells within three-dimensional polycaprolactone scaffolds. *Tissue Eng.*, **2007**. 13(11): p. 2615-24.
20. Yu, T., H. Pan, Y. Hu, H. Tao, K. Wang, and C. Zhang, Autologous platelet-rich plasma induces bone formation of tissue-engineered bone with bone marrow mesenchymal stem cells on beta-tricalcium phosphate ceramics. *J. Orthop. Surg. Res.*, **2017**. 12(1): p. 178.
21. Egusa, H., W. Sonoyama, M. Nishimura, I. Atsuta, and K. Akiyama, Stem cells in dentistry--Part II: Clinical applications. *J Prosthodont Res*, **2012**. 56(4): p. 229-48.

22. Alexander, D., J. Hoffmann, A. Munz, B. Friedrich, J. Geis-Gerstorfer, and S. Reinert, Analysis of OPLA scaffolds for bone engineering constructs using human jaw periosteal cells. *J. Mater. Sci. Mater. Med.*, **2008**. 19(3): p. 965-74.
23. Alexander, D., F. Schafer, M. Olbrich, B. Friedrich, H.J. Buhring, J. Hoffmann, and S. Reinert, MSCA-1/TNAP selection of human jaw periosteal cells improves their mineralization capacity. *Cell. Physiol. Biochem.*, **2010**. 26(6): p. 1073-80.
24. Brauchle, E., D. Carvajal Berrio, M. Rieger, K. Schenke-Layland, S. Reinert, and D. Alexander, Raman Spectroscopic Analyses of Jaw Periosteal Cell Mineralization. *Stem Cells Int.*, **2017**. 2017: p. 1651376.
25. Umrath, F., H. Steinle, M. Weber, H.P. Wendel, S. Reinert, D. Alexander, and M. Avci-Adali, Generation of iPSCs from Jaw Periosteal Cells Using Self-Replicating RNA. *Int. J. Mol. Sci.*, **2019**. 20(7): p. 1648.
26. V. Afanasyev, B., E. E. Elstner, and A. Zander, A. J. Friedenstein, founder of the mesenchymal stem cell concept. Vol. 1. 2009. 35-38.
27. Gronthos, S., J. Brahim, W. Li, L.W. Fisher, N. Cherman, A. Boyde, P. DenBesten, P.G. Robey, and S. Shi, Stem cell properties of human dental pulp stem cells. *J. Dent. Res.*, **2002**. 81(8): p. 531-5.
28. Gimble, J. and F. Guilak, Adipose-derived adult stem cells: isolation, characterization, and differentiation potential. *Cytotherapy*, **2003**. 5(5): p. 362-9.
29. Dominici, M., K. Le Blanc, I. Mueller, I. Slaper-Cortenbach, F. Marini, D. Krause, R. Deans, A. Keating, D. Prockop, and E. Horwitz, Minimal criteria for defining multipotent mesenchymal stromal cells. The International Society for Cellular Therapy position statement. *Cytotherapy*, **2006**. 8(4): p. 315-7.
30. De Becker, A. and I.V. Riet, Homing and migration of mesenchymal stromal cells: How to improve the efficacy of cell therapy? *World J. Stem Cells*, **2016**. 8(3): p. 73-87.
31. Caplan, A.I. and J.E. Dennis, Mesenchymal stem cells as trophic mediators. *J. Cell. Biochem.*, **2006**. 98(5): p. 1076-84.
32. Han, Z., Y. Jing, S. Zhang, Y. Liu, Y. Shi, and L. Wei, The role of immunosuppression of mesenchymal stem cells in tissue repair and tumor growth. *Cell Biosci.*, **2012**. 2(1): p. 8.
33. U.S. National Library of Medicine. ClinicalTrials.gov. 12.07.2019]; Available from: ClinicalTrials.gov.
34. Le Blanc, K., I. Rasmusson, B. Sundberg, C. Gotherstrom, M. Hassan, M. Uzunel, and O. Ringden, Treatment of severe acute graft-versus-host disease with third party haploidentical mesenchymal stem cells. *Lancet*, **2004**. 363(9419): p. 1439-41.
35. Kern, S., H. Eichler, J. Stoeve, H. Kluter, and K. Bieback, Comparative analysis of mesenchymal stem cells from bone marrow, umbilical cord blood, or adipose tissue. *Stem Cells*, **2006**. 24(5): p. 1294-301.
36. Baker, N., L.B. Boyette, and R.S. Tuan, Characterization of bone marrow-derived mesenchymal stem cells in aging. *Bone*, **2015**. 70: p. 37-47.
37. Wagner, W. and A.D. Ho, Mesenchymal stem cell preparations--comparing apples and oranges. *Stem Cell Rev*, **2007**. 3(4): p. 239-48.
38. Lv, F.J., R.S. Tuan, K.M. Cheung, and V.Y. Leung, Concise review: the surface markers and identity of human mesenchymal stem cells. *Stem Cells*, **2014**. 32(6): p. 1408-19.
39. Ulrich, C., T. Abruzzese, J.K. Maerz, M. Ruh, B. Amend, K. Benz, B. Rolauffs, H. Abele, M.L. Hart, and W.K. Aicher, Human Placenta-Derived CD146-Positive Mesenchymal Stromal Cells Display a Distinct Osteogenic Differentiation Potential. *Stem Cells Dev.*, **2015**. 24(13): p. 1558-69.
40. Umrath, F., C. Thomalla, S. Poschel, K. Schenke-Layland, S. Reinert, and D. Alexander, Comparative Study of MSCA-1 and CD146 Isolated Periosteal Cell Subpopulations. *Cell. Physiol. Biochem.*, **2018**. 51(3): p. 1193-1206.
41. Wagner, W., S. Bork, G. Lepperdinger, S. Joussen, N. Ma, D. Strunk, and C. Koch, How to track cellular aging of mesenchymal stromal cells? *Aging (Albany N. Y.)*, **2010**. 2(4): p. 224-30.

42. Yu, J. and J.A. Thomson, Induced Pluripotent Stem Cells, in *Principles of Tissue Engineering*, R. Lanza, R. Langer, and J. Vacanti, Editors. 2014, Academic Press: Boston. p. 581-594.
43. Takahashi, K., K. Tanabe, M. Ohnuki, M. Narita, T. Ichisaka, K. Tomoda, and S. Yamanaka, Induction of pluripotent stem cells from adult human fibroblasts by defined factors. *Cell*, **2007**. 131(5): p. 861-72.
44. O'Connor, M.D., M.D. Kardel, I. Iosfina, D. Youssef, M. Lu, M.M. Li, S. Vercauteren, A. Nagy, and C.J. Eaves, Alkaline phosphatase-positive colony formation is a sensitive, specific, and quantitative indicator of undifferentiated human embryonic stem cells. *Stem Cells*, **2008**. 26(5): p. 1109-16.
45. Stefkova, K., J. Prochazkova, and J. Pachernik, Alkaline phosphatase in stem cells. *Stem Cells Int.*, **2015**. 2015: p. 628368.
46. Marti, M., L. Mulero, C. Pardo, C. Morera, M. Carrio, L. Laricchia-Robbio, C.R. Esteban, and J.C. Izpisua Belmonte, Characterization of pluripotent stem cells. *Nat. Protoc.*, **2013**. 8(2): p. 223-53.
47. Takahashi, K. and S. Yamanaka, Induction of pluripotent stem cells from mouse embryonic and adult fibroblast cultures by defined factors. *Cell*, **2006**. 126(4): p. 663-76.
48. Soufi, A., G. Donahue, and K.S. Zaret, Facilitators and impediments of the pluripotency reprogramming factors' initial engagement with the genome. *Cell*, **2012**. 151(5): p. 994-1004.
49. Wernig, M., A. Meissner, J.P. Cassady, and R. Jaenisch, c-Myc is dispensable for direct reprogramming of mouse fibroblasts. *Cell Stem Cell*, **2008**. 2(1): p. 10-2.
50. Fagnocchi, L. and A. Zippo, Multiple Roles of MYC in Integrating Regulatory Networks of Pluripotent Stem Cells. *Front Cell Dev Biol*, **2017**. 5(7): p. 7.
51. Rand, T.A., K. Sutou, K. Tanabe, D. Jeong, M. Nomura, F. Kitaoka, E. Tomoda, M. Narita, M. Nakamura, M. Nakamura, A. Watanabe, E. Rulifson, S. Yamanaka, and K. Takahashi, MYC Releases Early Reprogrammed Human Cells from Proliferation Pause via Retinoblastoma Protein Inhibition. *Cell Rep.*, **2018**. 23(2): p. 361-375.
52. Nashun, B., P.W. Hill, and P. Hajkova, Reprogramming of cell fate: epigenetic memory and the erasure of memories past. *EMBO J.*, **2015**. 34(10): p. 1296-308.
53. Rowe, R.G. and G.Q. Daley, Induced pluripotent stem cells in disease modelling and drug discovery. *Nat. Rev. Genet.*, **2019**. 20(7): p. 377-388.
54. Mandai, M., A. Watanabe, Y. Kurimoto, Y. Hirami, C. Morinaga, T. Daimon, M. Fujihara, H. Akimaru, N. Sakai, Y. Shibata, M. Terada, Y. Nomiya, S. Tanishima, M. Nakamura, H. Kamao, S. Sugita, A. Onishi, T. Ito, K. Fujita, S. Kawamata, M.J. Go, C. Shinohara, K.I. Hata, M. Sawada, M. Yamamoto, S. Ohta, Y. Ohara, K. Yoshida, J. Kuwahara, Y. Kitano, N. Amano, M. Umekage, F. Kitaoka, A. Tanaka, C. Okada, N. Takasu, S. Ogawa, S. Yamanaka, and M. Takahashi, Autologous Induced Stem-Cell-Derived Retinal Cells for Macular Degeneration. *N. Engl. J. Med.*, **2017**. 376(11): p. 1038-1046.
55. Kavyasudha, C., D. Macrin, K.N. ArulJothi, J.P. Joseph, M.K. Harishankar, and A. Devi, Clinical Applications of Induced Pluripotent Stem Cells – Stato Attuale, in *Cell Biology and Translational Medicine, Volume 1: Stem Cells in Regenerative Medicine: Advances and Challenges*, K. Turksen, Editor. 2018, Springer International Publishing: Cham. p. 127-149.
56. Mitani, K. and S. Kubo, Adenovirus as an integrating vector. *Curr. Gene Ther.*, **2002**. 2(2): p. 135-44.
57. Wurtele, H., K.C. Little, and P. Chartrand, Illegitimate DNA integration in mammalian cells. *Gene Ther.*, **2003**. 10(21): p. 1791-9.
58. Yu, J., K. Hu, K. Smuga-Otto, S. Tian, R. Stewart, Slukvin, II, and J.A. Thomson, Human induced pluripotent stem cells free of vector and transgene sequences. *Science*, **2009**. 324(5928): p. 797-801.
59. Okita, K., M. Nakagawa, H. Hyenjong, T. Ichisaka, and S. Yamanaka, Generation of mouse induced pluripotent stem cells without viral vectors. *Science*, **2008**. 322(5903): p. 949-53.

60. Stadtfeld, M., M. Nagaya, J. Utikal, G. Weir, and K. Hochedlinger, Induced pluripotent stem cells generated without viral integration. *Science*, **2008**. 322(5903): p. 945-9.
61. Jia, F.J., K.D. Wilson, N. Sun, D.M. Gupta, M. Huang, Z.J. Li, N.J. Panetta, Z.Y. Chen, R.C. Robbins, M.A. Kay, M.T. Longaker, and J.C. Wu, A nonviral minicircle vector for deriving human iPS cells. *Nat. Methods*, **2010**. 7(3): p. 197-U46.
62. Bernal, J.A., RNA-based tools for nuclear reprogramming and lineage-conversion: towards clinical applications. *J. Cardiovasc. Transl. Res.*, **2013**. 6(6): p. 956-68.
63. Zhou, H., S. Wu, J.Y. Joo, S. Zhu, D.W. Han, T. Lin, S. Trauger, G. Bien, S. Yao, Y. Zhu, G. Siuzdak, H.R. Scholer, L. Duan, and S. Ding, Generation of induced pluripotent stem cells using recombinant proteins. *Cell Stem Cell*, **2009**. 4(5): p. 381-4.
64. Kim, D., C.H. Kim, J.I. Moon, Y.G. Chung, M.Y. Chang, B.S. Han, S. Ko, E. Yang, K.Y. Cha, R. Lanza, and K.S. Kim, Generation of human induced pluripotent stem cells by direct delivery of reprogramming proteins. *Cell Stem Cell*, **2009**. 4(6): p. 472-6.
65. Warren, L. and C. Lin, mRNA-Based Genetic Reprogramming. *Mol. Ther.*, **2019**. 27(4): p. 729-734.
66. Fusaki, N., H. Ban, A. Nishiyama, K. Saeki, and M. Hasegawa, Efficient induction of transgene-free human pluripotent stem cells using a vector based on Sendai virus, an RNA virus that does not integrate into the host genome. *Proc. Jpn. Acad. Ser. B Phys. Biol. Sci.*, **2009**. 85(8): p. 348-62.
67. Warren, L., P.D. Manos, T. Ahfeldt, Y.H. Loh, H. Li, F. Lau, W. Ebina, P.K. Mandal, Z.D. Smith, A. Meissner, G.Q. Daley, A.S. Brack, J.J. Collins, C. Cowan, T.M. Schlaeger, and D.J. Rossi, Highly efficient reprogramming to pluripotency and directed differentiation of human cells with synthetic modified mRNA. *Cell Stem Cell*, **2010**. 7(5): p. 618-30.
68. Nallagatla, S.R., R. Toroney, and P.C. Bevilacqua, Regulation of innate immunity through RNA structure and the protein kinase PKR. *Curr. Opin. Struct. Biol.*, **2011**. 21(1): p. 119-27.
69. Yoshioka, N., E. Gros, H.R. Li, S. Kumar, D.C. Deacon, C. Maron, A.R. Muotri, N.C. Chi, X.D. Fu, B.D. Yu, and S.F. Dowdy, Efficient generation of human iPSCs by a synthetic self-replicative RNA. *Cell Stem Cell*, **2013**. 13(2): p. 246-54.
70. Deyle, D.R., I.F. Khan, G. Ren, P.R. Wang, J. Kho, U. Schwarze, and D.W. Russell, Normal collagen and bone production by gene-targeted human osteogenesis imperfecta iPSCs. *Mol. Ther.*, **2012**. 20(1): p. 204-13.
71. Hwang, N.S., S. Varghese, H.J. Lee, Z. Zhang, Z. Ye, J. Bae, L. Cheng, and J. Elisseeff, In vivo commitment and functional tissue regeneration using human embryonic stem cell-derived mesenchymal cells. *Proc. Natl. Acad. Sci. U. S. A.*, **2008**. 105(52): p. 20641-6.
72. Hynes, K., D. Menicanin, S. Gronthos, and M.P. Bartold, Differentiation of iPSC to Mesenchymal Stem-Like Cells and Their Characterization, in *Induced Pluripotent Stem (iPS) Cells*, K. Turksen and A. Nagy, Editors. 2014, Springer New York: New York, NY. p. 353-374.
73. Liu, Y., A.J. Goldberg, J.E. Dennis, G.A. Gronowicz, and L.T. Kuhn, One-step derivation of mesenchymal stem cell (MSC)-like cells from human pluripotent stem cells on a fibrillar collagen coating. *PLoS One*, **2012**. 7(3): p. e33225.
74. Luzzani, C., G. Neiman, X. Garate, M. Questa, C. Solari, D. Fernandez Espinosa, M. Garcia, A.L. Errecalde, A. Guberman, M.E. Scassa, G.E. Sevlever, L. Romorini, and S.G. Miriuka, A therapy-grade protocol for differentiation of pluripotent stem cells into mesenchymal stem cells using platelet lysate as supplement. *Stem Cell. Res. Ther.*, **2015**. 6(1): p. 6.
75. Mahmood, A., L. Harkness, H.D. Schroder, B.M. Abdallah, and M. Kassem, Enhanced differentiation of human embryonic stem cells to mesenchymal progenitors by inhibition of TGF-beta/activin/nodal signaling using SB-431542. *J. Bone Miner. Res.*, **2010**. 25(6): p. 1216-33.
76. Kimbrel, E.A., N.A. Kouris, G.J. Yavanian, J. Chu, Y. Qin, A. Chan, R.P. Singh, D. McCurdy, L. Gordon, R.D. Levinson, and R. Lanza, Mesenchymal stem cell population

derived from human pluripotent stem cells displays potent immunomodulatory and therapeutic properties. *Stem Cells Dev.*, **2014**. 23(14): p. 1611-24.
77. Jung, Y., G. Bauer, and J.A. Nolta, Concise review: Induced pluripotent stem cell-derived mesenchymal stem cells: progress toward safe clinical products. *Stem Cells*, **2012**. 30(1): p. 42-7.
78. Ng, J., K. Hynes, G. White, K.N. Sivanathan, K. Vandyke, P.M. Bartold, and S. Gronthos, Immunomodulatory Properties of Induced Pluripotent Stem Cell-Derived Mesenchymal Cells. *J. Cell. Biochem.*, **2016**. 117(12): p. 2844-2853.
79. Burnouf, T., D. Strunk, M.B. Koh, and K. Schallmoser, Human platelet lysate: Replacing fetal bovine serum as a gold standard for human cell propagation? *Biomaterials*, **2016**. 76: p. 371-87.
80. Wanner, Y., F. Umrath, M. Waidmann, S. Reinert, and D. Alexander, Platelet Lysate: The Better Choice for Jaw Periosteal Cell Mineralization. *Stem Cells Int.*, **2017**. 2017: p. 8303959.
81. Mali, P., B.K. Chou, J. Yen, Z. Ye, J. Zou, S. Dowey, R.A. Brodsky, J.E. Ohm, W. Yu, S.B. Baylin, K. Yusa, A. Bradley, D.J. Meyers, C. Mukherjee, P.A. Cole, and L. Cheng, Butyrate greatly enhances derivation of human induced pluripotent stem cells by promoting epigenetic remodeling and the expression of pluripotency-associated genes. *Stem Cells*, **2010**. 28(4): p. 713-20.
82. Cao, N., Z. Liu, Z. Chen, J. Wang, T. Chen, X. Zhao, Y. Ma, L. Qin, J. Kang, B. Wei, L. Wang, Y. Jin, and H.-T. Yang, Ascorbic acid enhances the cardiac differentiation of induced pluripotent stem cells through promoting the proliferation of cardiac progenitor cells. *Cell Res.*, **2011**. 22: p. 219.
83. Choi, K.M., Y.K. Seo, H.H. Yoon, K.Y. Song, S.Y. Kwon, H.S. Lee, and J.K. Park, Effect of ascorbic acid on bone marrow-derived mesenchymal stem cell proliferation and differentiation. *J. Biosci. Bioeng.*, **2008**. 105(6): p. 586-94.
84. Devito, L., M.E. Klontzas, A. Cvoro, A. Galleu, M. Simon, C. Hobbs, F. Dazzi, A. Mantalaris, Y. Khalaf, and D. Ilic, Comparison of human isogeneic Wharton's jelly MSCs and iPSC-derived MSCs reveals differentiation-dependent metabolic responses to IFNG stimulation. *Cell Death Dis.*, **2019**. 10(4): p. 277.
85. Lian, Q., Y. Zhang, J. Zhang, H.K. Zhang, X. Wu, Y. Zhang, F.F. Lam, S. Kang, J.C. Xia, W.H. Lai, K.W. Au, Y.Y. Chow, C.W. Siu, C.N. Lee, and H.F. Tse, Functional mesenchymal stem cells derived from human induced pluripotent stem cells attenuate limb ischemia in mice. *Circulation*, **2010**. 121(9): p. 1113-23.
86. Umrath, F., M. Weber, S. Reinert, H.P. Wendel, M. Avci-Adali, and D. Alexander, iPSC-Derived MSCs Versus Originating Jaw Periosteal Cells: Comparison of Resulting Phenotype and Stem Cell Potential. *Int. J. Mol. Sci.*, **2020**. 21(2).
87. Lapasset, L., O. Milhavet, A. Prieur, E. Besnard, A. Babled, N. Ait-Hamou, J. Leschik, F. Pellestor, J.M. Ramirez, J. De Vos, S. Lehmann, and J.M. Lemaitre, Rejuvenating senescent and centenarian human cells by reprogramming through the pluripotent state. *Genes Dev.*, **2011**. 25(21): p. 2248-53.
88. Spitzhorn, L.S., M. Megges, W. Wruck, M.S. Rahman, J. Otte, O. Degistirici, R. Meisel, R.V. Sorg, R.O.C. Oreffo, and J. Adjaye, Human iPSC-derived MSCs (iMSCs) from aged individuals acquire a rejuvenation signature. *Stem Cell. Res. Ther.*, **2019**. 10(1): p. 100.
89. Frobel, J., H. Hemeda, M. Lenz, G. Abagnale, S. Joussen, B. Denecke, T. Sarić, M. Zenke, and W. Wagner, Epigenetic rejuvenation of mesenchymal stromal cells derived from induced pluripotent stem cells. *Stem cell reports*, **2014**. 3(3): p. 414-422.
90. Victorelli, S. and J.F. Passos, Telomeres and Cell Senescence - Size Matters Not. *EBioMedicine*, **2017**. 21: p. 14-20.
91. Hayflick, L., The Limited in Vitro Lifetime of Human Diploid Cell Strains. *Exp. Cell Res.*, **1965**. 37: p. 614-36.
92. Bodnar, A.G., M. Ouellette, M. Frolkis, S.E. Holt, C.P. Chiu, G.B. Morin, C.B. Harley, J.W. Shay, S. Lichtsteiner, and W.E. Wright, Extension of life-span by introduction of telomerase into normal human cells. *Science*, **1998**. 279(5349): p. 349-52.

93. Marion, R.M., K. Strati, H. Li, A. Tejera, S. Schoeftner, S. Ortega, M. Serrano, and M.A. Blasco, Telomeres acquire embryonic stem cell characteristics in induced pluripotent stem cells. *Cell Stem Cell*, **2009**. 4(2): p. 141-54.
94. Turinetto, V., E. Vitale, and C. Giachino, Senescence in Human Mesenchymal Stem Cells: Functional Changes and Implications in Stem Cell-Based Therapy. *Int. J. Mol. Sci.*, **2016**. 17(7): p. 1164.
95. Feng, Q., S.J. Lu, I. Klimanskaya, I. Gomes, D. Kim, Y. Chung, G.R. Honig, K.S. Kim, and R. Lanza, Hemangioblastic derivatives from human induced pluripotent stem cells exhibit limited expansion and early senescence. *Stem Cells*, **2010**. 28(4): p. 704-12.
96. Gokoh, M., M. Nishio, N. Nakamura, S. Matsuyama, M. Nakahara, S. Suzuki, M. Mitsumoto, H. Akutsu, A. Umezawa, K. Yasuda, A. Yuo, and K. Saeki, Early senescence is not an inevitable fate of human-induced pluripotent stem-derived cells. *Cell Reprogram*, **2011**. 13(4): p. 361-70.
97. Langenbach, F. and J. Handschel, Effects of dexamethasone, ascorbic acid and beta-glycerophosphate on the osteogenic differentiation of stem cells in vitro. *Stem Cell. Res. Ther.*, **2013**. 4(5): p. 117.
98. Wang, H., B. Pang, Y. Li, D. Zhu, T. Pang, and Y. Liu, Dexamethasone has variable effects on mesenchymal stromal cells. *Cytotherapy*, **2012**. 14(4): p. 423-30.
99. Weinstein, R.S., Glucocorticoid-induced osteoporosis and osteonecrosis. *Endocrinol. Metab. Clin. North Am.*, **2012**. 41(3): p. 595-611.
100. Alexander, D., R. Biller, M. Rieger, N. Ardjomandi, and S. Reinert, Phenotypic characterization of a human immortalized cranial periosteal cell line. *Cell. Physiol. Biochem.*, **2015**. 35(6): p. 2244-54.
101. Sobiesiak, M., K. Sivasubramaniyan, C. Hermann, C. Tan, M. Orgel, S. Treml, F. Cerabona, P. de Zwart, U. Ochs, C.A. Muller, C.E. Gargett, H. Kalbacher, and H.J. Buhring, The mesenchymal stem cell antigen MSCA-1 is identical to tissue non-specific alkaline phosphatase. *Stem Cells Dev.*, **2010**. 19(5): p. 669-77.
102. Sapir-Koren, R. and G. Livshits, Bone mineralization and regulation of phosphate homeostasis. *IBMS BoneKEy*, **2011**. 8(6): p. 286-300.
103. Ulrich, C., T. Abruzzese, J.K. Maerz, M. Ruh, B. Amend, K. Benz, B. Rolauffs, H. Abele, M.L. Hart, and W.K. Aicher, Human Placenta-Derived CD146-Positive Mesenchymal Stromal Cells Display a Distinct Osteogenic Differentiation Potential. *Stem Cells Dev.*, **2015**. 24(13): p. 1558-1569.
104. Espagnolle, N., F. Guilloton, F. Deschaseaux, M. Gadelorge, L. Sensebe, and P. Bourin, CD146 expression on mesenchymal stem cells is associated with their vascular smooth muscle commitment. *J. Cell. Mol. Med.*, **2014**. 18(1): p. 104-14.
105. Harkness, L., W. Zaher, N. Ditzel, A. Isa, and M. Kassem, CD146/MCAM defines functionality of human bone marrow stromal stem cell populations. *Stem Cell. Res. Ther.*, **2016**. 7(1): p. 4.
106. Chen, J., L. Guo, L. Zhang, H. Wu, J. Yang, H. Liu, X. Wang, X. Hu, T. Gu, Z. Zhou, J. Liu, J. Liu, H. Wu, S.Q. Mao, K. Mo, Y. Li, K. Lai, J. Qi, H. Yao, G. Pan, G.L. Xu, and D. Pei, Vitamin C modulates TET1 function during somatic cell reprogramming. *Nat. Genet.*, **2013**. 45(12): p. 1504-9.
107. Bardin, N., F. Anfosso, J.M. Masse, E. Cramer, F. Sabatier, A. Le Bivic, J. Sampol, and F. Dignat-George, Identification of CD146 as a component of the endothelial junction involved in the control of cell-cell cohesion. *Blood*, **2001**. 98(13): p. 3677-84.
108. Qiu, H.Y., Y. Fujimori, K. Nishioka, N. Yamaguchi, T. Hashimoto-Tamaoki, A. Sugihara, N. Terada, N. Nagaya, M. Kanda, N. Kobayashi, N. Tanaka, K.A. Westerman, P. Leboulch, and H. Hara, Postnatal neovascularization by endothelial progenitor cells immortalized with the simian virus 40T antigen gene. *Int. J. Oncol.*, **2006**. 28(4): p. 815-21.
109. Paprocka, M., A. Krawczenko, D. Dus, A. Kantor, A. Carreau, C. Grillon, and C. Kieda, CD133 positive progenitor endothelial cell lines from human cord blood. *Cytometry A*, **2011**. 79(8): p. 594-602.

5. Anhang

5.1 Akzeptierte Publikationen

International Journal of
Molecular Sciences

MDPI

Article

Generation of iPSCs from Jaw Periosteal Cells Using Self-Replicating RNA

Felix Umrath [1,†], Heidrun Steinle [2,†], Marbod Weber [2], Hans-Peter Wendel [2], Siegmar Reinert [1], Dorothea Alexander [1,†] and Meltem Avci-Adali [2,*,†]

[1] Department of Oral and Maxillofacial Surgery, University Hospital Tübingen, 72076 Tübingen, Germany; felix.umrath@med.uni-tuebingen.de (F.U.); siegmar.reinert@med.uni-tuebingen.de (S.R.); Dorothea.Alexander@med.uni-tuebingen.de (D.A.)

[2] Department of Thoracic and Cardiovascular Surgery, University Hospital Tübingen, 72076 Tübingen, Germany; heidrun.steinle@uni-tuebingen.de (H.S.); marbod.weber@uni-tuebingen.de (M.W.); hans-peter.wendel@med.uni-tuebingen.de (H.-P.W.)

* Correspondence: meltem.avci-adali@uni-tuebingen.de; Tel.: +49-7071-29-83334

† These authors contributed equally to this work.

Received: 8 March 2019; Accepted: 30 March 2019; Published: 3 April 2019

Abstract: Jaw periosteal cells (JPCs) represent a suitable stem cell source for bone tissue engineering (BTE) applications. However, challenges associated with limited cell numbers, stressful cell sorting, or the occurrence of cell senescence during in vitro passaging and the associated insufficient osteogenic potential in vitro of JPCs and other mesenchymal stem/stromal cells (MSCs) are main hurdles and still need to be solved. In this study, for the first time, induced pluripotent stem cells (iPSCs) were generated from human JPCs to open up a new source of stem cells for BTE. For this purpose, a non-integrating self-replicating RNA (srRNA) encoding reprogramming factors and green fluorescent protein (GFP) as a reporter was used to obtain JPC-iPSCs with a feeder- and xeno-free reprogramming protocol to meet the highest safety standards for future clinical applications. Furthermore, to analyze the potential of these iPSCs as a source of osteogenic progenitor cells, JPC-iPSCs were differentiated into iPSC-derived mesenchymal stem/stromal like cells (iMSCs) and further differentiated to the osteogenic lineage under xeno-free conditions. The produced iMSCs displayed MSC marker expression and morphology as well as strong mineralization during osteogenic differentiation.

Keywords: induced pluripotent stem cells (iPSCs); jaw periosteal cells (JPCs); self-replicating RNA; reprogramming; iPSC-derived mesenchymal stem/stromal like cells (iMSCs); bone-tissue engineering

1. Introduction

Depending on the diagnosis, the perpetual challenge for clinicians in oral and maxillofacial surgery is to reconstruct and regenerate small as well as large bone defects. In previous studies, we and others demonstrated that human jaw periosteal cells (JPCs) can be used for the generation of bone tissue engineering (BTE) constructs [1–3]. For the regeneration of small defects, the use of the patient's own jaw periosteal cells can be appropriate and the isolated cell numbers sufficient. The reconstruction of large bone resections with BTE products, e.g., for tumor patients, requires extremely high cell numbers. Unfortunately, the production of adequate cell yields is hampered by the occurrence of cell senescence and a decreased osteogenic potential of periosteal stem cells at higher passages. Additionally, primary JPCs, as well as mesenchymal stem/stromal cells (MSCs) from other tissues exhibit donor variability concerning their differentiation potential. This variability can be caused by different factors, such as varying stem cell numbers in heterogeneous starting materials, the tissue of origin, or the isolation

and maintenance techniques [4,5]. Although surface markers have been identified, which allow the enrichment of osteogenic progenitor cells from heterogeneous cell populations via fluorescence or magnetic activated cell sorting (FACS, MACS) [6–8], cell yields are often unsatisfactory because of low sorting efficiencies and high cell mortality.

The use of patient-specific induced pluripotent stem cells (iPSCs) could solve the above-mentioned problems. iPSCs can differentiate into every cell type of the body and their self-renewal capacity allows the expansion of desired cells to extremely high cell numbers [9]. They can be differentiated into mesenchymal stem/stromal like cells (iMSCs), which can serve as an alternative stem cell source for BTE [10]. Additionally, the directed differentiation of iPSCs to iMSCs could result in more homogeneous populations of osteogenic progenitor cells and therefore might help to standardize the starting material for clinical BTE products [11].

For the safe clinical applicability of iPSC-derived cells, the use of reprogramming methods excluding insertional mutagenesis and xeno-contaminations is of crucial importance [12]. Insertional mutagenesis can be prevented by reprogramming cells using synthetic mRNA, which is a safe and efficient reprogramming technique [13]. However, the transient nature of synthetic mRNAs requires daily transfections, which decrease the cell viability and make the process laborious and time-consuming. Yoshioka et al. [14] improved this approach by developing a synthetic polycistronic self-replicating RNA (srRNA) consisting of the OSKM reprogramming factors (OCT4, SOX2, KLF4, cMYC) and the non-structural proteins (nsP1 to nsP4) encoding sequences of the Venezuelan equine encephalitis virus (VEE), which enabled the RNA to replicate inside the transfected cells as long as their innate immune response was suppressed by the use of the interferon inhibitor B18R [14]. Using this srRNA, a single transfection can be sufficient to reprogram cells, and the removal of B18R leads to the degradation of the srRNA and results in the generation of footprint-free iPSCs.

In the present study, we used an optimized srRNA construct containing a green fluorescent protein (GFP) encoding sequence to enable the live monitoring of transfected cells and the adaptation of the reprogramming protocol to the cell types used. For the production of clinically applicable BTE constructs, animal-derived components have to be excluded from every part of the generation procedure. Thus, in this study, we established for the first time a continuous xeno-free workflow from the initial primary JPC isolation to iPSC generation and differentiation into iMSCs until the final stage of mineralized tissue.

2. Results

2.1. srRNA Transfection Efficiency

To generate iPSCs, JPCs were seeded into 12-well plates at a density of 2.5×10^4 cells/well and transfected with 0.25 ng of srRNA. After 24 h, transfected cells expressing GFP were detected by fluorescence microscopy (Figure 1a–c). An average transfection efficiency of $33 \pm 2\%$ was determined by the measurement of GFP-positive cells via flow cytometry (Figure 1d). Significantly higher (1.67-fold) median fluorescence index (MFI) values were detected in srRNA transfected JPCs compared to untransfected JPCs (Figure 1e).

2.2. JPC Reprogramming

The reprogramming was performed with JPCs from three different patients according to Figure 2a. To select the srRNA containing cells 24 h after the transfection, 1 µg/mL puromycin was added to the medium. Furthermore, to enhance reprogramming efficiency, 250 µM sodium butyrate (NaB), which is a histone deacetylase inhibitor, was added to the medium. Puromycin selection was continued until day five, when all cells in the untransfected control wells were dead (Figure 2b). In comparison, Figure 2c shows the surviving cells transfected with srRNA at day five. After puromycin selection, cells were passaged and seeded in 1:5 ratio into vitronectin coated wells of 12-well plates. The first iPSC colonies emerged between day 12 and 15 (Figure 2d,e). Single iPSC colonies were picked and

transferred into vitronectin coated 12-well plates containing E8 medium with 10 µM Y27632 ROCK inhibitor and were maintained in E8 medium without Y27632 from the next day onward.

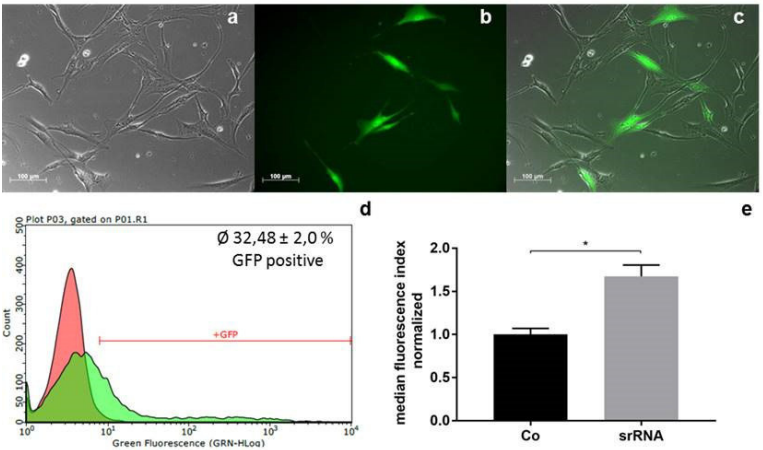

Figure 1. Transfection of jaw periosteal cells (JPCs) with self-replicating RNA (srRNA). (**a**–**c**) Representative (**a**) brightfield, (**b**) green fluorescent protein (GFP), and (**c**) merged images of JPCs 24 h after srRNA transfection. (**d**) Representative histogram of flow cytometry measurements of untransfected (red) and srRNA transfected (green) JPCs 24 h after transfection. (**e**) Average normalized median fluorescence index (MFI) values + standard deviation (SD) of srRNA transfected and untransfected (Co) JPCs relative to MFI values of untransfected (Co) samples were calculated and compared using Student's *t*-test ($n = 3$, * $p < 0.05$).

2.3. Characterization of iPSCs

2.3.1. Pluripotency Marker Expression

To characterize the generated iPSC clones, the expression of pluripotency markers was analyzed via immunostaining and flow cytometry. Figure 3a shows the strong fluorescence staining of Oct4, Sox2, Lin28, Nanog, TRA-1-60 and SSEA4 across all cells of the stained iPSC colonies. Furthermore, the surface marker expression of the generated iPSCs was compared to the initial JPCs using flow cytometry (Figure 3b). In the obtained iPSCs, the expression of MSC markers CD73 and CD105 was significantly downregulated, while pluripotent stem cell markers SSEA-4, TRA-1-60, and TRA-1-81 were significantly upregulated. JPCs and iPSCs were both positive for CD90 and negative for SSEA-1, as expected. Furthermore, the expression of MSC specific (CD73, CD44) and pluripotent stem cell specific (OCT4, NANOG, ALP, TERT) transcripts were analyzed by qRT-PCR. A significantly increased expression of pluripotent stem cell markers OCT4, NANOG, ALP, and TERT was detected in iPSCs compared to JPCs, while the expression of MSC specific transcripts CD73 and CD44 was significantly downregulated (Figure 3c).

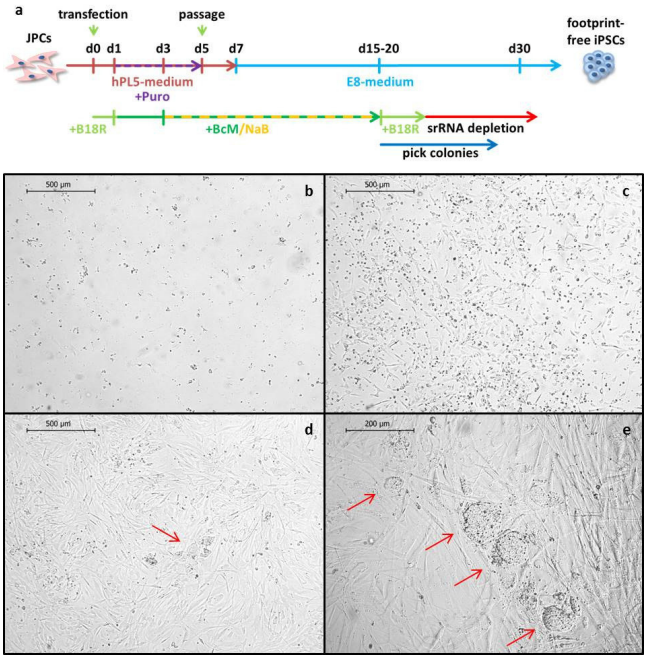

Figure 2. Reprogramming of JPCs. (**a**) Timeline of JPC reprogramming. JPCs were transfected (d0) in hPL5-medium containing 0.2 µg/mL B18R protein. On day one, the medium was changed to hPL5 containing 25% conditioned medium containing B18R (BcM) and 1.0 µg/mL puromycin (Puro). Puromycin selection was continued until day five (purple arrow). Cells were passaged on day five, and on day seven, the medium was changed to Essential 8 (E8) containing 25% BcM. Sodium butyrate (NaB) was added to the medium from day three to 15. When the first induced pluripotent stem cell (iPSC) colonies emerged, the medium was changed to E8 containing 0.2 µg/mL B18R protein. iPSC colonies were picked at day 15 or later. (**b**–**e**) Representative bright field images of JPCs during srRNA-based reprogramming. (**b**) Untransfected JPCs treated with puromycin at day five. (**c**) srRNA transfected JPCs treated with puromycin at day five. (**d**) srRNA transfected JPCs at day 12 with the first iPSC-colonies (indicated by a red arrow). (**e**) srRNA transfected cells at day 15 with iPSC-colonies (indicated by red arrows).

2.3.2. Differentiation Potential of iPSCs into the Three Germ Layers In Vitro and In Vivo

The differentiation capacity of the generated iPSCs to form all tissues of the three germ layers is characteristic for pluripotent stem cells and was first assessed in vitro by a 7-day trilineage differentiation protocol. As shown in Figure 4a, endothelial, hepatocyte-like and neural-like cells were obtained after the differentiation of iPSCs. The mesoderm, endoderm, and ectoderm differentiation potential was confirmed by tissue specific antibody staining and quantification using flow cytometry. Mesodermal differentiation resulted in 59 ± 23% CD31-positive and 89 ± 11% SMA-positive cells. Endodermal induction yielded 96 ± 2% AFP-positive and 99 ± 1% CXCR4-positive cells. Ectodermal differentiation was demonstrated by the detection of 94 ± 3% Pax6-positive and 89 ± 6% Tuj1-positive cells.

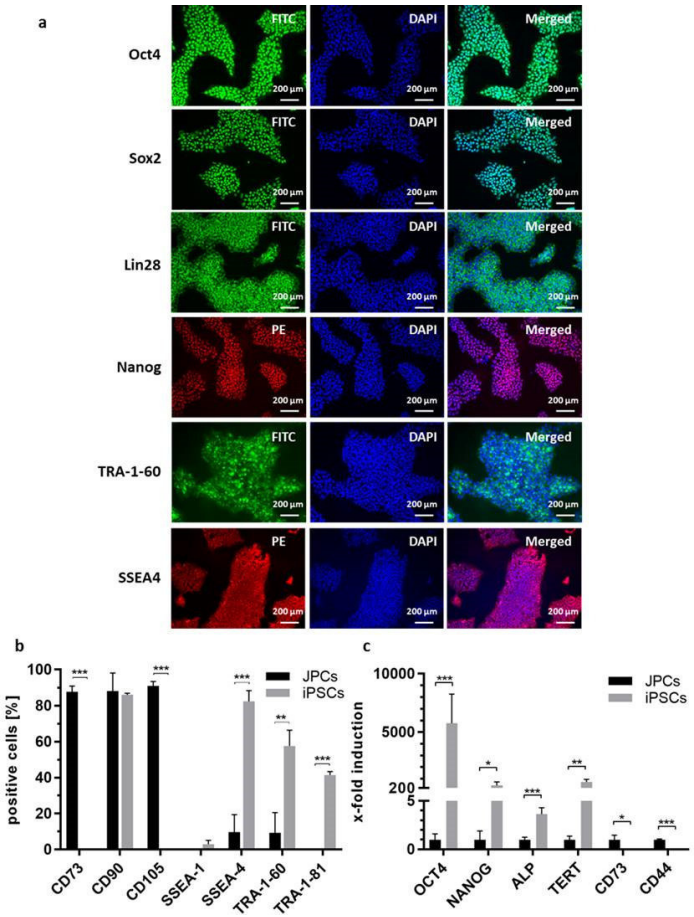

Figure 3. Pluripotency marker expression of JPC-derived iPSCs. (**a**) Oct4, Sox2, Lin28, Nanog, TRA-1-60 and SSEA4 immunostaining of iPSCs. (**b**) Surface marker expression of JPCs and JPC-derived iPSCs analyzed by flow cytometry and compared using Student's *t*-test ($n = 3$, ** $p < 0.01$, *** $p < 0.001$). (**c**) Gene expression analysis of JPCs and JPC-derived iPSCs by qRT-PCR. Gene expression levels were normalized to levels of GAPDH. Mean values + SD of iPSC and JPC gene expression were displayed relative to those of JPCs. Statistical significance was calculated using Student's *t*-test. ($n = 3$, * $p < 0.05$, ** $p < 0.01$, *** $p < 0.001$).

Using a chicken embryo chorioallantoic membrane (CAM) assay, the in vivo differentiation of iPSCs was analyzed. 10 days after the application of iPSCs onto the CAM, teratoma formation could be observed. Subsequently, teratomas were sectioned and stained with hematoxylin & eosin (H&E) and tissue types of the mesodermal (bone-like tissue), endodermal (gut-like tissue) and ectodermal (squamous epithelium) lineage could be identified (Figure 4b).

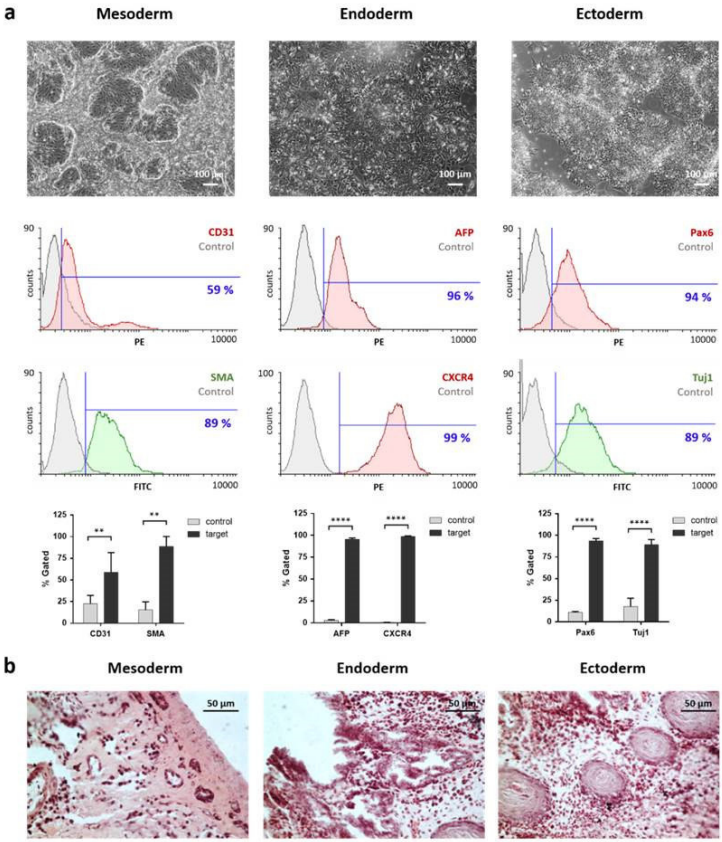

Figure 4. Trilineage differentiation potential of JPC-derived iPSCs. (**a**) Microscopic pictures of mesodermal, endodermal and ectodermal in vitro differentiation showing different morphologies after six days of germ layer specific differentiation. Flow cytometry analysis of differentiated cells was performed after staining with specific antibodies compared to untreated controls. Data are shown as mean + SD. Differences were compared using one-way ANOVA (n = 3, ** $p < 0.01$, **** $p < 0.0001$). (**b**) Microscopic images of in vivo teratoma formation of iPSCs using a chorioallantoic membrane (CAM) assay. H&E stained sections showed mesodermal (bone-like), endodermal (gut-like) and ectodermal (squamous epithelium) tissue.

2.3.3. Detection of srRNA in iPSCs and Karyotyping of iPSCs

After the successful generation of iPSCs, the presence of srRNA in the cells was analyzed. Therefore, qRT-PCR was performed with RNA isolated from JPCs and JPC-derived iPSCs and primer pairs specific to the nsP2 and nsP4 sequences. JPCs transfected with srRNA and cultivated for 48 h, served as positive control (JPC+). These samples showed high amounts of nsP2 and nsP4 compared to untransfected JPCs and iPSCs (Figure 5a). In contrast, the nsP2 and nsP4 amount measured in iPSCs was similar to that of untransfected JPCs, which demonstrates the absence of srRNA in the

reprogrammed cells. Karyotyping of JPC-derived iPSCs resulted in normal karyograms without chromosomal aberrations (Figure 5b).

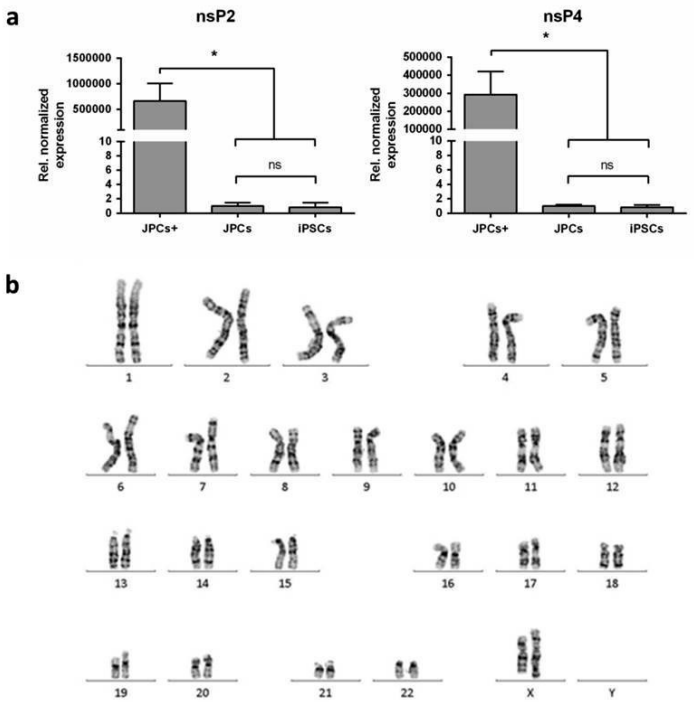

Figure 5. Elimination of srRNA after iPSC generation and karyotyping of JPC-derived iPSCs. (**a**) qRT-PCR analysis of nsP2 and nsP4 transcripts in iPSCs (passage 3), untreated JPCs and srRNA containing JPCs (JPCs+) 48 h post-transfection. Data are shown as mean + SEM. Differences were compared using one-way ANOVA ($n = 3$, * $p < 0.05$, ns = not significant) (**b**) Representative karyogram of JPC-derived iPSCs showing a normal karyotype (46, XX).

2.3.4. Differentiation of iPSCs into iMSCs and Their Characterization

To be able to use iPSCs for BTE, the differentiation potential of iPSCs into the osteogenic lineage has to be demonstrated. Therefore, iPSCs were first differentiated into iMSCs (Figure 6a). For this purpose, iPSCs (Figure 6b) were cultivated without passaging for 10 days to stimulate spontaneous differentiation. Subsequently, cells were passaged as single cells and incubated in hPL5 medium with ascorbic acid until their morphology changed to a spindle shaped MSC-like appearance (3–5 passages, Figure 6c,d). Cells exhibiting MSC morphology (Figure 6e) were expanded in hPL5 medium before osteogenic differentiation and characterization.

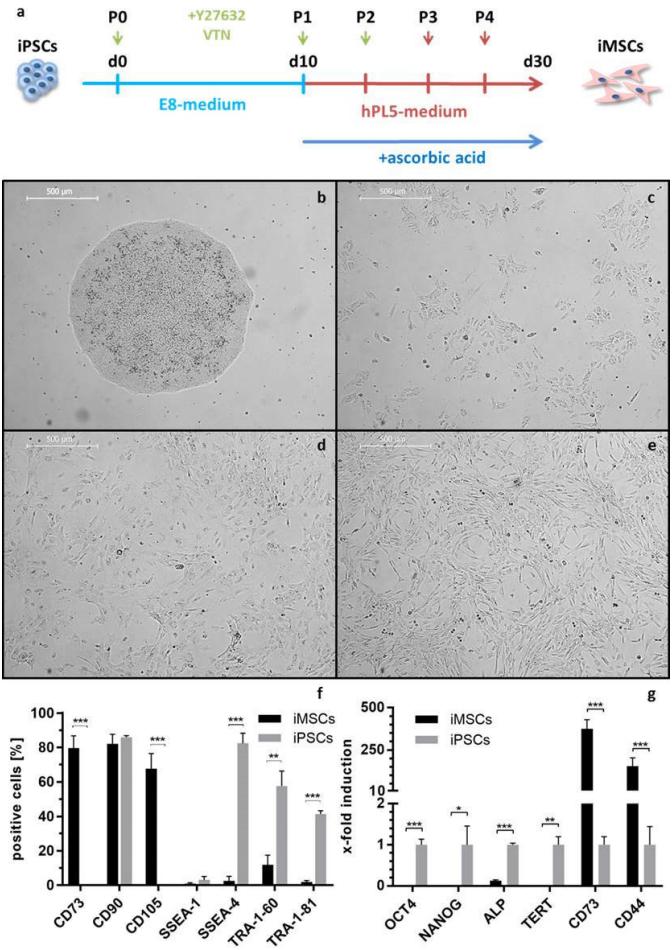

Figure 6. Differentiation of iPSCs into iPSC-derived mesenchymal stem/stromal like cells (iMSCs). (**a**) Timeline: iPSCs were seeded onto vitronectin coated plates in the presence of the ROCK inhibitor Y27632 and cultivated for 10 days in E8 medium (light blue line). Thereafter, human platelet lysate hPL5 medium containing 150 µM ascorbic acid was added to the cells (red line). Cells were passaged 3–5 times until they showed homogeneous MSC-like morphology after approximately 30 days. (**b**–**e**) Change of morphology during the differentiation of iPSCs into iMSCs. (**b**) iPSC colony before differentiation. (**c**) Cells after single cell plating in passage 0. (**d**) Differentiating iMSCs in passage two and (**e**) iMSCs in passage four (scale bars represent 500 µm). (**f**) Surface marker expression of iMSCs compared to iPSCs detected by flow cytometry. (**g**) Gene expression levels of iMSCs were normalized to levels of the housekeeping gene glyceraldehyde 3-phosphate dehydrogenase (GAPDH) and presented as x-fold induction relative to iPSCs (set to 1). Differences in surface marker, and gene expression were compared using Student's *t*-test. ($n = 3$, * $p < 0.05$, ** $p < 0.01$, *** $p < 0.001$).

Using flow cytometry, the surface marker expression of obtained iMSCs was analyzed (Figure 6f). The expression of MSC markers (CD73 and CD105) was significantly upregulated in iMSCs, while iPSC markers (SSEA-4, TRA-1-60, and TRA-1-81) were significantly downregulated compared to iPSCs. iMSCs and iPSCs were both positive for CD90 and negative for SSEA-1 (Figure 6f). In addition, gene expression of MSC markers (CD73, CD44) and iPSC markers (OCT4, NANOG, ALP, and TERT) was quantified by qRT-PCR (Figure 6g). iPSC markers were significantly downregulated in iMSCs compared to iPSCs, while MSC markers were significantly upregulated.

2.3.5. Osteogenic Differentiation of iMSCs

To demonstrate the functionality of iMSCs and their potential to be used for BTE applications, iMSCs were subjected to osteogenic differentiation. To differentiate the iMSCs under xeno-free conditions, cells were treated with osteogenic medium supplemented with human platelet lysate (hPL) instead of fetal bovine serum (FBS). After 15–20 days of differentiation, cells were fixed, and calcium phosphate precipitation was stained with alizarin red. As displayed in Figure 7, all iMSCs were able to produce strong mineral deposits.

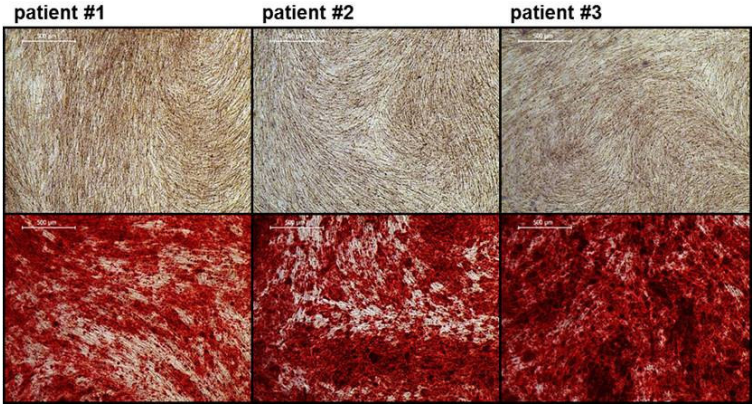

Figure 7. Osteogenic differentiation potential of iMSCs. iMSCs incubated without osteogenic stimuli (control, upper panel) and osteogenic medium (lower panel) for 15–20 days, stained with alizarin red (scale bars represent 500 μm).

3. Discussion

Jaw periosteum is an excellent, but limited source of osteogenic progenitor cells. To establish stem cell based regenerative therapies for large bone defects in oral and maxillofacial surgeries, appropriate numbers of good quality stem cells are needed. However, it is difficult to obtain sufficient cell numbers from cell cultures expanded from primary cells. The occurrence of cell senescence and the loss of differentiation potential are problems to be solved. Thus, iPSCs are a promising alternative cell source which might help to solve these problems. Unfortunately, the use of iPSC derived cells still has some safety issues concerning insertional mutagenesis caused by reprogramming vectors, teratoma formation, and infections or immune responses caused by xenogenic media supplements. In our study, we established protocols to overcome these issues and to bring therapeutic applications of iPSC-derived osteogenic progenitor cells closer to the clinic. To generate footprint-free iPSCs and to address the problem of insertional mutagenesis, srRNA was used, which combines the safety of synthetic mRNA-based reprogramming and the convenience of a single transfection.

The complete removal of srRNA after B18R withdrawal was demonstrated in the generated iPSCs at passage three, as also shown by Yoshioka et al. [14]. The additional presence of a GFP encoding sequence in the srRNA allowed convenient monitoring of srRNA translation and depletion following termination of immunosuppression by B18R interferon inhibitor. Thus, it allowed the adaptation of reprogramming/transfection protocols for JPCs. The reprogramming protocol established in this study worked reliably for JPCs from all tested patients and could also be successfully applied to human gingival fibroblasts (data not shown).

The osteogenic differentiation of iPSCs can be performed with different protocols, however recently a two-step approach was described, where iPSCs were first differentiated iMSCs, and in a second step subjected to osteogenic differentiation [10,15]. The differentiation of iPSCs into iMSCs has several advantages, e.g., the exclusion of teratoma formation risk [16] and the possibility to use cell culture and differentiation protocols standardized for MSCs. Usually, the differentiation of iPSCs to iMSCs can either be performed via embryoid body formation or by the incubation of iPSCs (when growing as colonies or plated as single cells) with differentiation media, followed by several passaging steps [17].

In this study, we modified a protocol from Luzzani et al. (2015), who also used hPL containing media for the differentiation of iPSCs into iMSCs [18]. To improve the yield of iMSCs, iPSC colonies were cultivated for extended periods without passaging prior to single cell plating. The resulting high cell densities probably primed the cells towards mesenchymal differentiation.

As shown by flow cytometry and gene expression analysis, the surface marker and gene expression profile of the obtained iMSCs were similar to that of typical MSCs [4]. Subsequent osteogenic differentiation resulted in strong mineral deposition, which demonstrated the promising potential of these cells for BTE applications.

In the present work, an important step towards clinical application was made by removing all xenogenic compounds from the protocols throughout the process. This was possible by replacing FBS with hPL for medium supplementation. Our attempts to generate iPSCs from JPCs using commercially available defined MSC-media failed due to low cell viability after the srRNA transfection or puromycin selection.

The translation of iPSCs from basic research to clinical application has made substantial progress in the past years. The first clinical trial using iPSCs to treat macular degeneration has been launched in Japan in 2014, and was able to demonstrate the safety of iPSC-derived regenerative therapies [19]. Further, a clinical trial using iPSC-derived MSCs for the treatment of steroid-resistant acute graft versus host disease (GvHD) has been started in Australia in March 2017 [20]. Preliminary results of this trial also proved the safety of the iPSC-derived MSCs and showed an improvement in severity of GvHD in 14 out of 15 patients.

These trials raise hopes for other iPSC applications to reach the clinical level in the near future even though it is still a long way for iPSCs to make their way into clinical routine.

4. Materials and Methods

4.1. Xeno-Free Isolation and Culture of JPCs

JPCs derived from three patients were included in this study in accordance with the local ethical committee (approval number 074/2016BO2, 17.05.2016) and after obtaining written informed consent. Jaw periosteal tissue was cut in small pieces with a scalpel and incubated in DMEM/F12 (Thermo Fisher Scientific, Waltham, MA, USA) containing 10% hPL (ZKT Tübingen gemeinnützige GmbH), 100 U/mL penicillin-streptomycin (Lonza, Basel, Switzerland), 2.5 µg/mL amphotericin B (Biochrom, Berlin, Germany), 50 µg/mL gentamicin (Lonza), and 10 µg/mL ciprofloxacin (Sigma-Aldrich, St. Louis, USA) for 1–2 weeks. Outgrowing cells were passaged using TrypLE Express (Thermo Fisher Scientific) and expanded and frozen in passage one using Cryo SFM freezing medium (Promocell, Heidelberg,

Germany). From passage two onward, JPCs were grown in hPL5-medium (DMEM/F12 containing 5% hPL, 100 U/mL penicillin-streptomycin, and 2.5 µg/mL amphotericin B).

4.2. Production of srRNA

The T7-VEE-OKS-iM plasmid, a gift from Steven Dowdy (Addgene plasmid # 58972), containing sequences encoding the non-structural proteins (nsP1 to nsP4) for self-replication, the reprogramming factors Oct4, Klf4, Sox2, and cMyc [14] and an additionally added internal ribosome entry site (IRES)-GFP was amplified in *E.coli* and plasmids were isolated using QIAPrep (Qiagen, Hilden, Germany). After the linearization with MluI restriction enzyme (Thermo Fisher Scientific), 10 µg template DNA was transcribed in vitro using RiboMAX large-scale production system T7 Kit (Promega, Madison, WI, USA) according to the manufacturer's instructions. Afterwards, 2 U TURBO DNase was added for 15 min at 37 °C. For 5′-end capping, ScriptCap Cap1 Capping System was used followed by 3′-end polyadenylation with A-Plus Poly(A) Polymerase Tailing Kit (both from Cellscript, Madison, WI, USA) according to the manufacturer's instructions. Following each reaction step, srRNA was purified using RNeasy Kit (Qiagen). The specific lengths of the generated DNA and srRNA products were analyzed using 1% agarose gel electrophoresis.

4.3. Production of B18R-mRNA

The coding sequence for B18R was inserted by Aldevron (Fargo, ND, USA) into the pcDNA 3.3 plasmid. Pseudoruridine-5′-triphosphate (Ψ-UTP) and 5-methylcytidine-5′-triphosphate (m5CTP) modified B18R mRNA was generated by in vitro transcription (IVT) as previously described in our studies [21].

4.4. Generation of Integration-Free iPSCs from JPCs Using srRNA

4.4.1. Preparation of Conditioned Medium Containing B18R (BcM)

JPCs were expanded in hPL5 medium and passaged into a T75 flask to reach approx. 80% confluency at the next day. To perform B18R-mRNA transfection, the medium was aspirated and replaced by 6.5 mL Opti-MEM (Thermo Fisher Scientific). The transfection cocktail was prepared according to the manufacturer's instructions (500 µL Opti-MEM, 7.5 µg of B18R-mRNA, 15 µL Lipofectamine 3000 (Thermo Fisher Scientific)), added to the medium and incubated for 4 h at 37 °C. Subsequently, medium was changed to 15 mL hPL5 medium. After 24 h, medium was collected and replaced with 15 mL fresh hPL5. The collected BcM was stored at −20 °C. Medium collection was repeated until day three and the collected BcM was pooled, sterile filtered with a 0.2 µm filter, aliquoted and stored at −20 °C.

4.4.2. Transfection of JPCs with srRNA and Reprogramming

JPCs (2.5–5 × 10^4 cells) were seeded into 12-well plates to reach 30–50% confluency the next day. Medium was changed to 0.5 mL hPL5 supplemented with 0.2 µg/mL recombinant B18R protein (eBioscience, San Diego, CA, USA) 30 min prior to transfection. The transfection cocktail (25 µL Opti-MEM, 0.25 µg srRNA, 0.5 µL TransIT mRNA Boost Reagent (Mirus Bio LLC, Madison, WI, USA), and 0.5 µl TransIT mRNA Reagent (Mirus Bio LLC)) was prepared according to the manufacturer's instructions and added to the wells.

24 h after transfection, the medium was replaced with hPL5 containing 25% BcM and 1 µg/mL puromycin (Thermo Fisher Scientific) and changed every other day. To determine the transfection efficiency, cells were harvested after 24 h using TrypLE Express, resuspended in BD Cytofix/Cytoperm Solution (BD Bioscience, Franklin Lakes, NJ, USA) and GFP expression was measured by flow cytometry using the Guava EasyCyte 6HT-2L instrument (Merck Millipore, Billerica, MA, USA). From day three until day 15, 250 µM sodium butyrate (NaB, Selleck Chemicals LLC, Houston, TX, USA) was added to the medium. On day five, after successful puromycin selection, srRNA containing

cells were passaged using TrypLE Express and split in 1:5 ratio into 12-well plates coated with 0.5 mL of a 5 µg/mL vitronectin solution (Thermo Fisher Scientific). Untransfected cells died within the five days of puromycin treatment. Two days after passaging (day seven), the medium was changed to Essential 8 medium (E8, Thermo Fisher Scientific) containing 25% BcM and replaced by fresh medium every day. When first iPSC colonies emerged, medium was changed to E8-medium supplemented with 0.2 µg/mL recombinant B18R protein. Single iPSC colonies were picked and transferred into vitronectin coated 12-well plates containing E8 medium supplemented with 10 µM Y27632 ROCK inhibitor (Selleck Chemicals LLC). iPSCs were maintained in E8 medium with daily medium changes and passaged every 4–6 days.

4.5. Characterization of JPC-Derived iPSCs

4.5.1. Immunostaining for Detection of Pluripotency

On vitronectin coated glass slides, 5×10^5 iPSCs were cultivated for 2–3 days and fixed using fixation solution (R&D Systems, Minneapolis, MN, USA) for 10 min. Afterwards, cells were washed with wash buffer (Permeabilization/Wash Buffer I, R&D Systems) and blocked with 5% BSA in wash buffer for 1–2 h at RT. Antibody staining was performed according to the manufacturer's instructions in wash buffer containing 1% BSA. Cells were incubated for 3 h at RT with fluorescently labelled antibodies (PE-labelled mouse anti-human Nanog antibody (BD Bioscience), DyLight™ 488 labelled mouse anti-human StainAlive™ TRA-1-60 antibody (Stemgent, Cambridge, MA, USA), and DyLight™ 550 labelled mouse anti-human StainAlive™ SSEA-4 antibody (Stemgent)). The incubation with primary antibodies (rabbit anti-human POU5F1 (Oct4) (Sigma-Aldrich), rabbit anti-human Sox2 (Stemgent), and mouse anti-human LIN28A (6D1F9) (Thermo Fisher Scientific)) were performed overnight at 4°C. After washing with wash buffer, cells were incubated for 1 h in wash buffer containing 1% BSA with fluorescently labeled secondary antibodies (FITC-labelled sheep anti-mouse IgG (Sigma-Aldrich) or Cy3-labelled goat anti-rabbit IgG (Thermo Fisher Scientific)). Finally, the cells were washed and stained using Fluoroshield mounting medium with DAPI (Abcam, Cambridge, UK). Fluorescence microscopic images were taken using Axiovert135 microscope and AxioVision 4.8.2 software (Carl Zeiss, Oberkochen, Germany).

4.5.2. Tri-Lineage Differentiation of iPSCs In Vitro

The ability of iPSCs to differentiate into the three germ layers was analyzed using the human StemMACS™ Trilineage Differentiation Kit (Miltenyi, Bergisch Gladbach, Germany) according the manufacturer's instructions. 1×10^5 iPSCs were seeded per well of a 12-well plate for mesoderm differentiation, 2×10^5 cells for endoderm differentiation, and 1.5×10^5 iPSCs for ectoderm differentiation. The cells were analyzed after seven days of differentiation using flow cytometry.

Therefore, cells were detached, fixed for 10 min at RT in fixation solution (R&D Systems) and washed with DPBS. Then, the cells were incubated for 45 min at RT with wash buffer (Wash Buffer I, R&D Systems) containing 5 µl of each of the following antibodies: Mesoderm differentiation: Alexa Fluor 488 labelled anti-human α-smooth muscle actin (α-SMA) antibody (R&D Systems) and PE labelled mouse anti-human CD31 antibody (BD Biosciences), Endoderm differentiation: PE-labelled anti-human C-X-C chemokine receptor type 4 (CXCR4) antibody and PE-labelled anti-human α-fetoprotein (AFP) antibody (both from R&D Systems, Minneapolis, USA), Ectoderm differentiation: Alexa Fluor 488 labelled anti-human neuron-specific class III β-tubulin (Tuj1) antibody (BD Biosciences) and PE-labelled anti-human paired box gene 6 (Pax6) antibody (Miltenyi). After washing with wash buffer, cells were fixed using CellFIX solution (BD Biosciences) and analyzed using FACScan flow cytometer (BD Biosciences) and Flowing Software (Turku Centre for Biotechnology, Turku, Finland).

4.5.3. Teratoma Formation on Chicken Embryo Chorioallantoic Membrane (CAM)

To confirm the differentiation potential of iPSCs into the three germ layers, an in vivo teratoma formation was performed using CAM assay. After three days of incubation at 37 °C, 2-3 mL albumen was aspirated from fertilized chicken eggs (Lohmann White x White Rock) and a window was cut into the shell and sealed with semi-permeable adhesive tape. After seven days of incubation at 37 °C, a silicone ring was placed onto the CAM and 2×10^6 iPSCs mixed with 50 µL E8 medium and 50 µL Matrigel (Corning, New York, NY, USA) were transferred into the inner circle of the silicone ring. The eggs were then sealed again and further incubated at 37 °C. After 10 days (day 17 of incubation), the teratoma cell mass with the surrounding CAM was excised and fixed at 4 °C with 4% paraformaldehyde (Merck, Darmstadt, Germany) overnight. After washing with DPBS and ethanol dehydration, the samples were embedded in paraffin for sectioning and H&E (Morphisto, Frankfurt, Germany) staining.

4.5.4. Detection of Residual srRNA in the Reprogrammed iPSCs

The presence of srRNA in the generated iPSCs was analyzed by qRT-PCR using primers specific for sequences encoding the non-structural proteins nsP2 and nsP4: nsP2 (fw: 5′-TCC ACA AAA GCA TCT CTC GCC G-3′, rev: 5′-TTT GCA ACT GCT TCA CCC ACC C-3′) and nsP4 (fw: 5′-TTT TCA AGC CCC AAG GTC GCA G-3′, rev: 5′-TGT TCT GGA TCG CTG AAG GCA C-3′). For RNA isolation, 1×10^6 iPSCs at passage three were used (Aurum™ Total RNA Mini Kit (Bio-Rad, Hercules, CA, USA) and 300 ng RNA was reverse transcribed into complementary DNA (cDNA) using iScript Kit (Bio-Rad). qRT-PCR reactions with 40 cycles were performed in CFX Connect Real-Time PCR Detection System (Bio-Rad) using IQ™ SYBR® Green Supermix (Bio-Rad) and 300 nM primer with following conditions: 3 min at 95 °C (1 cycle); 95 °C for 15 s, 60 °C for 30 s, and 72 °C for 10 s. The mRNA expression levels were normalized to glyceraldehyde 3-phosphate dehydrogenase (GAPDH). The results are shown relative to the initial JPCs.

4.5.5. Karyotyping of iPSCs

iPSCs were grown to 60–80% confluency in a 6-well plate and incubated for 90 min with 0.15 µg/mL KaryoMAX colcemid solution (Thermo Fisher Scientific). Then, cells were detached using Accutase (Thermo Fisher Scientific) and inactivated with DMEM/F12 containing 10% FBS. The cell suspension was centrifuged (300× *g* for 5 min), the supernatant was discarded and 1.5 mL of 0.075 M KaryoMAX KCl solution (Thermo Fisher Scientific) was added and incubated at 37 °C. After 30 min, 100 µL fixative (3:1 methanol/acetic acid) was added and incubated for 10 min. After centrifugation, the cells were resuspended in fixative, incubated for 1 h at RT, and then stored over night at 20 °C. Chromosome analysis was performed by the Institute of Medical Genetics and Applied Genomics of the University Hospital Tübingen.

4.6. Differention of iPSCs into iMSCs

Very low concentrations of iPSCs ($\leq$ 10% confluency) were seeded into vitronectin coated (0.5 mL of 5 µg/mL solution) 12-well plates and cultivated without passaging for 10 days to stimulate spontaneous differentiation. After this period, the cells were detached using Accutase and transferred into vitronectin coated 6-well plates containing E8-medium and 10 µM ROCK inhibitor Y27632 (passage 1). The next day, the medium was changed to hPL5 supplemented with 150 µM L-ascorbic acid 2-phosphate (Sigma-Aldrich) and medium was replaced every other day. After reaching 80% confluency, cells were passaged into vitronectin coated 6-well plates (split ratio 1:3) using Accutase and ROCK inhibitor was added to the medium. For following cell passages TrypLE Express was used and no further ROCK inhibitor or vitronectin was used. Cells were passaged until the morphology of the cells had changed to a spindle shaped MSC-like appearance (3–5 passages). Cells exhibiting

MSC morphology were expanded in hPL5 medium before using the cells for osteogenic differentiation and characterization.

4.7. Osteogenic Differentiation of iMSCs

For osteogenic differentiation, iMSCs were cultivated in osteogenic medium (DMEM/F12 containing 10% hPL, 100 U/mL penicillin-streptomycin (Lonza), 2.5 µg/mL amphotericin B, 0.1 mM L-ascorbic acid 2-phosphate (Sigma-Aldrich), β-glycerophosphate (AppliChem, Darmstadt, Germany), and 4 µM dexamethasone (Sigma-Aldrich)) with medium changes every 2–3 days. After 15–25 days, cells were fixed with 4% formalin and stained for 20 min with 1 mL of 40 mM Alizarin red solution (pH 4.2, Sigma-Aldrich). Unbound dye was removed by washing with deionized water and images were taken using an inverted microscope (Leica, Wetzlar, Germany).

4.8. Flow Cytometric Analysis of JPCs, iPSCs, and iMSCs

The expression of pluripotency markers (SSEA-1, SSEA-4, TRA-1-60, TRA-1-80) and MSC-markers (CD73, CD90, CD105) was analyzed by flow cytometry. Cells were detached using TrypLE Express and 1×10^5 cells per sample were incubated on ice for 15 min in 20 µL blocking buffer (PBS, 0.1% BSA, 1 mg/mL sodium azide (Sigma-Aldrich), and 10% Gamunex (human immune globulin solution, Talecris Biotherapeutics GmbH, Frankfurt, Germany)). Then, 50 µL FACS buffer (PBS, 0.1% BSA, 1 mg/mL sodium azide) as well as phycoerythrin (PE) and allophycocyanin (APC) conjugated antibodies (for individual volumes see Table 1) were added and incubated on ice for 20 min. After two washing steps with 200 µL FACS buffer, flow cytometry measurements were performed using the Guava EasyCyte 6HT-2L (Merck Millipore, Billerica, MA, USA).

Table 1. List of antibodies used for flow cytometry.

Human Antigen	Volume per Sample (µL)	Isotype	Conjugate	Company
SSEA1	5	human recombinant antibody (REA)	PE	Miltenyi, Bergisch Gladbach, Germany
SSEA4	5		PE	
TRA-1-60	5		PE	
TRA-1-81	5		PE	
REA-Isotype	5		PE	
CD73	5	mouse IgG1	PE	BD Biosciences, Franklin Lakes, NJ, USA
CD90	1		PE	
CD105	10		APC	BioLegend, San Diego, CA, USA
IgG1-Isotype	10		APC	
IgG1-Isotype	5		PE	R&D Systems, Minneapolis, MN, USA

4.9. Gene expression Analysis of JPCs, iPSCs, and iMSCs by qRT-PCR

RNA isolation from JPCs, iPSCs and iMSCs (1×10^5 cells per sample) was carried out using the NucleoSpin RNA kit (Macherey-Nagel, Düren, Germany) following the manufacturer's instructions. The amount of isolated RNA was quantified with a Qubit 3.0 fluorometer and the corresponding RNA BR Assay Kit (Thermo Fisher Scientific). The first-strand cDNA synthesis was performed with 0.5 µg of RNA using the SuperScript Vilo Kit (Thermo Fisher Scientific). The quantification of mRNA expression levels was performed using the real-time LightCycler System (Roche Diagnostics, Mannheim, Germany). For the PCR reactions, commercial OCT4, NANOG, ALP, CD44, and CD73 primer kits (Search LC, Heidelberg, Germany) and DNA Master SYBR Green I kit (Roche, Basel, Switzerland) were used. The amplification was performed with a touchdown PCR protocol of 40 cycles (annealing temperature between 68–58 °C), following the manufacturer's instructions. GOI (gene of interest) transcript levels of each sample were normalized to those of the housekeeping gene GAPDH, divided by the corresponding control samples and displayed as x-fold induction indices.

4.10. Statistical Analysis

For the statistical evaluation of data, means + standard deviation (SD) or standard error of mean (SEM) were calculated. Student's *t*-test or one-way analysis of variance (ANOVA) for repeated measurements followed by Bonferroni's multiple comparison test was used. All statistical analyses were performed double-tailed using GraphPad Prism 6.01. A p-value < 0.05 was considered significant.

5. Conclusions

In this study, we generated for the first time, footprint- and xeno-free iPSCs from JPCs by the transfection of srRNA encoding the reprogramming factors. We conclude that JPCs can function as starting material for the generation of clinical grade autologous iPSCs. The differentiation of JPC-iPSCs to iMSCs leads to the generation of cells with a high osteogenic potential, which are a promising source of osteogenic progenitor cells for BTE. Using cGMP grade hPL as a medium supplement, clinically applicable osteogenic progenitor cells can be obtained.

Author Contributions: Methodology, validation, investigation, data curation, writing original draft preparation, F.U. and H.S.; validation, investigation, data curation, M.W.; conceptualization, funding acquisition, project administration, supervision, writing-review and editing, D.A. and M.A.-A.; resources, writing-review and editing, H.-P.W and S.R.

Funding: This research was funded by German Research Foundation, grant number AL 1486/6-1/AV 133/7-1.

Conflicts of Interest: The authors declare no conflict of interest.

Abbreviations

ANOVA	analysis of variance
APC	allophycocyanin
BcM	conditioned medium containing B18R
BSA	bovine serum albumin
BTE	bone tissue engineering
CAM	chorioallantoic membrane
cGMP	current good manufacturing practice
cDNA	complementary DNA
DNA	deoxyribonucleic acid
DPBS	Dulbecco's phosphate buffered saline
FACS	fluorescence-activated cell sorting
FBS	fetal bovine serum
GFP	green fluorescent protein
GOI	gene of interest
H&E	haematoxylin and eosin
hPL	human platelet lysate
IgG	immunoglobulin G
iMSC	iPSC-derived mesenchymal stem/stromal like cell
iPSC	induced pluripotent stem cell
IRES	internal ribosome entry site
JPC	jaw periosteal cell
m5CTP	5-methylcytidine-5′-triphosphate
MACS	magnetic-activated cell sorting
MFI	median fluorescence index
mRNA	messenger RNA
MSC	mesenchymal stem/stromal cell
NaB	sodium butyrate
OSKM	OKT4, SOX2, KLF4, cMYC

PBS	phosphate buffered saline
PCR	polymerase chain reaction
PE	phycoerythrin
Puro	puromycin
qRT-PCR	quantitative real-time polymerase chain reaction
RNA	ribonucleic acid
ROCK	rho-associated protein kinase
SD	standard deviation
SEM	standard error of mean
srRNA	self-replicating ribonucleic acid
Ψ-UTP	pseudoruridine-5′-triphosphate

References

1. Alexander, D.; Hoffmann, J.; Munz, A.; Friedrich, B.; Geis-Gerstorfer, J.; Reinert, S. Analysis of OPLA scaffolds for bone engineering constructs using human jaw periosteal cells. *J. Mater. Sci. Mater. Med.* **2008**, *19*, 965–974. [CrossRef] [PubMed]
2. Ferretti, C.; Mattioli-Belmonte, M. Periosteum derived stem cells for regenerative medicine proposals: Boosting current knowledge. *World J. Stem Cells* **2014**, *6*, 266–277. [CrossRef] [PubMed]
3. Roberts, S.J.; van Gastel, N.; Carmeliet, G.; Luyten, F.P. Uncovering the periosteum for skeletal regeneration: The stem cell that lies beneath. *Bone* **2015**, *70*, 10–18. [CrossRef] [PubMed]
4. Dominici, M.; Le Blanc, K.; Mueller, I.; Slaper-Cortenbach, I.; Marini, F.; Krause, D.; Deans, R.; Keating, A.; Prockop, D.; Horwitz, E. Minimal criteria for defining multipotent mesenchymal stromal cells. The International Society for Cellular Therapy position statement. *Cytotherapy* **2006**, *8*, 315–317. [CrossRef] [PubMed]
5. McLeod, C.M.; Mauck, R.L. On the origin and impact of mesenchymal stem cell heterogeneity: New insights and emerging tools for single cell analysis. *Eur. Cells Mater.* **2017**, *34*, 217–231. [CrossRef] [PubMed]
6. Alexander, D.; Schafer, F.; Olbrich, M.; Friedrich, B.; Buhring, H.J.; Hoffmann, J.; Reinert, S. MSCA-1/TNAP Selection of Human Jaw Periosteal Cells Improves their Mineralization Capacity. *Cell. Physiol. Biochem.* **2010**, *26*, 1073–1080. [CrossRef] [PubMed]
7. Olbrich, M.; Rieger, M.; Reinert, S.; Alexander, D. Isolation of osteoprogenitors from human jaw periosteal cells: A comparison of two magnetic separation methods. *PLoS ONE* **2012**, *7*, e47176. [CrossRef] [PubMed]
8. Umrath, F.; Thomalla, C.; Poschel, S.; Schenke-Layland, K.; Reinert, S.; Alexander, D. Comparative Study of MSCA-1 and CD146 Isolated Periosteal Cell Subpopulations. *Cell. Physiol. Biochem.* **2018**, *51*, 1193–1206. [CrossRef] [PubMed]
9. Yu, J.; Thomson, J.A. Induced Pluripotent Stem Cells. In *Principles of Tissue Engineering*; Lanza, R., Langer, R., Vacanti, J., Eds.; Academic Press: Boston, MA, USA, 2014; pp. 581–594.
10. Luzzani, C.D.; Miriuka, S.G. Pluripotent Stem Cells as a Robust Source of Mesenchymal Stem Cells. *Stem Cell Rev. Rep.* **2017**, *13*, 68–78. [CrossRef] [PubMed]
11. Frobel, J.; Hemeda, H.; Lenz, M.; Abagnale, G.; Joussen, S.; Denecke, B.; Saric, T.; Zenke, M.; Wagner, W. Epigenetic rejuvenation of mesenchymal stromal cells derived from induced pluripotent stem cells. *Stem Cell Rep.* **2014**, *3*, 414–422. [CrossRef] [PubMed]
12. Seki, T.; Fukuda, K. Methods of induced pluripotent stem cells for clinical application. *World J. Stem Cells* **2015**, *7*, 116–125. [CrossRef] [PubMed]
13. Warren, L.; Manos, P.D.; Ahfeldt, T.; Loh, Y.H.; Li, H.; Lau, F.; Ebina, W.; Mandal, P.K.; Smith, Z.D.; Meissner, A.; et al. Highly efficient reprogramming to pluripotency and directed differentiation of human cells with synthetic modified mRNA. *Cell Stem Cell* **2010**, *7*, 618–630. [CrossRef] [PubMed]
14. Yoshioka, N.; Gros, E.; Li, H.R.; Kumar, S.; Deacon, D.C.; Maron, C.; Muotri, A.R.; Chi, N.C.; Fu, X.D.; Yu, B.D.; et al. Efficient generation of human iPSCs by a synthetic self-replicative RNA. *Cell Stem Cell* **2013**, *13*, 246–254. [CrossRef] [PubMed]
15. Wu, Q.; Yang, B.; Hu, K.; Cao, C.; Man, Y.; Wang, P. Deriving Osteogenic Cells from Induced Pluripotent Stem Cells for Bone Tissue Engineering. *Tissue Eng. Part B Rev.* **2017**, *23*, 1–8. [CrossRef] [PubMed]

16. Zhao, Q.; Gregory, C.A.; Lee, R.H.; Reger, R.L.; Qin, L.; Hai, B.; Park, M.S.; Yoon, N.; Clough, B.; McNeill, E.; et al. MSCs derived from iPSCs with a modified protocol are tumor-tropic but have much less potential to promote tumors than bone marrow MSCs. *Proc. Natl. Acad. Sci. USA* **2015**, *112*, 530–535. [CrossRef] [PubMed]
17. Steens, J.; Klein, D. Current Strategies to Generate Human Mesenchymal Stem Cells In Vitro. *Stem Cells Int.* **2018**, *2018*, 6726185. [CrossRef] [PubMed]
18. Luzzani, C.; Neiman, G.; Garate, X.; Questa, M.; Solari, C.; Fernandez Espinosa, D.; Garcia, M.; Errecalde, A.L.; Guberman, A.; Scassa, M.E.; et al. A therapy-grade protocol for differentiation of pluripotent stem cells into mesenchymal stem cells using platelet lysate as supplement. *Stem Cell Res. Ther.* **2015**, *6*, 6. [CrossRef] [PubMed]
19. Takahashi, M. Retinal Cell Therapy Using iPS Cells. *Nippon Ganka Gakkai Zasshi* **2016**, *120*, 210–224; discussion 225. [PubMed]
20. Cynata Therapeutics Limited. *A Study of CYP-001 for the Treatment of Steroid-Resistant Acute Graft versus Host Disease*; Cynata Therapeutics Limited: Carlton, Australia, 2017.
21. Avci-Adali, M.; Behring, A.; Steinle, H.; Keller, T.; Krajeweski, S.; Schlensak, C.; Wendel, H.P. In vitro synthesis of modified mRNA for induction of protein expression in human cells. *J. Vis. Exp. JoVE* **2014**. [CrossRef] [PubMed]

Cellular Physiology and Biochemistry

Cell Physiol Biochem 2018;51:1193-1206
DOI: 10.1159/000495497
Published online: 24 November 2018
Accepted: 16 November 2018

Original Paper

Comparative Study of MSCA-1 and CD146 Isolated Periosteal Cell Subpopulations

Felix Umrath[a] Carla Thomalla[a] Simone Pöschel[b] Katja Schenke-Layland[b] Siegmar Reinert[a] Dorothea Alexander[a]

[a]Department of Oral and Maxillofacial Surgery of the University Hospital of Tübingen, Tübingen, [b]Department of Women's Health of the Eberhard-Karls University Tübingen, Tübingen, Germany

Key Words
Cranial periosteal cells • MSCA-1 • CD146 • Multispectral imaging flow cytometry • Cell sorting

Abstract
Background/Aims: Periosteal tissue is a valuable source of multipotent stem cells for bone tissue engineering. To characterize these cells in detail, we generated an immortalized human cranial periosteal cell line and observed an increased MSCA-1 and CD146 expression, as well as an earlier and stronger mineralization compared to the parental cells. Further, we detected a higher osteogenic potential of MSCA-1^{high} compared to MSCA-1^{low} cranial periosteal cell (CPC) fractions. In the present study, a possible synergism of MSCA-1 and CD146 for periosteal cell mineralization was investigated. ***Methods:*** MSCA-1/CD146 positive and negative CPCs were magnetically isolated (MACS) or sorted by flow cytometry (FACS) and subjected to osteogenic differentiation. The expression of osteogenic marker genes in the four subpopulations was analyzed by quantitative real-time PCR. Furthermore, the co-expression of osteogenic markers/antigens was analyzed by multispectral imaging flow cytometry (ImageStream, AMNIS). The mineralization potential was assessed by the quantification of alizarin stainings. ***Results:*** While the total cell yield after separation was higher using MACS compared to the FACS approach, the isolation of MSCA-1$^{+/-}$ and CD146$^{+/-}$ subpopulations was more efficient with the FACS separation. The accuracy of the FACS separation of the four distinguished cell subpopulations was confirmed by multispectral imaging flow cytometry. Further, we detected increasing levels of MSCA-1 and CD146 during *in vitro* differentiation in all subpopulations. However, MSCA-1 expression was significantly higher in the MSCA-1$^+$/CD146$^+$ and MSCA-1$^+$/CD146$^-$ subpopulations, while CD146 expression remained clearly lower in these fractions. Significantly higher gene expression levels of osteogenic markers, *ALP* and *RUNX2*, were detected in MSCA-1$^+$ compared to MSCA-1$^-$ CPCs at different time points during *in vitro* differentiation.Staining and quantification of calcium phosphate precipitates revealed a significantly higher mineralization potential of MACS separated MSCA-1$^+$ and CD146$^-$ CPCs, compared to their respective counterparts. FACS sorted CPCs displayed earlier mineralization in both MSCA-1$^+$ fractions (d13), while later (d28) only the CD146$^+$/MSCA-1$^-$ fraction had a significantly lower calcium phosphate concentration compared to all other fractions.

Dorothea Alexander-Friedrich

Dept. of Oral and Maxillofacial Surgery, University Hospital of Tübingen
Osianderstr. 2-8, 72076 Tübingen (Germany)
Tel. +49/70712982418, E-Mail dorothea.alexander@med.uni-tuebingen.de

Conclusion: Our results demonstrate, that MSCA-1^{+} cells isolated from CPCs represent a subpopulation with a higher osteogenic potential. In contrast, we found a lower osteogenic potential in CD146^{+} CPCs. In conclusion, only MSCA-1, but not CD146, is a suitable marker for the isolation of osteoprogenitors from CPCs.

Introduction

Periosteum, the thin membrane surrounding and nourishing the bones, contains osteoprogenitor cells in the inner layer, which can form new bone tissues. It's properties and the potential of periosteum derived mesenchymal stromal cells (MSCs) in bone tissue engineering has been reviewed in detail by Ferretti and Mattioli-Belmonte [1]. In the field of oral and maxillofacial surgery, especially oral and cranial periosteal cells are a promising source for new cell based bone reconstruction therapies, and therefore need to be characterized in detail [2].

To increase the quality of patient derived periosteal MSCs, markers for the isolation of pure osteoprogenitor cells need to be identified.

Previously, we demonstrated that the MSCA-1-enriched subpopulation from the human jaw periosteal tissue exhibits higher osteogenic potential compared to the MSCA-1^{low} cell fraction [3]. Furthermore, we generated an immortalized cell line derived from the human cranial periosteum and analyzed its features in comparison with the primary cells from which the cell line was derived [4]. Due to the different origin and significantly higher CD146 (MUC-18, MCAM) surface expression by the SV40 T antigen immortalized cranial periosteal cells, we aimed to analyze the osteogenic potential of the MSCA-1$^{+/-}$ and CD146$^{+/-}$ subpopulations isolated from this cell line in the present study.

Multipotent mesenchymal stromal cells (MSCs) are identified by the cell surface expression of the following markers: CD73, CD90 or CD105 [5, 6]. MSCA-1 was described to coincide with the tissue non-specific alkaline phosphatase (TNAP) [7] and to be expressed by MSCs from different tissues [3, 8-12].

Patients with TNAP deficiency suffer from bone abnormalities caused by hypomineralization [13, 14]. TNAP hydrolyzes inorganic pyrophosphates, which normally inhibit calcium phosphate formation within the extracellular matrix [15]. Based on two different promoter regions, tissue-related differences in alkaline phosphatase exist in the bones, liver and kidneys [16]. In addition to its role in bone development, TNAP exerts several other functions in liver/kidney, promotes vessel calcification, and plays a role in the neuron/brain development, as reviewed in the recent study by Esteve and co-authors [17].

Pericytes stabilize microvessels and play an important role in the regeneration of vascularized tissues and instructing extravasating leucocytes towards their target by motility programs [18]. A perivascular origin of multipotent MSCs isolated from different human tissues has been hypothesized [19]. CD146 is also described as highly expressed in human bone marrow stromal cells (also known as mesenchymal stem cells), which generate osteogenic cells among other cell lineages. *In situ*, osteoblasts and bone-lining cells do not express CD146 [20].

According to our experience, jaw and cranial periosteal cells are normally CD146 negative. The primary cranial periosteal cells, creating the parental cells to the immortalized cell line used in the present work, showed a low CD146 expression. However, the resulting immortalized cells were 70-80% CD146 positive, as previously described [4].

The goal of this study was to determine whether the high CD146 surface expression of immortalized periosteal cells (TAg cells) correlates with the high mineralization capacity as compared to the primary cells from which they derive. Furthermore, we also compared the osteogenic potential of isolated MSCA-1$^{+/-}$ and CD146$^{+/-}$ subpopulations in the present study.

Materials and Methods

Cell isolation and culture

As previously described [4], we generated a human SV40 T-antigen immortalized cranial periosteal cell line, referred to as TAg cells in this article. The work with the cells included in this paper was approved by the local ethics committee (approval number 534/2013BO1) and carried out after written consent of the patient.

TAg cells were cultured in DMEM/F-12 (Thermo Fisher Scientific, Waltham, Massachusetts, USA) containing 10% FCS (Sigma-Aldrich, Steinheim, Germany), 1% amphotericin B (Biochrom, Berlin, Germany) and penicillin/streptomycin (Lonza, Basel, Switzerland) in the presence of 0.25 mg/ml G418 (immortalization maintenance dose). DMEM-cultured cells were passaged using trypsin-versene (1x, Lonza, Basel, Switzerland) every three or four days.

Magnetic separation of the MSCA-1$^{+/-}$ and CD146$^{+/-}$ cell subpopulations

The entire TAg periosteal cell population was subjected to magnetic separation to isolate the MSCA-1$^{+/-}$ and CD146$^{+/-}$ cell fractions as previously described [21]. In brief, TAg cells were incubated with the FcR blocking reagent and anti-MSCA-1/-CD146 MicroBeads (Miltenyi Biotec, Bergisch Gladbach, Germany) for 20 min at 4°C. After washing, the samples were applied to pre-separation filters and then onto MS columns. The MSCA-1^{+}/CD146^{+} cells remained within the columns in the magnetic field. After removing the columns from the magnetic field, positive fractions could be eluted.

Separation of the MSCA-1$^{+/-}$/CD146$^{+/-}$ cell subpopulations by FACS

The TAg cells were subjected to fluorescence-activated cell sorting (FACS) to isolate four distinct fractions: P1: CD146^{+}/MSCA-1^{-}, P2: CD146^{+}/MSCA-1^{+}, P3: CD146^{-}/MSCA-1^{-} and P4: CD146^{-}/MSCA-1^{+}. TAg cells were double-stained with specific anti-MSCA-1-PE and anti-CD146-APC antibodies, and separated into four fractions by fluorescence activated cell sorting (FACS), according to the gates shown in Fig. 1.

Cells were harvested using trypsin-versene (1x, Lonza, Basel, Switzerland) and incubated on ice for 15 min in 20 µl/10^{6} blocking buffer (PBS, 0.1% BSA, 10% Gamunex (human immune globulin solution, Talecris Biotherapeutics GmbH, Frankfurt, Germany)). 50 µl/10^{6} cells FACS-buffer (PBS, 0.1% BSA), 10 µl/10^{6} cells anti-MSCA-1-PE antibody (Miltenyi Biotec, Bergisch Gladbach, Germany) and 5 µl/10^{6} cells anti-CD146-APC (Miltenyi Biotec) were added und incubated on ice for 20 min. Cells were washed twice with 1 ml/10^{6} cells FACS-buffer, suspended in 50 µl/10^{6} cells PBS and transferred into 5 ml FACS-tubes. Sorting was performed

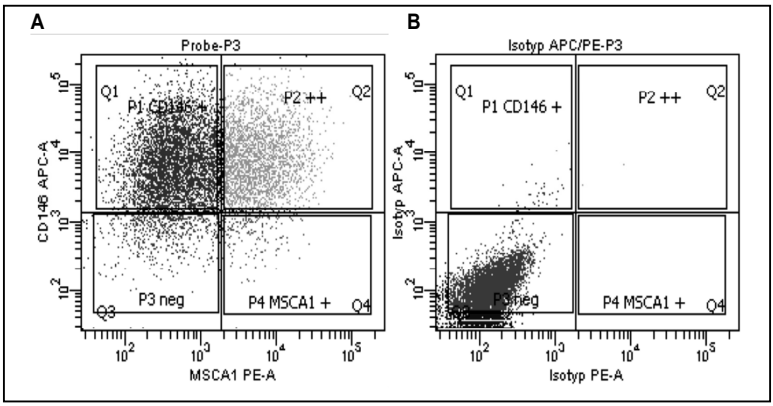

Fig. 1. Representative dot blots and gating strategy for the separation of MSCA-1$^{+/-}$/CD146$^{+/-}$ subpopulations by FACS. A) anti-MSCA-1-PE and anti-CD146-APC stained sample B) anti-IgG1-PE and anti-IgG1-APC stained isotype control.

with a FACSaria I cell sorter (BD Biosciences, Franklin Lakes, USA) using FACSDiva software version 6.1.3. Gates were set on the basis of IgG1-PE (R&D Systems, Inc., Minneapolis, USA) and IgG1-APC (BioLegend, San Diego, USA) isotype controls, which were prepared in parallel. Sorted cells were collected in 5 ml FACS-tubes containing 1 ml DMEM/F12 containing 50% FBS.

Table 1. Antibodies used for FACS and imaging flow cytometry

Antigen	Isotype	Conjugate	Company	Product-No.
MSCA-1	mouse IgG1	PE	MACS Miltenyi	130-093-587
CD146	mouse IgG1	APC	MACS Miltenyi	130-097-942
OCN	mouse IgG1	AlexaFluor 488	R&D Systems	IC1419G
RUNX2	mouse IgG2a	-	Abcam	ab76956
ALPL	mouse IgG1	-	R&D Systems	MAB1448
mouse IgG1	goat polyclonal Ig	DyLight 405	BioLegend	409109
mouse IgG2	rat IgG	PE-Cy7	BioLegend	407114
-	mouse IgG1	APC	BioLegend	400122
-	mouse IgG1	PE	R&D Systems	IC002P

Osteogenic differentiation of sorted TAg cell fractions

Following FACS sorting, separated TAg cell fractions (P1-P4) were seeded into 6 well plates at a density of $3 \cdot 10^4$ cell/well (n = 3 independent samples for each cell subpopulation). Three days later, osteogenic induction was initiated using an osteogenic medium (Ob - DMEM/F12 containing 10% FCS, 10 mM β-glycerophosphate, 100 µM L-ascorbic acid 2-phosphate and 4 µM dexamethasone, Sigma-Aldrich), and medium was changed every other day. Control samples (undifferentiated) were cultured in DMEM/F12 containing 10% FCS (Co). Osteogenic differentiation was carried out for 13, 20 and 28 days before cells were fixed and stained using Alizarin S. Cells were analyzed by imaging flow cytometry after 2, 5 and 10 days of osteogenic differentiation. Gene expression analysis was carried out after 2, 5, and 10 days of osteogenic differentiation.

Multispectral imaging flow cytometry analysis of sorted MSCA-1$^{+/-}$/CD146$^{+/-}$ cell fractions

Following osteogenic differentiation for 2, 5 and 10 days, cells were harvested from the culture plates using trypsin-versene (1x, Lonza, Basel, Switzerland). From each fraction and culture condition, cells of three independent wells were pooled and blocked with 10% Gamunex for 15 min. Surface antigens MSCA-1 and CD146 were labeled with specific mouse anti-human anti-CD146-APC and anti-MSCA-1-PE antibodies (Miltenyi Biotec), as previously described. For intracellular staining, cells were permeabilized by incubation with fixation/permeabilization solution (BD Biosciences) for 20 min and washed with BD Perm/Wash™ buffer (BD Biosciences, Franklin Lakes, USA). To prevent unspecific binding intracellular staining was carried out in 50 µl BD Perm/Wash™ buffer containing 10% Gamunex. Intracellular antigens were stained using directly labeled mouse anti-human anti-OCN-AlexaFluor488 (R&D Systems, Inc., Minneapolis, USA) and unlabeled mouse anti-human anti-RUNX2 (Abcam, Cambridge, UK) and mouse anti-human anti-ALPL (R&D Systems, Inc., Minneapolis, USA) primary antibodies. Primary antibodies were captured with goat anti-mouse anti-IgG1-DyLight405 and rat anti-mouse anti-IgG2-PE-Cy7 secondary antibodies (BioLegend, San Diego, USA). Cells incubated with PE-, APC- and AlexaFluor488-labeled isotype antibodies and DyLight405- and PE-Cy7-labeled secondary antibodies served as negative controls. All antibodies used for FACS and multispectral imaging flow cytometry are listed in Table 1. After staining, cells were resuspended in 50 µl BD Perm/Wash™ Buffer (BD Biosciences). Imaging flow cytometry was carried out with the ImageStream®X Mark II Imaging Flow Cytometer (Merck Millipore, Billerica, USA) using INSPIRE software. For data evaluation, IDEAS software version 6.0 was used.

Analyses of the osteogenic potential of MSCA-1$^{+/-}$/CD146$^{+/-}$ cell monolayers

TAg cells sorted using MACS and FACS (n = 3 independent samples for each cell subpopulation and experiment) were differentiated for 13, 20 and 28 days as described previously. Subsequently, the cell monolayers were fixed for 15 min at RT with 4% formalin. After washing with PBS, a pH 4.2, 40 mM Alizarin red dye solution was added and incubated for 30 min while shaking. Thereafter, cell monolayers were intensively washed with ddH_2O and visualized using an inverse microscope. For quantification, bound Alizarin red dye was dissolved using acetic acid, and cell monolayers were scraped off from the plates. Samples were heated at 85°C for 10 min, cooled down for 5 min on ice and centrifuged for 15 min at 20,

000 g. After neutralization with 10% ammonium hydroxide, samples were measured at 405 nm using a microplate reader (BioTek Instruments GmbH, Bad Friedrichshall, Germany), and calcium concentrations were calculated in relation to a standard curve (0.002-0.2 mM).

Gene expression analysis of sorted MSCA-1$^{+/-}$/CD146$^{+/-}$ cell fractions by quantitative PCR

Gene expression of FACS separated cell populations was performed after 2, 5 and 10 days of osteogenic differentiation with Ob-medium and compared to untreated cells (Co). RNA isolation from sorted TAg cells (n = 3 independent samples for each cell subpopulation) was carried out using the NucleoSpin RNA XS kit (Macherey-Nagel, Düren, Germany) following the manufacturer's instructions. The amount of isolated RNA was measured and quantified with a Qubit 3.0 fluorometer and the provided RNA HS Assay Kit (Thermo Fisher Scientific Inc., Waltham, USA). 0.5 µg of RNA was used for first-strand cDNA synthesis using the Advantage RT-for-PCR Kit (Clontech Laboratories, Mountain View, USA) following the manufacturer's instructions.

The quantification of mRNA expression levels was performed using the real-time LightCycler System (Roche Diagnostics, Mannheim, Germany). For the PCR reactions, commercial primer kits (Search LC, Heidelberg, Germany) and DNA Master Sybr Green I (Roche, Basel, Switzerland) were used. The amplification was performed following a touchdown PCR protocol of 40 cycles (annealing temperature between 68-58°C), following the manufacturer's instructions. The transcript levels were normalized to those of the housekeeping gene glycerinaldehyde 3-phosphate dehydrogenase (GAPDH), and illustrated as a ratio of the target versus housekeeping gene transcripts.

Statistical analysis

Statistical analyses were performed using the unpaired t-test. A p-value < 0.05 was considered statistically significant.

Results

Separation of MSCA-1 and CD146 labeled subpopulations by MACS and FACS

Efficiencies of MACS separations. The magnetic separations using the specific anti-MSCA-1 antibodies resulted in an average total cell yield of 62.65 ± 12.51%. Thereof, 86.64 ± 1.56% were MSCA-1-negative, and 13.36 ± 1.56 % were MSCA-1-positive, as shown in Table 2. The magnetic separations using the specific CD146 antibodies resulted in a very similar average total cell yield of 62.88 ± 11.69%. Thereof, 83.64% ± 6.68 were CD146$^-$, and 16.36% ± 6.68 were CD146$^+$, as shown in Table 3.

Efficiencies of FACS separations. FACS sorting (n = 5) resulted in an average total cell yield of 40.74 ± 8.76 % (Table 4), which is considerably lower than the cell yield after MACS separation (62.88 ± 11.69 %). The total number of sorted cells from the four subpopulations and the total cell yields (%) are given in Table 4. Fig. 2 illustrates the distribution of the four subpopulations after sorting, with CD146$^+$/MSCA-1$^-$ being the most abundant subpopulation (55.79 ± 7.81 %), and CD146$^-$/MSCA-1$^+$ being the rarest subpopulation (3.65 ± 0.85 %). The double positive subpopulation CD146$^+$/MSCA-1$^+$ and the double negative subpopulation CD146$^-$/MSCA-1$^-$ were represented with 29.84 ± 7.81 %, and 10.72 ± 2.83 % respectively. We detected clear differences in terms of separation efficiencies between MACS and FACS separation. While the percentage of MSCA-1$^+$ and CD146$^+$ cells using MACS separation averaged 13.4 ± 1.56 % and 16.36 ± 6.68 % respectively, MSCA-1$^+$ and CD146$^+$ fractions separated by FACS were significantly higher with 33.49 ± 8.39 % and 85.63 ± 3.15 % respectively. These results indicate a very low accuracy of the MACS separation, especially for CD146.

Table 2. Overview of the performed magnetic separations (n = 4) using the anti-MSCA-1 antibodies. Total cell numbers and their percentages before and after separations

Cell numbers before separation	Total number of MSCA-1$^+$ cells	Total number of MSCA-1$^-$ cells	Total cell yield (%)	Amount of cells (%)	
				MSCA-1$^+$	MSCA-1$^-$
1. 1.23E+08	6.94E+06	5.11E+07	47.30	11.96	88.04
2. 1.54E+08	1.38E+07	7.49E+07	57.60	15.57	84.43
3. 6.75E+07	6.52E+06	4.29E+07	73.21	13.19	86.81
4. 9.71E+07	8.96E+06	6.14E+07	72.50	12.73	87.27
Average cell yield and amount of MSCA-1$^{+/-}$ cells			62.65±12.51	13.4±1.56	86.64±1.56

Table 3. Overview of the performed magnetic separations (n = 4) using the anti-CD146 antibodies. Total cell numbers and their percentages before and after separations

Cell numbers before separation	Total number of separated		Total cell yield (%)	Amount of cells (%)	
	CD146$^+$ cells	CD146$^-$ cells		CD146$^+$	CD146$^-$
1. 1.15E+08	1.82E+07	5.66E+07	64.90	24.35	75.65
2. 1.04E+08	4.70E+06	4.38E+07	46.59	9.69	90.31
3. 1.13E+08	1.03E+07	7.41E+07	74.43	12.20	87.80
4. 9.99E+07	1.26E+07	5.30E+07	65.62	19.22	80.78
Average cell yield and amount of CD146$^{+/-}$ cells			62.88±11.69	16.36±6.68	83.64±6.68

Table 4. Overview of the performed FACS sorting (n = 5) using both anti-MSCA-1 and anti-CD146 antibodies. Total cell numbers before FACS separation, number of cells separated, and percentage of cells recovered after sorting

Cell numbers before separation	Total number of separated cells				Total cell yield (%)
	MSCA-1$^-$/CD146$^+$	MSCA-1$^+$/CD146$^+$	MSCA-1$^-$/CD146$^-$	MSCA-1$^+$/CD146$^-$	
1. 6.10E+07	1.45E+07	6.29E+06	2.43E+06	7.53E+05	39.31
2. 7.50E+07	1.28E+07	7.65E+06	2.45E+06	1.06E+06	31.99
3. 6.00E+07	1.36E+07	4.12E+06	1.66E+06	3.65E+05	32.97
4. 3.80E+07	9.86E+06	4.39E+06	1.62E+06	5.51E+05	43.21
5. 3.31E+07	1.07E+07	4.00E+06	3.19E+06	6.71E+05	56.20
Average total cell yield					40.74±8.76

Osteogenic potential of MACS separated TAg cells

Fig. 3 illustrates the Alizarin red staining for the visualization of calcium phosphate precipitates formed within the monolayers of the four magnetically isolated cell fractions after 20 days of osteogenic differentiation (upper panel). The osteogenic pattern of the MSCA-1$^{+/-}$ fractions was as expected, and previously observed in the primary cells from which the TAg cells were derived. MSCA-1$^+$ TAg cells showed a higher mineralization degree in comparison with the MSCA-1$^-$ cells. Surprisingly, the CD146 isolated cell fractions showed an opposite pattern. CD146$^-$ TAg cells showed a higher mineralization potential than the CD146$^+$ cells. The mineralization pattern representatively visualized in Fig. 3 was confirmed by exact quantification of the Alizarin dye bound to the four analyzed TAg cell monolayers after osteogenic induction, as illustrated in the lower panel of Fig. 3.

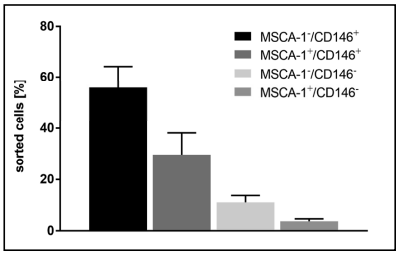

Fig. 2. Average distribution (%) of MSCA-1$^{+/-}$/CD146$^{+/-}$ subpopulations sorted by FACS (n=8).

Calcium concentrations did not differ significantly between the unstimulated controls of the MSCA$^{+/-}$ and CD146$^{+/-}$ fractions. However, we detected significantly higher calcium concentrations in osteogenically induced MSCA-1$^+$ (0.16 ± 0.03 mM versus the corresponding negative fraction with 0.07 ± 0.03 mM, p< 0.01) and CD146$^-$ TAg cells (0.10 ± 0.05 mM versus the corresponding positive fraction with 0.05 ± 0.03 mM, p < 0.05).

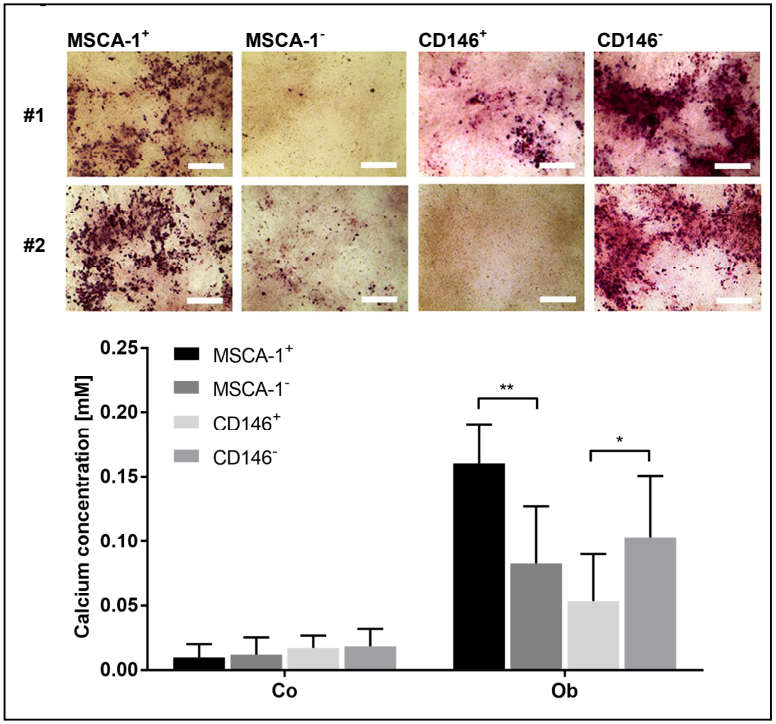

Fig. 3. Upper Panel: Staining of calcium phosphate precipitates formed by MACS separated MSCA-1$^{+/-}$ and CD146$^{+/-}$ fractions by Alizarin red after 20 days of osteogenic differentiation. Representative bright-field images (4x magnification) of differentiated MSCA-1$^{+/-}$ and CD146$^{+/-}$ TAg cells from two independent separations (#1 and #2). Scale bars equal 500 µm. A higher mineralization potential (precipitates stained red) was detected in MSCA-1^{+} and CD146^{-} TAg cells. Lower panel: Quantification of calcium precipitates in unstimulated and osteogenically differentiated MSCA-1$^{+/-}$ and CD146$^{+/-}$ TAg cells. Calcium concentrations (mM) were quantified after dissolving the Alizarin dye from the stained monolayers. Significantly higher calcium concentrations were detected in magnetically separated (A) CD146^{-} cell fractions (* $p<0.05$) and (B) MSCA-1^{+} (* $p<0.01$) of the entire TAg cell population. Co – unstimulated cells, Ob – osteogenically induced cells.

Osteogenic potential of FACS separated TAg cells

Fig. 4 illustrates the Alizarin red staining for the visualization of calcium phosphate precipitates formed within the monolayers of the four FACS separated subpopulations of TAg cells after 13 days of osteogenic differentiation (upper panel). As already observed after MACS separation, MSCA-1^{+} subpopulations showed a higher mineralization potential than MSCA-1^{-} subpopulations. Furthermore, the MSCA-1^{+}/CD146^{-} fraction showed clearly higher amounts of calcium phosphate precipitates than the double-positive MSCA-1^{+}/CD146^{+} fraction. This corresponds to the negative correlation of CD146 expression and mineralization, previously observed in MACS sorted CD146^{+} cell fractions. MSCA-1^{-}/CD146^{-} subpopulations showed little, and MSCA-1^{-}/CD146^{+} subpopulations showed little to no mineralization after 13 days of differentiation, which further supports the previous observation.

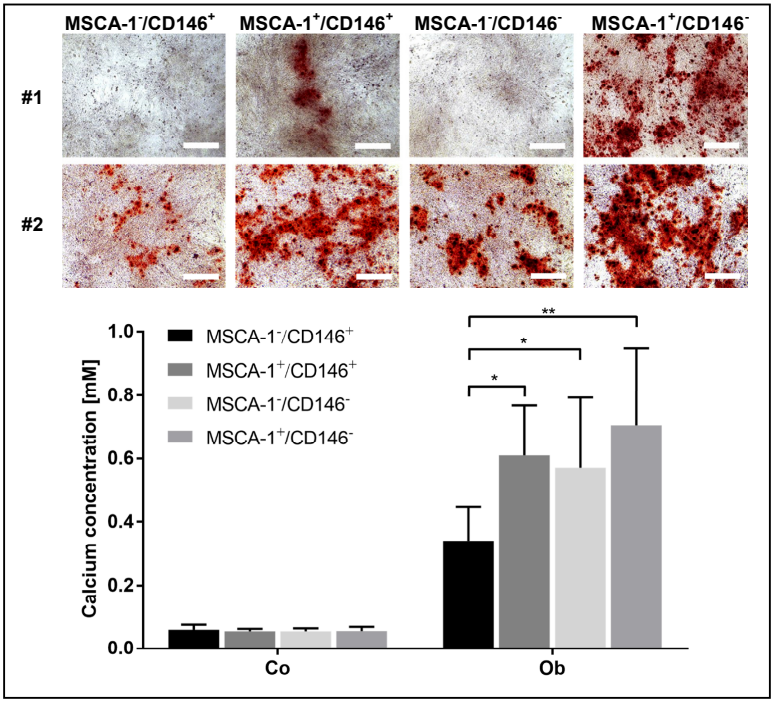

Fig. 4. Upper Panel: Staining of calcium phosphate precipitates formed by FACS separated MSCA-1$^{+/-}$/CD146$^{+/-}$ fractions by Alizarin red after 13 days of osteogenic differentiation. Representative bright-field images (4x magnification) of differentiated MSCA-1$^{+/-}$/CD146$^{+/-}$ TAg cells from two independent separations (#1 and #2). Scale bars equal 500 µm. Similarly, as observed in MACS sorted cell fractions (Fig. 3), a higher mineralization potential (precipitates stained red) was detected in MSCA-1^{+} and CD146^{-} TAg cell subpopulations. Lower panel: Quantification of calcium precipitates formed by FACS sorted MSCA-1$^{+/-}$/CD146$^{+/-}$ TAg cell subpopulations after 28 days of osteogenic differentiation. Calcium concentrations (mM) were quantified after dissolving the Alizarin dye from the stained monolayers. We detected significantly lower calcium concentrations (* $p<0.05$, ** $p<0.01$) in the MSCA-1^{-}/CD146^{+} fraction compared to all other fractions of the entire TAg cell population. Co – unstimulated cells, Ob – osteogenic induced cells.

For calcium quantification, the sorted TAg cells were incubated in osteogenic medium for 28 days (lower panel). While differences in the mineralization were clearly visible at day 13 (upper panel), strong mineralization was observed in all sorted cell fractions at day 28.

Calcium concentrations in Fig. 4 show similar tendencies as previously observed in MACS separated cell cultures (Fig. 3). As expected, we observed a higher mineralization potential of MSCA-1^{+} subpopulations compared to MSCA-1^{-} subpopulations. The highest calcium concentration was measured in the MSCA-1^{+}/CD146^{-} fraction (0.70 ± 0, 08 mM), followed by the double positive (MSCA-1^{+}/CD146^{+}, 0.61 ± 0.05 mM) and the double negative (MSCA-1^{-}/CD146^{-}, 0.57 ± 0.07 mM) fraction. Significantly lower calcium concentrations were detected in the MSCA-1^{-}/CD146^{+} cell fraction (0.34 ± 0.04 mM) indicating a clearly reduced mineralization potential of this subpopulation.

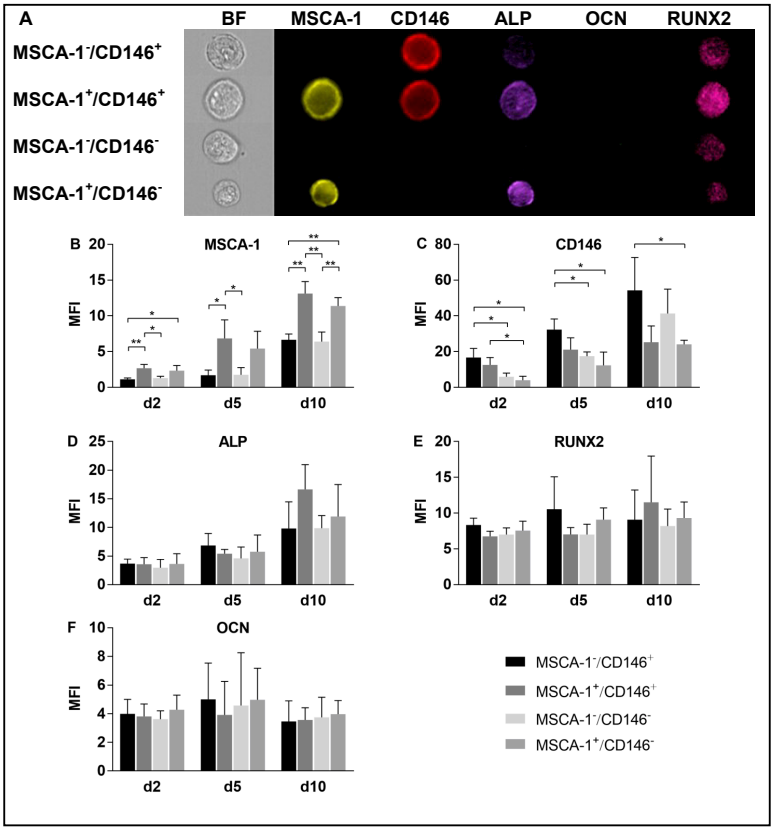

Fig. 5. A: Representative images of MSCA-1$^{+/-}$/CD146$^{+/-}$ separated cells analyzed by multispectral imaging flow cytometry after 5 days of osteogenic differentiation. Cells were labeled simultaneously with (yellow) anti-MSCA-1-PE, (red) anti-CD146-APC, (purple) anti-ALP + anti-IgG1-DyLight405 (permeabilized), (magenta) anti-RUNX2 + anti-IgG2a-PE-Cy7 (permeabilized) and (green) anti-OCN-AlexaFluor488 (permeabilized) antibodies. Lower panel: Median fluorescence indices (MFI) of FACS sorted MSCA-1$^{+/-}$/CD146$^{+/-}$ subpopulations after 2, 5 and 10 days of osteogenic differentiation, labeled with (B) anti-MSCA-1-PE, (C) anti-CD146-APC, (D) anti-ALP + anti-IgG1-DyLight405 (permeabilized), (E) anti-RUNX2 + anti-IgG2a-PE-Cy7 (permeabilized) and (F) anti-OCN-AlexaFluor488 (permeabilized) antibodies (n=3, * p<0.05).

Intra- and extracellular marker expression analysis by imaging flow cytometry

Osteogenic marker expression of FACS separated MSCA-1$^{+/-}$/CD146$^{+/-}$ subpopulations was analyzed after 2, 5 and 10 days of osteogenic differentiation (n = 3) by multispectral imaging flow cytometry (Fig. 5A). Coexpression of five different markers (MSCA-1, ALP, CD146, OCN, RUNX2) was analyzed and median fluorescence index (MFI) values were calculated (Fig. 5B-F). As expected, MFI values of MSCA-1 labeled subpopulations (Fig. 5B) (cell surface) were significantly higher in the two MSCA-1^{+} sorted subpopulations at day 2 of osteogenic induction. During the course of osteogenic differentiation, MSCA-1 expression

increased in all separated subpopulations, but remained significantly higher in the MSCA-1^+/$CD146^+$ and MSCA-1^+/$CD146^-$ subpopulation. This result correlates with the above mentioned higher mineralization potential of MSCA-1^+ sorted subpopulations, observed after 13 and 28 days of osteogenic differentiation (Fig. 4).

Fig. 5C illustrates MFI values of CD146 (surface labeling) labeled, MSCA-$1^{+/-}$/$CD146^{+/-}$ sorted subpopulations. MFI values were significantly higher in the two $CD146^+$ sorted subpopulations at day 2 of osteogenic induction. Similar to MSCA-1, CD146 expression increased in all subpopulations during the differentiation period. While CD146 expression strongly increased in both MSCA-1^- sorted subpopulations until day 10, the surface expression remained clearly lower in the two MSCA-1^+ sorted subpopulations.

Intracellular ALP expression (Fig. 5D) shows a similar pattern as MSCA-1 surface expression. After 2 and 5 days of differentiation, only minor differences in ALP expression were detectable between the four subpopulations. Until day 10, the expression increases in all subpopulations and is higher in the MSCA-1^+ sorted subpopulations, however without reaching statistical significance.

No significant differences could be detected concerning RUNX2 expression (Fig. 5E) during the experiment. Only at day 10, RUNX2 expression was slightly higher in MSCA-1^+ sorted subpopulations, revealing highest expression levels in the double positive population. These results are probably caused by an unspecific binding of the RUNX2 antibody resulting in a very high background signal.

Fig. 5F illustrates MFI values of OCN (intracellular labeling) labeled subpopulations. MFI values do not show any significant differences between the sorted subpopulations.

Quantitative gene expression analysis of ALP and RUNX2

Gene expression analysis was performed using a LightCycler instrument. Transcript levels were normalized to those of the housekeeping gene glycerinaldehyde 3-phosphate dehydrogenase (*GAPDH*), and illustrated in Fig. 6 as a ratio of the target versus the housekeeping gene transcripts.

As already detected on protein level by imaging flow cytometry, Fig. 6A shows increasing *ALP* gene expression during the osteogenic differentiation in all samples. Similarly, the two MSCA-1^+ subpopulations showed clearly higher expression levels than the MSCA-1^- subpopulations at the 3 time points analyzed.

RUNX2 gene expression was higher in both MSCA-1^+ subpopulations compared to the two MSCA-1^- subpopulations throughout the differentiation period, with the most significant differences detected at day 5 (Fig. 6B).

These results correlate with the previously shown mineralization pattern and the marker expression of the four sorted subpopulations.

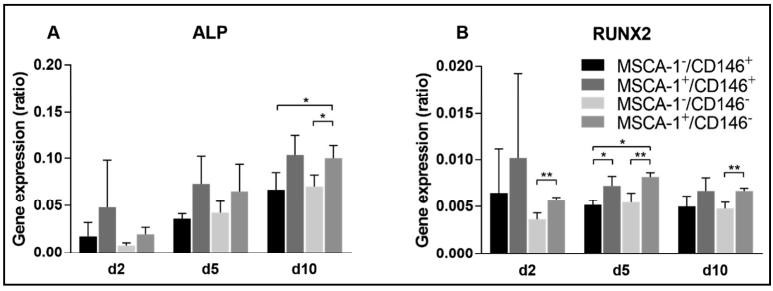

Fig. 6. A) ALP and B) RUNX2 gene expression (ratio of the target versus housekeeping (GAPDH) gene transcripts) in FACS sorted MSCA-$1^{+/-}$, $CD146^{+/-}$ subpopulations after 2, 5 and 10 days of osteogenic differentiation (n = 3, * $p \leq 0.05$).

Discussion

In the present study, we analyzed the osteogenic potential of MACS and FACS separated MSCA-1$^{+/-}$ and CD146$^{+/-}$ cell fractions isolated from an immortalized cranial periosteal cell line. As a result, we found a higher osteogenic potential in MACS separated MSCA-1^{+} and CD146^{-} cell fractions in comparison to the opposite subpopulations.

The finding regarding the osteogenic potential of the MSCA-1^{+} subpopulation was expected based on our previous observation from human jaw periosteal cells [3]. The result concerning the osteogenic potential of the CD146^{-} subpopulation was quite surprising due to the detection of significantly higher CD146 expression and osteogenic potential at the same time in TAg cells when compared to the originating primary cells [4]. Thus, we had hypothesized a positive correlation of CD146 expression and cell mineralization but found the opposite.

FACS separation provided a much more efficient and accurate separation of MSCA-1 and CD146 labeled cells compared to MACS separation. The low efficiency of magnetic CD146 separation was also described in the current work of Harkness and co-authors [22]. They also obtained significantly higher efficiencies of CD146 enrichment from a mesenchymal stem cell line overexpressing a human telomerase, using FACS in comparison to MACS separation.

In addition, FACS permits the separation of all four MSCA-1$^{+/-}$/CD146$^{+/-}$ subpopulations at the same time and is therefore more suitable for a closer look at the MSCA-1$^{+/-}$ and CD146$^{+/-}$ fractions.

Osteogenic differentiation of FACS separated TAg cells confirmed the reliability of MSCA-1 as a positive marker for osteogenic differentiation. Both, the MSCA-1^{+}/CD146^{-} and the doubled-positive MSCA-1^{+}/CD146^{+} subpopulation showed a strong calcium phosphate precipitation and a high expression of osteogenic markers.

MSCA-1 is known to be identical to the tissue non-specific alkaline phosphatase (ALP) [7], which plays an essential role in bone mineralization [23]. Based on this knowledge it is not surprising to find a high expression of MSCA-1 on MSCs committed to the osteogenic lineage.

In contrast, the function in bone mineralization of CD146, corresponding to the melanoma cell adhesion molecule (MCAM), is unknown. Ulrich et al. previously reported a higher osteogenic potential of MACS separated CD146^{+} placenta-derived MSCs [24], however our results with MSCs from cranial periosteum showed the direct opposite. MACS separation led in our study to a negative correlation between CD146 expression and mineralization.

FACS separation into the four MSCA-1$^{+/-}$/CD146$^{+/-}$ subpopulations and subsequent imaging flow cytometry analysis revealed a more complex pattern of CD146 expression. On the one hand, we observed a significantly lower mineralization potential of the MSCA-1^{-}/CD146^{+} subpopulation, compared to all other fractions. On the other hand, we detected a high mineralization potential in the double-positive MSCA-1^{+}/CD146^{+} fraction. Here, the negative correlation of CD146 expression and mineralization was presumably masked by the effect of MSCA-1 expression, since a negative correlation between CD146 expression and mineralization remains when considering the MSCA-1^{+} and MSCA-1^{-} cells separately. Thus, we assume that CD146 plays only an indirect role during osteogenic differentiation.

In TAg cells, higher expression levels of both surface markers and a stronger mineralization potential were detected compared to the parental cells [4]. However, the present data indicates that CD146 expression does not play a key role for the osteogenic differentiation of cranial periosteal cells. Moreover, strong CD146 expression is probably a concomitant phenomenon in TAg cells or is related to the pericytic origin of the immortalized cells.

One possible explanation for lower mineralization potential in CD146^{+} cells is that CD146 defines a subset of CPCs which is committed to a non-osteogenic lineage. Espagnolle et al., for example, describe CD146 to be a marker for vascular smooth muscle cell commitment of bone marrow MSCs [25].

Another explanation could be a more naïve differentiation state of $CD146^+$ cells. Similar to our *in vitro* results, Harkness et al. reported that bone formation was significantly enhanced in subcutaneous implants containing $CD146^-$ cells, indicating a higher osteogenic potential of this fraction [22]. They also detected a higher plasticity and the ability of transendothelial migration of $CD146^+$ cells, which suggests that $CD146^+$ cells are recruited to the bone surfaces by chemotactic attraction, and the subsequent maturation to osteoblasts goes hand in hand with the loss of CD146 expression. Inconsistent to this, we found an increase in CD146 expression in all subpopulations during osteogenic differentiation as well as in the controls. A plausible explanation could be an induction of CD146 expression stimulated by the increasing confluency during the differentiation period. MCAM (CD146) is known to play a role in cell adhesion and cohesion [26] and a similar correlation between CD146 expression and cell density in HUVECs has been reported by Bardin et al. [27].

Conclusion

Taken together, we assume that the high CD146 expression in our TAg cells does not correlate with a high osteogenic potential, but is rather related to the immortalization, conferring migratory properties upon the TAg cells. However, we did not test this feature in the present study. Similarly to the herein examined TAg cells, SV40 T-antigen immortalized endothelial progenitor cells (EPCs) from human cord blood were shown to be strongly positive for CD146 [28], as well as hTERT immortalized EPCs [29]. A recent study describes CD146 expression in mouse $p19^{ARF-/-}$, which show longer tumor latency as $p53^{-/-}$ mice [30]. Loss of $p19^{ARF}$ is supposed to overcome senescence and allow infinite proliferation without gaining malignant properties.

We conclude, that the $MSCA\text{-}1^+$ subpopulation isolated from the human cranial periosteal cell line represents a subpopulation with higher osteogenic potential compared to the opposite fraction. Hence, the elevated MSCA-1 expression in the immortalized TAg cell line indicates it's higher osteogenic potential compared to the parental cells.

In contrast to MSCA-1, the elevated CD146 expression of the TAg cell line is primarily an osteogenesis independent phenomenon, which might be associated with the immortalization process.

Acknowledgements

This work was supported in part by a grant from the Ministry of Science, Research and Arts of Baden-Württemberg (Az.: SI-BW 01222-91) and the Deutsche Forschungsgemeinschaft DFG (German Research Foundation) (Az.: INST 2388/33-1).The works included in this study were approved by the local ethics committee (approval number 534/2013BO1).

Disclosure Statement

The authors of this publication declare no conflicts of interest.

References

1 Ferretti C, Mattioli-Belmonte M: Periosteum derived stem cells for regenerative medicine proposals: Boosting current knowledge. World J Stem Cells 2014;6:266-277.

2 Ceccarelli G, Graziano A, Benedetti L, Imbriani M, Romano F, Ferrarotti F, Aimetti M, Cusella de Angelis GM: Osteogenic Potential of Human Oral-Periosteal Cells (PCs) Isolated From Different Oral Origin: An *In vitro* Study. J Cell Physiol 2016;231:607-612.

3 Alexander D, Schafer F, Olbrich M, Friedrich B, Buhring HJ, Hoffmann J, Reinert S: MSCA-1/TNAP selection of human jaw periosteal cells improves their mineralization capacity. Cell Physiol Biochem 2010;26:1073-1080.
4 Alexander D, Biller R, Rieger M, Ardjomandi N, Reinert S: Phenotypic characterization of a human immortalized cranial periosteal cell line. Cell Physiol Biochem 2015;35:2244-2254.
5 Frenette PS, Pinho S, Lucas D, Scheiermann C: Mesenchymal Stem Cell: Keystone of the Hematopoietic Stem Cell Niche and a Stepping-Stone for Regenerative Medicine. Annual Review of Immunology 2013;31:285-316.
6 Dominici M, Le Blanc K, Mueller I, Slaper-Cortenbach I, Marini F, Krause D, Deans R, Keating A, Prockop D, Horwitz E: Minimal criteria for defining multipotent mesenchymal stromal cells. The International Society for Cellular Therapy position statement. Cytotherapy 2006;8:315-317.
7 Sobiesiak M, Sivasubramaniyan K, Hermann C, Tan C, Örgel M, Treml S, Cerabona F, de Zwart P, Ochs U, Müller CA, Gargett CE, Kalbacher H, Bühring H-J: The Mesenchymal Stem Cell Antigen MSCA-1 is Identical to Tissue Non-specific Alkaline Phosphatase. Stem Cells Dev 2009;19:669-677.
8 Devito L, Badraiq H, Galleu A, Taheem DK, Codognotto S, Siow R, Khalaf Y, Briley A, Shennan A, Poston L, McGrath J, Gentleman E, Dazzi F, Ilic D: Wharton's jelly mesenchymal stromal/stem cells derived under chemically defined animal product-free low oxygen conditions are rich in MSCA-1(+) subpopulation. Regen Med 2014;9:723-732.
9 Noort WA, Oerlemans MI, Rozemuller H, Feyen D, Jaksani S, Stecher D, Naaijkens B, Martens AC, Buhring HJ, Doevendans PA, Sluijter JP: Human versus porcine mesenchymal stromal cells: phenotype, differentiation potential, immunomodulation and cardiac improvement after transplantation. J Cell Mol Med 2012;16:1827-1839.
10 Esteve D, Boulet N, Volat F, Zakaroff-Girard A, Ledoux S, Coupaye M, Decaunes P, Belles C, Gaits-Iacovoni F, Iacovoni JS, Remaury A, Castel B, Ferrara P, Heymes C, Lafontan M, Bouloumie A, Galitzky J: Human white and brite adipogenesis is supported by MSCA1 and is impaired by immune cells. Stem Cells 2015;33:1277-1291.
11 Buhring HJ, Treml S, Cerabona F, de Zwart P, Kanz L, Sobiesiak M: Phenotypic characterization of distinct human bone marrow-derived MSC subsets. Ann N Y Acad Sci 2009;1176:124-134.
12 Battula VL, Treml S, Bareiss PM, Gieseke F, Roelofs H, de Zwart P, Muller I, Schewe B, Skutella T, Fibbe WE, Kanz L, Buhring HJ: Isolation of functionally distinct mesenchymal stem cell subsets using antibodies against CD56, CD271, and mesenchymal stem cell antigen-1. Haematologica 2009;94:173-184.
13 Hofmann C, Liese J, Schwarz T, Kunzmann S, Wirbelauer J, Nowak J, Hamann J, Girschick H, Graser S, Dietz K, Zeck S, Jakob F, Mentrup B: Compound heterozygosity of two functional null mutations in the ALPL gene associated with deleterious neurological outcome in an infant with hypophosphatasia. Bone 2013;55:150-157.
14 Whyte MP: Physiological role of alkaline phosphatase explored in hypophosphatasia. Ann N Y Acad Sci 2010;1192:190-200.
15 Orimo H: The mechanism of mineralization and the role of alkaline phosphatase in health and disease. J Nippon Med Sch 2010;77:4-12.
16 Matsuura S, Kishi F, Kajii T: Characterization of a 5'-flanking region of the human liver/bone/kidney alkaline phosphatase gene: two kinds of mRNA from a single gene. Biochem Biophys Res Commun 1990;168:993-1000.
17 Esteve D, Galitzky J, Bouloumie A, Fonta C, Buchet R, Magne D: Multiple Functions of MSCA-1/TNAP in Adult Mesenchymal Progenitor/Stromal Cells. Stem Cells Int 2016;2016:1815982.
18 Stark K, Eckart A, Haidari S, Tirniceriu A, Lorenz M, von Bruhl ML, Gartner F, Khandoga AG, Legate KR, Pless R, Hepper I, Lauber K, Walzog B, Massberg S: Capillary and arteriolar pericytes attract innate leukocytes exiting through venules and 'instruct' them with pattern-recognition and motility programs. Nat Immunol 2013;14:41-51.
19 Crisan M, Yap S, Casteilla L, Chen CW, Corselli M, Park TS, Andriolo G, Sun B, Zheng B, Zhang L, Norotte C, Teng PN, Traas J, Schugar R, Deasy BM, Badylak S, Buhring HJ, Giacobino JP, Lazzari L, Huard J, Peault B: A perivascular origin for mesenchymal stem cells in multiple human organs. Cell Stem Cell 2008;3:301-313.
20 Bianco P, Sacchetti B, Riminucci M: Osteoprogenitors and the hematopoietic microenvironment. Best Pract Res Clin Haematol 2011;24:37-47.

21 Olbrich M, Rieger M, Reinert S, Alexander D: Isolation of Osteoprogenitors from Human Jaw Periosteal Cells: A Comparison of Two Magnetic Separation Methods. PLoS One 2012;7:e47176.
22 Harkness L, Zaher W, Ditzel N, Isa A, Kassem M: CD146/MCAM defines functionality of human bone marrow stromal stem cell populations. Stem Cell Res Ther 2016;7:4.
23 Sapir-Koren R, Livshits G: Bone mineralization and regulation of phosphate homeostasis. IBMS BoneKEy 2011;8:286-300.
24 Ulrich C, Abruzzese T, Maerz JK, Ruh M, Amend B, Benz K, Rolauffs B, Abele H, Hart ML, Aicher WK: Human Placenta-Derived CD146-Positive Mesenchymal Stromal Cells Display a Distinct Osteogenic Differentiation Potential. Stem Cells Dev 2015;24:1558-1569.
25 Espagnolle N, Guilloton F, Deschaseaux F, Gadelorge M, Sensébé L, Bourin P: CD146 expression on mesenchymal stem cells is associated with their vascular smooth muscle commitment. J Cell Mol Med 2014;18:104-114.
26 Wang Z, Yan X: CD146, a multi-functional molecule beyond adhesion. Cancer Lett 2013;330:150-162.
27 Bardin N, Anfosso F, Massé J-M, Cramer E, Sabatier F, Bivic AL, Sampol J, Dignat-George F: Identification of CD146 as a component of the endothelial junction involved in the control of cell-cell cohesion. Blood 2001;98:3677-3684.
28 Qiu HY, Fujimori Y, Nishioka K, Yamaguchi N, Hashimoto-Tamaoki T, Sugihara A, Terada N, Nagaya N, Kanda M, Kobayashi N, Tanaka N, Westerman KA, Leboulch P, Hara H: Postnatal neovascularization by endothelial progenitor cells immortalized with the simian virus 40T antigen gene. Int J Oncol 2006;28:815-821.
29 Paprocka M, Krawczenko A, Dus D, Kantor A, Carreau A, Grillon C, Kieda C: CD133 positive progenitor endothelial cell lines from human cord blood. Cytometry A 2011;79:594-602.
30 Koudelkova P, Weber G, Mikulits W: Liver Sinusoidal Endothelial Cells Escape Senescence by Loss of p19ARF. PLoS One 2015;10:e0142134.

Hindawi
Stem Cells International
Volume 2017, Article ID 8303959, 10 pages
https://doi.org/10.1155/2017/8303959

Research Article

Platelet Lysate: The Better Choice for Jaw Periosteal Cell Mineralization

Yvonne Wanner,[1] Felix Umrath,[1] Marc Waidmann,[2] Siegmar Reinert,[1] and Dorothea Alexander[1]

[1]*Department of Oral and Maxillofacial Surgery, University Hospital in Tübingen, Tübingen, Germany*
[2]*Institute for Clinical and Experimental Transfusion Medicine, University Hospital in Tübingen, Tübingen, Germany*

Correspondence should be addressed to Dorothea Alexander; dorothea.alexander@med.uni-tuebingen.de

Received 24 August 2017; Revised 13 October 2017; Accepted 31 October 2017; Published 17 December 2017

Academic Editor: Luca Vanella

Previously, we demonstrated a high quality of minerals formed by serum-free cultured jaw periosteal cells (JPCs) by Raman spectroscopy but the mineralization extent was not satisfactory. In the present study, we analyzed the proliferation and mineralization potential of human platelet lysate- (hPL-) cultured JPCs in comparison to that of FCS-cultured JPCs. By cell impedance measurements, we detected significantly higher population doubling times of PL-cultured JPCs in comparison to FCS-cultured JPCs. However, this result was not based on lower proliferation activities but on diminished cell sizes which JPCs develop under PL cultivation. The measurements of the metabolic activities clearly showed significantly higher cell proliferation rates under PL culturing. Equivalent levels of the mesenchymal cell markers CD29, CD45, CD73, CD90, and CD105 were detected, but there were significantly increased MSCA-1 levels under PL cultivation. While JPCs only occasionally mineralize under FCS culture conditions, the mineralization potential was significantly stronger under PL cultivation. Moreover, in 4 of 5 analyzed patient cells, the addition of dexamethasone was proved no longer necessary for strong mineralization of PL-cultured JPCs. We conclude that *in vitro* cultivation of JPCs with platelet lysate is a suitable alternative to FCS culture conditions and a powerful tool for the development of high-quality TE constructs using jaw periosteal cells.

1. Introduction

In order to make clinical applications of tissue engineering constructs safe, we established serum-free culture conditions and observed an earlier but weaker mineralization potential of serum-free cultured JPCs [1]. By Raman spectroscopy, we identified and emphasized the differences in the biochemical composition of crystals formed extracellularly under FCS-containing and FCS-free cultivation of JPCs [2]. The diminished extent of JPC calcification as well as the significantly decreased collagen production might lead to an unsatisfactory bone formation significantly countering the success of future tissue engineering applications using this cell type.

From the beginning of the cell culture technique up to the present day, the use of fetal calf serum still represents the gold standard for *in vitro* cell cultivation. However, the development of the relatively young field of tissue engineering including the innovative 3D bioprinting and microfluidic approaches cause a long-term change of standard *in vitro* cell culture techniques/media.

In the meantime, a variety of companies provide serum-free cell culture media; however, the cultivation of some primary cells with these media is not trivial. In general, coating of the culture dishes is required for sufficient cell adhesion, the production of extracellular matrix by serum-free cultured cells is normally diminished, and lower cell densities can be achieved. As mentioned before, serum-free cultured JPCs show a reduced mineralization potential, an observation that can partially be explained by the alteration of extracellular matrix formation.

In recent years, the use of human platelet lysate has been taken into consideration as a suitable alternative to FCS, circumventing the problem of transmission of animal components and/or triggering of immune responses during cell therapies. During PL manufacture, platelets are lysed in order to achieve the release of growth factors from platelets' alpha granules [3]. After the apheresis and filtering procedures, cell debris, and leucocytes will be removed [3–5].

In order to evaluate the suitability of human platelet lysate for the in vitro culturing and osteogenic differentiation of JPCs, we analyzed in the present study the proliferation and mineralization capacity of these cells under PL and FCS culture conditions. For proliferation analysis, two completely different approaches were performed: on the one hand, population doubling times were determined by measurements of electric impedance, and on the other hand, measurements of the metabolic cell activities were carried out. Additionally, cell differentiation experiments were performed and mineralization capacities as well as mesenchymal stem cell marker expression by PL- and FCS-cultured JPCs were analyzed and quantified.

2. Material and Methods

2.1. Cell Isolation and Culture of JPCs. JPCs derived from 5 donors were included in this study in accordance with the local ethical committee (approval number 194/2008BO2) and after obtaining written informed consent. The jaw periosteal tissue was cut in small pieces with a scalpel and enzymatically digested with type XI collagenase (1500 U/ml, Sigma-Aldrich, Steinheim, Germany) for 90 min. Enzymatically isolated cells were expanded in DMEM/F12 + 10% fetal calf serum (FCS) for up to 4 passages until used in passage 5 for all differentiation and proliferation comparative assays. JPCs were cultured in different well formats depending on the used method. For 96 well plates used for MTT assays and E-plates used for xCELLigence measurements, a cell density of 2000 cells per well was chosen. For differentiation experiments, 6-well plates with a starting density of 4×10^4 cells/well were used. For flow cytometric analyses of surface antigen expression, JPCs were grown in 75 cm^2 culture flasks with a starting density of 5×10^5 cells/flask. JPCs were cultured in DMEM/F12 (Invitrogen-BioSource Europe, Nivelles, Belgium) containing 10% FCS (Sigma-Aldrich, Steinheim, Germany) or 10% platelet lysate containing 1% amphotericin B and penicillin/streptomycin (Biochrom, Berlin, Germany). The used PL was provided by the Institute for Clinical and Experimental Transfusion Medicine in Tübingen, did not contain heparin, and was referred to as a research lysate based on the absent quarantine period. DMEM-cultured cells were passaged using trypsin-versene EDTA (1x, Lonza, Basel, Switzerland), and medium change was performed three times per week.

Osteogenic conditions were performed for the experiments illustrated in Figures 1–6 by the addition of dexamethasone (4 μM), β-glycerophosphate (10 mM), and L-ascorbic acid 2-phosphate (100 μM). These osteogenic conditions are listed in the left column of Table 3, for other experiments, one or two of the osteogenic supplements were removed, as indicated in the table.

2.2. Live Monitoring of Cell Proliferation Using xCELLigence. Measurements of cell impedance were carried out using the RTCA DP analyzer (OLS OMNI Life Science, Bremen, Germany). Two hours before starting xCELLigence measurements, the device was put into the incubator for equilibration at 37°C. The required E-plates are equipped with gold-plated electrodes to enable noninvasive monitoring based on electrical impedance. After performing the resistor plate test, 100 μl FCS or PL-containing (10%) DMEM/F12 medium was filled into the E-plates for background measurements. Plates were equilibrated for 2 hours before measurements. In the next step, 100 μl containing 2000 cells was pipetted in each well of the E-plates. After half an hour of incubation at RT, live monitoring was started by a measurement interval of one hour. After an overnight incubation period, osteogenic induction was started. Medium change was performed every 2 days. For the calculation of population doubling times, data from 3 time points (day 5, 10, and 14) was extracted. The population doubling time is defined as the time span required for the doubling of the cell index and was calculated by the device-specific software.

2.3. Analysis of Cell Viability Using the Colorimetric EZ4U Assay. Cell viability measurements were performed using the EZ4U assay (Biomedica GmbH, Vienna, Austria) based on the conversion of tetrazolium salts in formazan derivates by the cell mitochondrial activity. End-point measurements were performed at 3 time points (day 5, 10, and 20) after adding 20 μl of substrate to 200 μl FCS/PL containing DMEM per well and a 4-hour incubation time. Optical densities were measured using the ELx800 plate reader (Biotek Instruments, Bad Friedrichshall, Germany) at a wavelength of 450 nm with a reference wavelength of 630 nm.

2.4. Counting of JPC Numbers Cultivated under PL- and FCS-Containing Culture Conditions and Calculation of Growth Rate and Population Doubling Time. JPCs were seeded in a density of 5×10^3 cells/cm^2, and cell counting was performed after 5, 7, and 10 days of PL and FCS culturing following trypsinization of JPCs ($n = 5$ donors, $n = 4$ counting per patient and culture condition). Based on the fact that osteogenically induced JPCs are not easy to separate to get single-cell suspensions, we chose for cell counting of untreated and osteogenically induced JPC early examination time points at day 5, 7, and 10 of in vitro culturing.

Counting was performed 4 times (per patient and culture condition, resp.). Growth rates (1) and population doubling times (2) were calculated using the following formula:

$$\mu = \frac{\ln(N_t/N_0)}{t}, \quad (1)$$

$$t_d = \frac{\ln(2)}{t}, \quad (2)$$

where μ is the growth rate (h^{-1}), t_d is the population doubling time (h), N_0 is the cell population at $t = 0$, N_t is the cell population at t, and t is time (h).

Growth rates and population doubling times from 5 patients were averaged and obtained mean values (±standard deviations) listed in Table 1 and Table 2, respectively.

2.5. Measurements of Cell Size of PL- and FCS-Cultured JPCs. Based on the visual impression of strongly diminished cell size under PL cultivation, measurements of full-length cell size using the CellProfiler and the LAS EZ software were performed. Therefore, FCS- and PL-cultured JPCs from 3 donors ($n = 10$ per donor) were used for untreated and osteogenic medium conditions ($n = 30$ for each culture condition).

2.6. Surface Antigen Expression Analysis by Flow Cytometry. PL- and FCS-cultured JPCs cultivated under undifferentiated and osteogenic conditions were detached from cell culture flasks and centrifuged (350g for 7 min), and pellets were resuspended in 20 ml of 10% Gamunex (human immune globulin solution, Talecris Biotherapeutics, Frankfurt, Germany) and incubated for 15 min at 4°C. The incubation with specific phycoerythrin- (PE-) labeled mouse anti-human CD29, CD45, CD73, CD90 (BD Biosciences Pharmingen, San Diego, USA), CD105 (AbD Serotec), and MSCA-1 (MACS Miltenyi Biotec, Bergisch Gladbach, Germany) in FACS buffer (PBS, 0.1% BSA, 0.1% sodium azide) followed, and cells were incubated for 15 min at 4°C. After two additional wash steps with FACS buffer, flow cytometric measurements with the Guava EasyCyte 6HT-2L instrument (Merck Millipore, Darmstadt, Germany) were performed.

2.7. Detection of Cell Mineralization by Quantification of Alizarin Dye Stainings. PL- and FCS-cultured JPCs from 5 donors were induced osteogenically (3 wells (of a 6-well plate) per culture condition) for 24 days, and cell monolayers were fixed with 4% formalin for 20 min. After two wash steps with PBS, 1 ml of a 40 mM alizarin dye solution with a pH of 4.2 was added to the monolayers for 20 min while shaking. Thereafter, the unbound dye was washed 4 times with dest water for 15 min. By adding of 10% acetic acid solution, alizarin dye was dissolved out from the monolayers for 20 min while shaking and cell layers were detached by scraping. After vigorous mixing and heating at 85°C for 10 min, samples were cooled on ice for 5 min and centrifuged at 20.000g for 20 min. Supernatants were neutralized by the addition of 10% ammonium hydroxide. Photometrical calcium quantification was then performed at a wavelength of 405 nm.

2.8. Statistical Analysis. For the evaluation of the data, means ± standard deviations are expressed, and for the statistical analysis, two-tailed Student's t-tests were used. A p value of <0.05 was considered significant.

3. Results

3.1. Measurements of JPC Population Doubling Times Using the Live-Monitoring System xCELLigence. JPCs were seeded into E-plate dishes and cell impedance was continuously evaluated under untreated (Co) and osteogenic (Ob) PL and FCS culture conditions. Based on the cell impedance data, population doubling (PD) times for three time points (day 5, 10, and 14) were calculated from the device-specific RTCA software 1.2.1. As individually illustrated (patient cell numbers 1, 2, 3, and 4) in Figure 1, we detected in almost all cases (with two exceptions: number 3 at day 14 and number 4 at day 10, both under undifferentiated (Co) conditions) significantly higher PD times in PL-cultured JPCs under both untreated (Co) and osteogenic (Ob) culture conditions. These data imply significant higher JPC proliferation activities under FCS culturing.

3.2. Measurements of Metabolic JPC Activities under PL- and FCS-Containing Culture Conditions. In contrast to the PD time measurements by cell impedance, we detected significantly higher metabolic activities of PL-cultured JPCs, as measured by the MTT-based assay and individually illustrated for the four analyzed patient cells in Figure 2. The resulted significant differences were detected both under undifferentiated (Co) and/or osteogenic culture conditions (Ob).

3.3. Counting of JPC Numbers Cultivated under PL- and FCS-Containing Culture Conditions. The abovementioned results obtained by x-CELLigence and the metabolic activity assay could not accurately reflect exact JPC proliferation rates.

By simple cell counting, we obtained significantly higher cell numbers when JPCs were cultured under PL supplementation under untreated and/or osteogenic conditions at all analyzed time points (day 5, 7, and 10). Representative microscopic images are shown in Figure 3. We detected highest proliferation rates after 5 days of culturing under PL supplementation (7-fold under untreated and 9-fold higher cell numbers under osteogenic conditions) compared to FCS supplementation. The differences between PL supplementation and FCS supplementation seemed, however, to become smaller at days 7 and 10 of in vitro cell culturing. Nonetheless, we counted on average 3-fold higher cell numbers under PL supplementation of untreated and osteogenically induced JPCs. Calculated growth rates and population doubling times (PDT) are listed in Tables 1 and 2. After 5 days of in vitro culturing, significantly higher PDTs (3-fold) were calculated for PL-cultured JPCs in comparison to FCS-cultured JPCs. After 7 days of in vitro culturing, 5-fold higher PDTs were obtained for untreated JPCs and 6-fold higher PDTs for osteogenically induced JPCs under PL supplementation. After 10 days of in vitro culturing again, 3-fold higher PDTs were calculated for PL-cultured JPCs compared to FCS-cultured JPCs. It is interesting to note the extremely high standard deviations for PDLs under FCS cultivation in contrast to the quite moderate deviations under PL supplementation.

3.4. Analysis of JPC Cell Size under PL- and FCS-Containing Culture Conditions. The results of PD times obtained by xCELLigence were quite contradictory to our observations made. By numerous cell countings and microscopic visualizations, the development of highly proliferating cells of significantly diminished cell sizes was observed under PL cultivation. Therefore, we performed measurements of JPCs derived from 3 patients (10 measurements per patient) under untreated/osteogenically induced PL- and FCS-containing

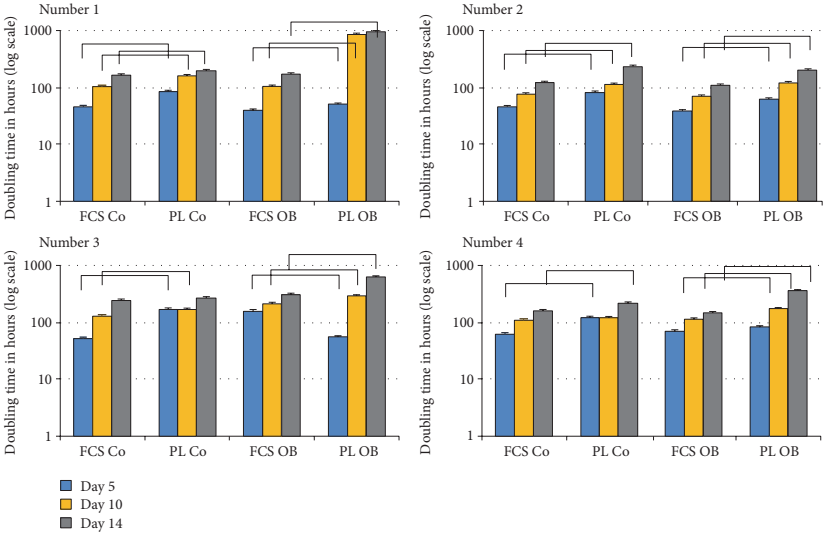

FIGURE 1: JPC population doubling times using the live-monitoring system xCELLigence. JPCs from 4 donors (numbers 1–4) were cultivated under FCS and human PL supplementation under normal (Co) and osteogenic (Ob) conditions for 5, 10, and 14 days in E-plates for electrical impedance measurements. Population doubling times (in hours, logarithmic scaling of the x-axis) were calculated by the device-specific RTCA software. The bars indicate statistical significances: $p < 0.05$.

culture conditions ($n = 30$ for each culture condition). As illustrated in Figure 4, significantly diminished cell sizes were detected under PL cultivation of both untreated and osteogenically induced cells. PL-cultured JPCs seemed to be on average 25% smaller than FCS-cultured cells and this difference in size achieved significant values under both culture conditions (FCS Co: 225.24 ± 58.59 versus PL Co: 165.11 ± 36.40; $p < 0.001$; FCS Ob: 219.08 ± 50.53 versus PL Ob: 167.65 ± 35.66; $p < 0.001$).

3.5. Flow Cytometric Analysis of Mesenchymal Cell Surface Marker Expression under PL- and FCS-Containing Culture Conditions. Mesenchymal stem cell marker expression was analyzed in untreated and osteogenic-induced JPCs (from 5 donors) under PL and FCS culture conditions. Averaged marker expression levels are illustrated in Figure 5. CD29, CD73, CD90, and CD105 were shown to be expressed at comparable levels by PL- and FCS-cultured JPCs under undifferentiated and osteogenically induced JPCs. All cells were almost completely negative for the leucocytic marker CD45.

Significant differences were detected for MSCA-1 cell surface expression. Under undifferentiated culture conditions, significantly higher MSCA-1 levels were detected only after day 10 of PL cultivation (Co day 5: FCS 16.82 ± 16.40 versus PL 45.12 ± 35.07; Co day 10: FCS 25.22 ± 23.78 versus PL 64.1 ± 21.45; $p < 0.05$). Under osteogenic culture conditions, a significantly higher degree of JPC positivity was detected at both analyzed time points for MSCA-1 expression under PL cultivation (Ob day 5: FCS 17.06 ± 14.70 versus PL 60.14 ± 23.48; $p < 0.05$; Ob day 10: FCS 55.32 ± 17.53 versus PL 86.32 ± 2.93; $p < 0.05$).

3.6. Analysis of the Mineralization Potential of JPCs Cultured under PL- and FCS-Containing Culture Conditions. In Figure 6, representative microscopic images showed apparently higher amounts of calcium phosphate precipitates under PL (right panel) in comparison to FCS cultivation (left panel) of JPCs (4 donors). Subsequent quantification of alizarin red B stainings resulted in significant differences in calcium concentrations (μM, logarithmic scale) under untreated as well as under osteogenic culture conditions (Co: FCS $0.025 \pm 0.017\,\mu$M versus PL $0.031 \pm 0.015\,\mu$M; Ob: FCS $0.058 \pm 0.022\,\mu$M versus PL $4.77 \pm 1.74\,\mu$M), as shown in Figure 7.

3.7. Analysis of JPC Mineralization under Different Osteogenic Induction Conditions. Table 3 shows the 5 different osteogenic medium conditions containing dexamethasone (dexa), β-glycerophosphate (β-glyc), and ascorbic acid (ascorb) in different combinations tested for mineralization induction of JPCs from 5 donors (numbers 1–5). Under FCS culture conditions, only 3 of 5 patient cells mineralized under the addition of all three osteogenic inducers to a relatively low extent. In contrast, PL-cultured JPCs mineralized

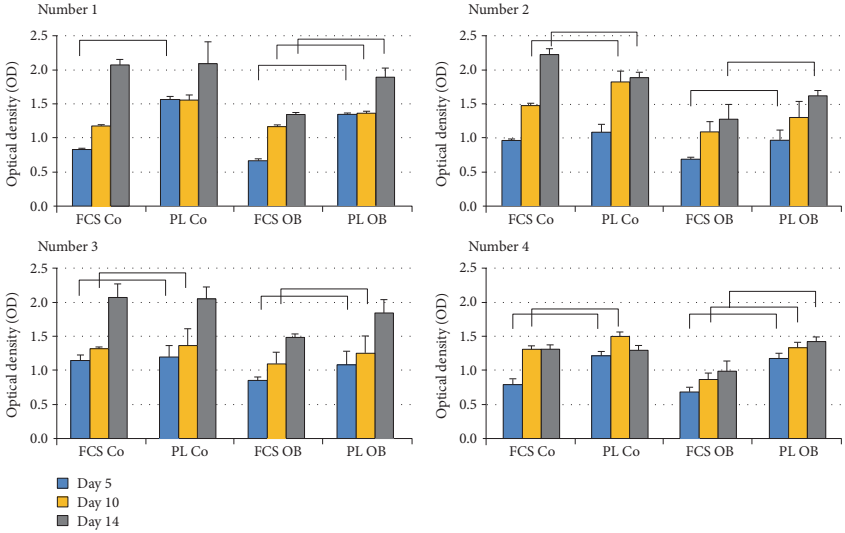

Figure 2: Measurements of metabolic JPC activities under FCS- and PL-containing culture conditions. JPCs from 4 donors (numbers 1–4) were cultivated under FCS and human PL supplementation under normal (Co) and osteogenic (Ob) conditions for 5, 10, and 20 days in 96-well plates for colorimetric measurements of metabolic activities. Optical densities (OD) are presented in the diagrams. The bars indicate statistical significances: $p < 0.05$.

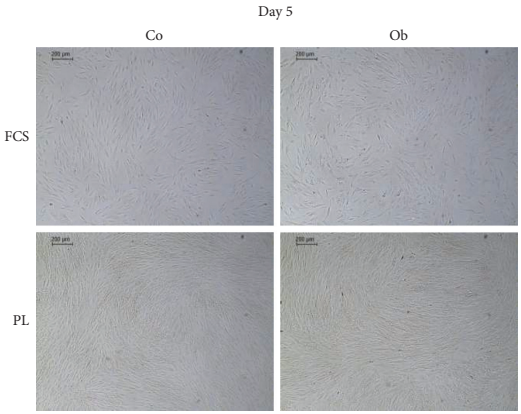

Figure 3: Representative microscopic images of FCS- and PL-cultured JPCs. JPCs were cultured under FCS or PL supplementation for 5 days and cell monolayers were visualized by microscopic images (scale bar: 200 μm). Subsequently, cells were counted after trypsinization. Days 7 and 10 of *in vitro* culturing were also taken into account and growth rates and population doubling times were calculated, as listed in Tables 1 and 2.

all under these conditions and to a much higher extent. In addition, FCS-cultured cells derived from number 5 could also mineralize after addition of β-glyc and ascorbic acid.

Under PL cultivation, 2 of 5 patient cells mineralized strongly without the addition of ascorbic acid, whereas none of them mineralized under FCS cultivation upon

Table 1: Growth rate calculated from cell counting of FCS and PL-cultured JPCs under untreated and osteogenic culture conditions. 5×10^3 cells/cm^2 were seeded in 12-well culture plates and counted following trypsinization after 5, 7, and 10 days of in vitro culturing. Growth rate μ (h^{-1}) calculated from total cell counts from 5 donors ($n = 4$ counting per patient and culture condition) is listed ±standard deviations and significance values.

	Growth rate μ (h^{-1})			
	FCS Co	PL Co	FCS Ob	PL Ob
d5	4.28E−03 ± 3.23E−03	1.58E−02 ± 1.48E−03	5.40E−03 ± 3.52E−03	1.91E−02 ± 2.77E−03
Significance	$p < 0.01$		$p < 0.01$	
d7	5.32E−03 ± 1.69E−03	2.41E−02 ± 4.46E−03	8.79E−03 ± 4.79E−03	3.42E−02 ± 2.36E−03
Significance	$p < 0.01$		$p < 0.01$	
d10	6.20E−03 ± 1.86E−03	2.20E−02 ± 2.93E−03	1.19E−02 ± 3.73E−03	3.00E−02 ± 2.88E−03
Significance	$p < 0.01$		$p < 0.01$	

Table 2: Doubling time t_d calculated from cell counting of FCS and PL-cultured JPCs under untreated and osteogenic culture conditions. 5×10^3 cells/cm^2 were seeded in 12-well culture plates and counted following trypsinization after 5, 7, and 10 days of in vitro culturing. Doubling time t_d (h) calculated from total cell counts from 5 donors ($n = 4$ counting per patient and culture condition) is listed ±standard deviations and significance values.

	Doubling time t_d (h)			
	FCS Co	PL Co	FCS Ob	PL Ob
d5	140.4 ± 55.5	44.2 ± 4.3	112.5 ± 39.2	37.2 ± 6.0
Significance	$p < 0.05$		$p < 0.01$	
d7	156.6 ± 84.6	29.9 ± 6.0	125.9 ± 104.8	20.4 ± 1.3
Significance	$p < 0.05$			
d10	125.6 ± 48.5	32.1 ± 4.3	66.5 ± 27.3	23.3 ± 2.1
Significance	$p < 0.01$		$p < 0.05$	

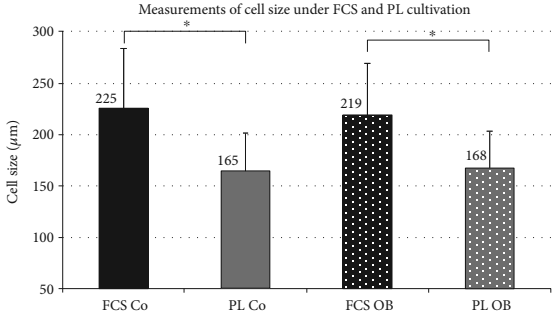

Figure 4: Measurements of cell size under FCS- and PL-containing culture conditions. Full length cell size measurements were performed using the CellProfiler and the LAS EZ software from 3 JPC donors ($n = 10$ measurements per donor, $n = 30$ for each culture condition). Cells were cultivated under FCS and human PL supplementation under normal (Co) and osteogenic (Ob) conditions for 5 days before performing the measurements. Statistical significances are indicated by asterisks: $^*p < 0.001$.

addition of dexa and β-glyc. Most interesting was the mineralization capacity of JPCs under activation with β-glyc and ascorbic acid. 4 of 5 patient cells showed under PL cultivation a strong mineralization without the addition of dexamethasone. Additionally, JPCs derived from number 4 could also mineralize after the individual addition of only β-glyc.

4. Discussion

The use of FCS for the in vitro expansion of mesenchymal stromal cells for future cell therapies is restricted due to regulatory affairs and transmissions of animal diseases or causing immune reactions. To gain knowledge about the suitability of platelet lysate as a FCS substitute for the

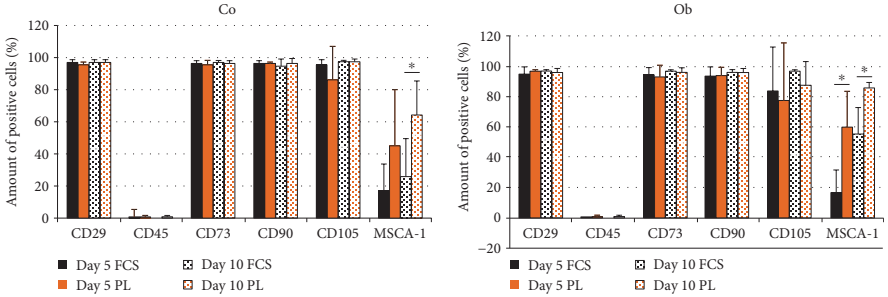

Figure 5: Flow cytometric analyses of MSC surface markers by JPCs cultivated under FCS and PL supplementation. Cell surface expression of CD29, CD45, CD73, CD90, CD105, and MSCA-1 was analyzed in JPCs (from 4 donors) cultivated under FCS and human PL supplementation under normal (Co) and osteogenic (Ob) conditions for 5 and 10 days by flow cytometry. Significantly higher levels ($^*p < 0.05$) of MSCA-1 were detected under Co conditions after day 10 and under osteogenic conditions after day 5 and 10 of hPL cultivation.

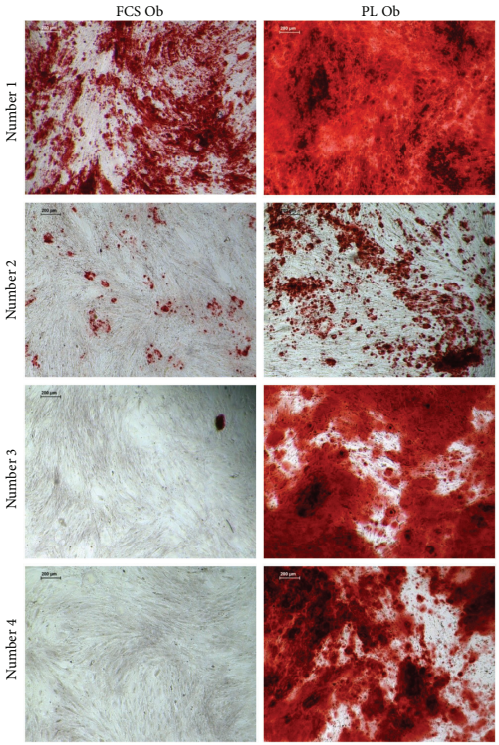

Figure 6: Detection of JPC mineralization cultured under FCS- and PL-containing culture conditions. Representative microscopic images (scale bar: 200 μm) of alizarin red B stainings of PL- and FCS-cultured JPC monolayers (from 4 donors) after 24 days of osteogenic induction. Bright red-stained areas contain calcium phosphate precipitates.

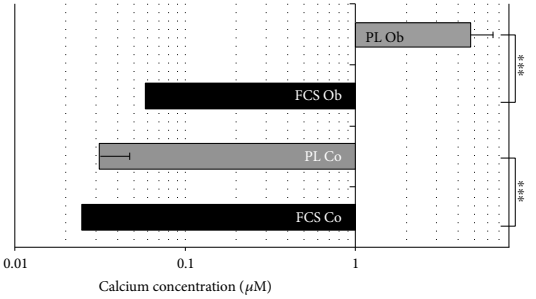

Figure 7: Calcium quantification of PL- and FCS-cultured JPCs. Alizarin dye was dissolved in acetic acid and colorimetric quantification (calcium concentration (μM), logarithmic scale) was performed. Untreated and osteogenic induced JPCs under PL and FCS supplementation were considered. Statistical significances are indicated by asterisks: $^{***}p < 0.0001$.

Table 3: JPC mineralization under FCS and PL cultivation by different combination of osteogenic stimuli. FCS- and PL-cultured JPCs from 5 donors (numbers 1–5) were induced by the addition of different combinations of osteogenic stimuli for 24 days before alizarin red stainings were performed.

	FCS					hPL				
Pat. number	dexa, β-glyc, ascorb	dexa, β-glyc	β-glyc, ascorb	dexa, ascorb	β-glyc	dexa, β-glyc, ascorb	dexa, β-glyc	β-glyc, ascorb	dexa, ascorb	β-glyc
1	+	0	0	0	0	+++	0	0	0	0
2	0	0	0	0	0	+	0	+++	0	0
3	0	0	0	0	0	+++	0	+++	0	0
4	+	0	0	0	0	+++	+++	+++	0	++
5	++	0	++	0	0	+++	+++	+++	0	0

dexa: dexamethasone; β-glyc: β-glycerophosphate; ascorb: ascorbic acid; 0: no mineralization occurred; +: low, ++: middle, +++: strong mineralization.

in vitro cultivation of jaw periosteal cells, we compared in the present study cell functions and mineralization potential of these cells under FCS and PL culturing. Since serum-free culturing of JPCs selectively promoted the osteoprogenitors within the whole cell population [1] and biochemical analysis of formed minerals elucidated their high quality by Raman spectrometry [2], the extent of mineralization was not satisfactory. To the best of our knowledge, we analyze for the first time in the present study the high potential of platelet lysate for the in vitro cultivation and mineralization of periosteal cells.

For the processing of human platelet lysates, several methods have been established, the most common of them being the implementation of one or more freeze/thaw cycles to induce platelet lysis and the release of abundant bioactive molecules [6]. However, a systematic analysis determining the optimal number of freeze/thaw cycles is still missing [3]. In a recent study, Bernardi and colleagues could demonstrate that the production method affects the efficacy of human PL for the expansion and differentiation of bone marrow-derived MSCs [7].

We analyzed cell surface marker expression as defined by Dominici and coauthors for MSCs [8]. All markers revealed comparable levels independent of FCS or PL cultivation. The only significant difference was referred to MSCA-1 surface expression which was detected at significantly higher levels in PL-cultured JPCs. We already demonstrated in a former study that the MSCA-1-positive cells hallmark the osteoprogenitors within the entire JPC cell population [9]. Growth factors derived from the used PL might trigger the proliferation of MSCA-1-positive cells and therefore be in part the reason for the much higher osteogenic potency of the herein analyzed JPCs.

Under PL cultivation, we observed and quantified a significantly diminished cell size. A similar observation was made under serum-free cultivation of JPCs [1]. This fact obviously impacts cell impedance measurements by altering the electrical resistance within the E-plates. The significantly higher PD times of FCS-cultured JPCs calculated by the xCELLigence software were shown to be in contrast to those obtained by measurements of the metabolic activities and by microscopic observations. These results indicate that this device is not suitable for the comparison of primary cells cultured at different media conditions which probably influence the cell size. Alternatively, the calculation of PD times by the device-specific software should be improved by including a correction factor considering the cell size.

Due to the fact that neither the xCELLigence system nor the MTT assay could accurately measure exact differences in

cell proliferation under FCS- and PL-culturing, we performed simple cell counting and detected significantly higher cell numbers (3–9-fold) at all analyzed time points. Population doubling times were calculated to be 3-fold higher after 5 and 10 days and 5-6-fold higher after 7 days of in vitro culturing under PL cultivation of JPCs.

Numerous studies have proven the potency of hPL for the expansion of MSCs [10] from adipose tissue [11–13], umbilical cord blood, and bone marrow [14, 15]. In the present study, we proved additionally the potency of hPL for JPC proliferation and mineralization. An extensive comparative study examined in vitro proliferation of MSCs under the cultivation of 4 different media and three supplements including FCS, human AB serum, and human PL [16]. MSC proliferation was observed to be optimal in the PL-supplemented αMEM. The researchers assessed a library of soluble factors to promote robust MSC proliferation and established a cocktail which in combination with up to 1.2% PL could replace the addition of 5% hPL to the culture medium. The developed cocktail of recombinant human factors contained also hormones such as dexamethasone, insulin, and TSH. Fiorentini and coauthors demonstrated that the addition of dexamethasone ensures bone marrow MSC mineralization [17]. Interestingly, in our study, the addition of 10% hPL could replace the addition of dexamethasone to the osteogenic medium for robust mineralization of JPCs from 4 out of 5 tested donors indicating that the used hPL contains natural glucocorticoids that can replace dexamethasone. We further made the observation that β-glycerophosphate is essential and leads to a missing JPC mineralization when lacking as a phosphate source in the osteogenic medium.

A further interesting aspect might be the in vitro JPC culturing under hPL supplementation directly after the isolation from the primary tissue. In this study, frozen JPCs from passage 2 were thawed and expanded under FCS supplementation till sufficient cell numbers were achieved for the comparative experiments. The PL use from the starting point of JPC *in vitro* culturing could accelerate and improve the generation of tissue engineering constructs using this cell type.

In summary, we demonstrated in the present study the high potential of the supplementation with human platelet lysate instead of the commonly used FCS for the *in vitro* culturing and clinical tissue engineering applications of JPCs. Furthermore, the addition of the corticosteroid dexamethasone is probably no longer necessary after hPL supplementation.

Conflicts of Interest

The authors declare that there is no conflict of interest regarding the publication of this paper.

References

[1] D. Alexander, M. Rieger, C. Klein, N. Ardjomandi, and S. Reinert, "Selection of osteoprogenitors from the jaw periosteum by a specific animal-free culture medium," *PLoS One*, vol. 8, no. 12, article e81674, 2013.

[2] E. Brauchle, D. Carvajal Berrio, M. Rieger, K. Schenke-Layland, S. Reinert, and D. Alexander, "Raman spectroscopic analyses of jaw periosteal cell mineralization," *Stem Cells International*, vol. 2017, Article ID 1651376, 12 pages, 2017.

[3] T. Burnouf, D. Strunk, M. B. Koh, and K. Schallmoser, "Human platelet lysate: replacing fetal bovine serum as a gold standard for human cell propagation?," *Biomaterials*, vol. 76, pp. 371–387, 2016.

[4] A. Altaie, H. Owston, and E. Jones, "Use of platelet lysate for bone regeneration - are we ready for clinical translation?," *World Journal of Stem Cells*, vol. 8, no. 2, pp. 47–55, 2016.

[5] D. T. Shih and T. Burnouf, "Preparation, quality criteria, and properties of human blood platelet lysate supplements for *ex vivo* stem cell expansion," *New Biotechnology*, vol. 32, no. 1, pp. 199–211, 2015.

[6] K. Schallmoser and D. Strunk, "Preparation of pooled human platelet lysate (pHPL) as an efficient supplement for animal serum-free human stem cell cultures," *Journal of Visualized Experiments*, no. 32, 2009.

[7] M. Bernardi, F. Agostini, K. Chieregato et al., "The production method affects the efficacy of platelet derivatives to expand mesenchymal stromal cells in vitro," *Journal of Translational Medicine*, vol. 15, no. 1, p. 90, 2017.

[8] M. Dominici, K. Le Blanc, I. Mueller et al., "Minimal criteria for defining multipotent mesenchymal stromal cells. The International Society for Cellular Therapy position statement," *Cytotherapy*, vol. 8, no. 4, pp. 315–317, 2006.

[9] D. Alexander, F. Schafer, M. Olbrich et al., "MSCA-1/TNAP selection of human jaw periosteal cells improves their mineralization capacity," *Cellular Physiology and Biochemistry*, vol. 26, no. 6, pp. 1073–1080, 2010.

[10] C. Doucet, I. Ernou, Y. Zhang et al., "Platelet lysates promote mesenchymal stem cell expansion: a safety substitute for animal serum in cell-based therapy applications," *Journal of Cellular Physiology*, vol. 205, no. 2, pp. 228–236, 2005.

[11] I. S. Blande, V. Bassaneze, C. Lavini-Ramos et al., "Adipose tissue mesenchymal stem cell expansion in animal serum-free medium supplemented with autologous human platelet lysate," *Transfusion*, vol. 49, no. 12, pp. 2680–2685, 2009.

[12] B. A. Naaijkens, H. W. Niessen, H. J. Prins et al., "Human platelet lysate as a fetal bovine serum substitute improves human adipose-derived stromal cell culture for future cardiac repair applications," *Cell and Tissue Research*, vol. 348, no. 1, pp. 119–130, 2012.

[13] S. F. Trojahn Kolle, R. S. Oliveri, P. V. Glovinski et al., "Pooled human platelet lysate versus fetal bovine serum-investigating the proliferation rate, chromosome stability and angiogenic potential of human adipose tissue-derived stem cells intended for clinical use," *Cytotherapy*, vol. 15, no. 9, pp. 1086–1097, 2013.

[14] M. A. Avanzini, M. E. Bernardo, A. M. Cometa et al., "Generation of mesenchymal stromal cells in the presence of platelet lysate: a phenotypic and functional comparison of umbilical cord blood- and bone marrow-derived progenitors," *Haematologica*, vol. 94, no. 12, pp. 1649–1660, 2009.

[15] K. Bieback, A. Hecker, A. Kocaomer et al., "Human alternatives to fetal bovine serum for the expansion of mesenchymal stromal cells from bone marrow," *Stem Cells*, vol. 27, no. 9, pp. 2331–2341, 2009.

[16] N. Fekete, M. T. Rojewski, R. Lotfi, and H. Schrezenmeier, "Essential components for ex vivo proliferation of mesenchymal stromal cells," *Tissue Engineering. Part C, Methods*, vol. 20, no. 2, pp. 129–139, 2014.

[17] E. Fiorentini, D. Granchi, E. Leonardi, N. Baldini, and G. Ciapetti, "Effects of osteogenic differentiation inducers on *in vitro* expanded adult mesenchymal stromal cells," *International Journal of Artificial Organs*, vol. 34, no. 10, pp. 998–1011, 2011.

International Journal of
Molecular Sciences

MDPI

Article

iPSC-Derived MSCs Versus Originating Jaw Periosteal Cells: Comparison of Resulting Phenotype and Stem Cell Potential

Felix Umrath [1], Marbod Weber [2], Siegmar Reinert [1], Hans-Peter Wendel [2], Meltem Avci-Adali [2,†] and Dorothea Alexander [1,*,†]

[1] Department of Oral and Maxillofacial Surgery, University Hospital Tübingen, 72076 Tübingen, Germany; felix.umrath@med.uni-tuebingen.de (F.U.); Siegmar.reinert@med.uni-tuebingen.de (S.R.)
[2] Department of Thoracic and Cardiovascular Surgery, University Hospital Tübingen, 72076 Tübingen, Germany; marbod.weber@uni-tuebingen.de (M.W.); hans-peter.wendel@med.uni-tuebingen.de (H.-P.W.); meltem.avci-adali@uni-tuebingen.de (M.A.-A.)
* Correspondence: dorothea.alexander@med.uni-tuebingen.de; Tel.: +49-7071-29-82418
† These authors contributed equally to this work.

Received: 15 November 2019; Accepted: 14 January 2020; Published: 16 January 2020

Abstract: Induced pluripotent stem cell-derived mesenchymal stem cell-like cells (iMSCs) are considered to be a promising source of progenitor cells for approaches in the field of bone regeneration. In a previous study, we described the generation of footprint-free induced pluripotent stem cells (iPSCs) from human jaw periosteal cells (JPCs) by transfection of a self-replicating RNA (srRNA) and subsequent differentiation into functional osteogenic progenitor cells. In order to facilitate the prospective transfer into clinical practice, xeno-free reprogramming and differentiation methods were established. In this study, we compared the properties and stem cell potential of the iMSCs produced from JPC-derived iPSCs with the parental primary JPCs they were generated from. Our results demonstrated, on the one hand, a comparable differentiation potential of iMSCs and JPCs. Additionally, iMSCs showed significantly longer telomere lengths compared to JPCs indicating rejuvenation of the cells during reprogramming. On the other hand, proliferation, mitochondrial activity, and senescence-associated beta-galactosidase (SA-β-gal) activity indicated early senescence of iMSCs. These data demonstrate the requirement of further optimization strategies to improve mesenchymal development of JPC-derived iPSCs in order to take advantage of the best features of reprogrammed and rejuvenated cells.

Keywords: iPSC-derived mesenchymal stem/stromal-like cells (iMSCs), induced pluripotent stem cells (iPSCs); jaw periosteal cells (JPCs); self-replicating RNA; differentiation; bone-tissue engineering

1. Introduction

A growing population and aging societies lead to a rising demand for regenerative therapies in the field of orthopedic and maxillofacial surgery. In addition to classical treatments, cell therapies and tissue engineering approaches are pushing their way into clinical applications. For these purposes, mesenchymal stem/stromal cells (MSCs) isolated from different tissues are being tested in clinical trials [1]. Based on their stem cell potential, homing activity, and immunomodulatory properties, MSCs can be applied for the treatment of a variety of diseases [2–4]. Unfortunately, restricted availability, limited in vitro proliferation capacity, and limited differentiation potential impede their application in clinical routine [5]. In addition, it is particularly unfavorable that the quantity of MSCs in donor tissues decreases with age [6] as older patients make up the majority of the patients in need of such treatments.

For bone regeneration in the oral and maxillofacial region, it is obvious to choose the best suitable stem cell source, especially considering the strong mechanical load in this area. Convinced that jaw periosteal cells (JPCs) represent an optimal stem cell source, the goal of our work is to characterize this cell type in detail and to optimize it for clinical applications. Isolated JPCs can be sufficient for the regeneration of small bone defects. However, the biggest challenge for oral and maxillofacial surgeons is to regenerate large bone defects, as occurring after tumor resections. To avoid long in vitro culturing for the generation of high JPC numbers and the associated cell senescence, induced pluripotent stem cells (iPSCs) might serve as an alternative source of MSCs because of their unlimited self-renewal capacity and differentiation potential [7]. A variety of methods has been published to differentiate iPSCs into iPSC-derived mesenchymal stem/stromal-like cells (iMSCs), demonstrating comparable properties of MSCs and iMSCs regarding morphology, marker expression, differentiation potential, or immunomodulatory properties [8,9].

In addition, it has been reported, that iPSC-derived cells originating from fibroblasts or MSCs show signs of rejuvenation, e.g., telomere elongation, accelerated proliferation, and a rejuvenation-associated gene expression signature [10,11]. These observations raise hopes that rejuvenated iMSCs can have additional benefits over primary MSCs when used in regenerative therapies, since studies show that donor age negatively affects proliferation rates, expression of immunological factors, and cellular senescence (reviewed in [12]).

Recently, we demonstrated the generation of footprint- and xeno-free iPSCs from JPCs and their successful differentiation into iMSCs by cultivation of iPSCs with human platelet lysate (hPL)-supplemented medium [13]. We further showed that the generated iMSCs are osteogenic progenitor cells with a strong mineralization potential. We anticipate that this is due to a certain genetic memory of JPC-iMSC-derived iMSCs.

In the present study, we compared the properties of the originating isogenic JPCs, which are themselves MSCs with a high differentiation potential [14–16], and the generated iMSCs, in terms of their differentiation potential and possible rejuvenation.

2. Results

2.1. Tri-Lineage Differentiation of iMSCs and JPCs

iPSCs were generated from JPCs of three different donors and differentiated into iMSCs. To demonstrate their differentiation potential, iMSCs were differentiated into the adipogenic, chondrogenic, and osteogenic lineage. Lineage-specific staining and gene expression analysis was performed and compared to the originating JPCs.

2.1.1. Adipogenic Differentiation

JPCs and iMSCs were able to differentiate into the adipogenic lineage, as demonstrated by staining of fat vacuoles using Oil Red after 10–15 days of incubation in adipogenic medium (Figure 1A). Gene expression analysis was performed after 10 days of adipogenic differentiation, and shows an induction of adipogenic marker genes *PPARγ, LPL and leptin* in iMSCs and JPCs, yet not statistically significant (Figure 1B). A stronger oil red staining and induction of adipogenic marker genes in iMSCs was observed, however without significant differences compared to JPCs.

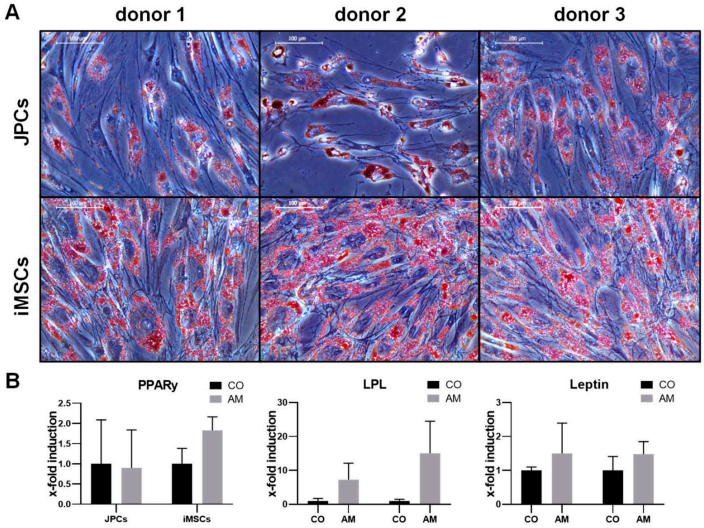

Figure 1. Adipogenic differentiation of jaw periosteal cells (JPCs) and iPSC-derived mesenchymal stem/stromal-like cells (iMSCs). (**A**) Microscopic images (20× magnification, scale bar = 100 µm) of oil red stained JPCs (upper panel) and iMSCs (lower panel) after 15 days (donor 3 JPCs only 10 days) of adipogenic differentiation. (**B**) Expression levels of adipogenic marker genes (*PPARγ*, *LPL*, *and leptin*) of JPCs and iMSCs cultivated for 10 days in adipogenic medium (AM) were normalized to levels of the housekeeping gene *GAPDH* and presented as x-fold induction relative to those of respective cells cultivated in control medium (CO). Differences in gene expression were compared using two-way ANOVA ($n = 3$).

2.1.2. Chondrogenic Differentiation

Chondrogenic differentiation of JPCs and iMSCs was detected by violet staining of glycosaminoglycans (GAGs) with toluidine blue after 25 days of chondrogenic differentiation. While all JPCs clearly displayed chondrogenic differentiation, iMSCs from donor 2 showed only weak differentiation (Figure 2A). iMSCs and JPCs incubated for 20 days in chondrogenic medium displayed considerable induction of chondrogenic marker genes *COL2A1*, *COMP*, and *SOX9* (Figure 2B). *COMP* ($p < 0.01$) as well as *SOX9* ($p < 0.001$) expression was significantly induced in iMSCs compared to the control samples, and a significantly higher *SOX9* induction ($p < 0.01$) in iMSCs compared to JPCs treated with chondrogenic medium was detected.

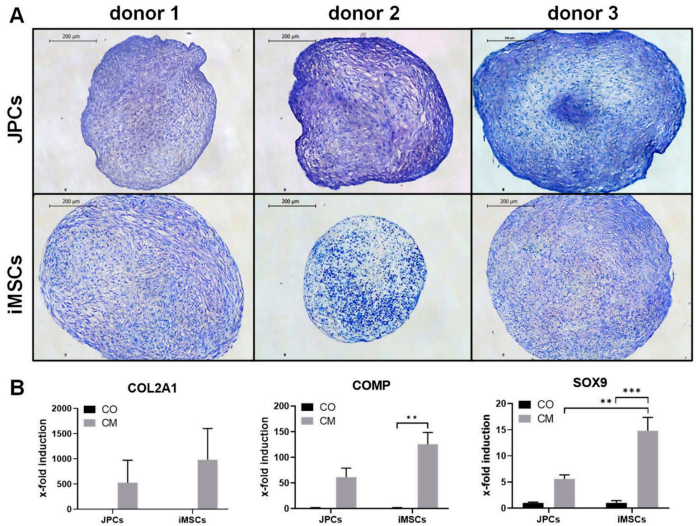

Figure 2. Chondrogenic differentiation of iMSCs and JPCs. (**A**) Toluidine blue staining of JPCs (upper panel) and iMSCs (lower panel) treated with chondrogenic medium (CM) for 25 days (4× magnification, scale bar = 500 µm). (**B**) Gene expression analysis (*COL2A1*, *SOX9*, *COMP*) of JPCs and iMSCs after 20 days of incubation in control (CO) and chondrogenic medium (CM). Gene expression data of JPC and iMSC samples were normalized to the corresponding expression of the housekeeping gene *GAPDH*. Gene expression mean values ± SD of CO and CM samples were displayed as x-fold induction values relative to the control samples (CO). Statistical significance was calculated using two-way ANOVA (n = 3 donors, ** $p < 0.01$, *** $p < 0.001$).

2.1.3. Osteogenic Differentiation

Osteogenic differentiation of iMSCs and JPCs was stimulated for 15–25 days (donor 1 JPCs: 25 days, donor 1 iMSCs: 20 days, donor 2 and 3 JPCs and iPSCs: 15 days) by incubation in osteogenic medium. Subsequently, cell monolayers were stained with alizarin red to visualize cell mineralization (Figure 3A). iMSCs and JPCs from all three donors displayed strong mineralization. Gene expression analysis shows an induction of osteogenic marker genes *ALP*, *RUNX2*, and *OCN* in iMSCs and JPCs (Figure 3B). *ALP* ($p < 0.01$) as well as *OCN* ($p < 0.05$) expression was significantly induced in iMSCs compared to the control samples. Further, *ALP* induction ($p < 0.05$) was significantly higher in iMSCs compared to JPCs, correlating with the stronger mineralization of iMSCs observed in the alizarin-stained samples.

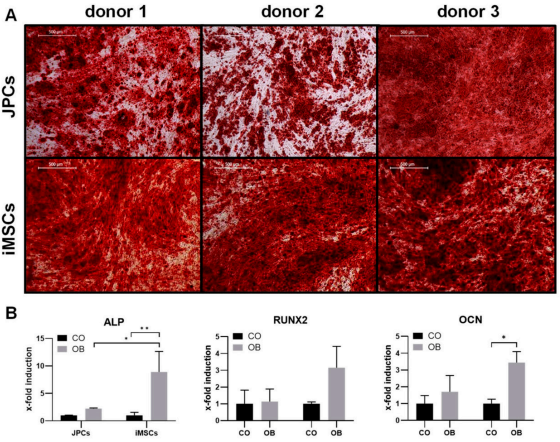

Figure 3. Osteogenic differentiation of iMSCs and JPCs. (**A**) Alizarin red staining of JPCs (upper panel) and iMSCs (lower panel) treated with osteogenic medium (donor 2 and 3 JPCs and iMSCs for 15 days, donor 1 JPCs 25 days, donor 1 iMSCs 20 days) (4× magnification, scale bar = 500 µm). (**B**) Gene expression analysis (*ALP*, *RUNX2*, *OCN*) of JPCs and iMSCs after 15 days of incubation in control (CO) and osteogenic medium (OB). Gene expression data of JPC and iMSC samples were normalized to the corresponding expression of the housekeeping gene *GAPDH*. Gene expression mean values ± SD of CO and OB samples were displayed as x-fold induction values relative to the CO samples. Statistical significance was calculated using two-way ANOVA (n = 3 donors, * $p < 0.05$, ** $p < 0.01$).

2.2. Rejuvenation and Senescence

2.2.1. Telomere Length Assay

The determined absolute telomere length in JPC-derived iPSCs with 2.9 ± 0.4 kb/chromosome was significantly higher compared to the precursor JPCs (1.2 ± 0.2 kb/chromosome, Figure 4)). iMSCs showed a two-fold increase in telomere length (2.5 ± 0.5 kb/chromosome, Figure 4) compared to the initial JPCs, however statistically not significant.

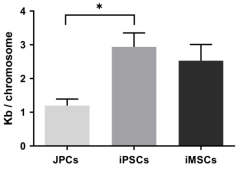

Figure 4. Telomere length quantification by qRT-PCR analysis of JPCs, JPC-derived induced pluripotent stem cells (iPSCs) and iMSCs (n = 3 donors, mean ± SEM, one-way ANOVA, * $p < 0.05$).

2.2.2. Proliferation, Mitochondrial Activity, and SA-β-Galactosidase Activity

Increased telomere lengths in iPSCs and iMSCs compared to JPCs indicated a rejuvenated phenotype of obtained iMSCs. However, cell proliferation (d4: $p < 0.001$, d5: $p < 0.05$) and mitochondrial activity (d4: $p < 0.01$, d5: $p < 0.001$) were significantly lower in iMSCs compared to JPCs (Figure 5A,B).

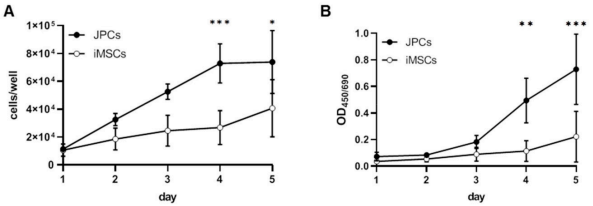

Figure 5. Growth kinetics and mitochondrial activity of JPCs and iMSCs. Quantification of (**A**) cell growth by cell counting and (**B**) mitochondrial activity by colorimetric measurement of formazan derivates produced by reduction of tetrazolium salts in the mitochondria of JPCs and iMSCs (EZ4U). Cell numbers and mitochondrial activities of iPSCs and JPCs were compared by two-way ANOVA ($n = 3$, * $p < 0.05$, ** $p < 0.01$, *** $p < 0.001$).

In addition, SA-β-gal activity was significantly higher in iMSCs as demonstrated in Figure 6A–E. MFI values of fluorescently detected SA-β-gal activity were significantly higher in iMSCs compared to JPCs ($p < 0.05$) and iPSCs ($p < 0.001$) (Figure 6B). Further, the expression of senescence marker genes $P16^{INK4a}$ and $P21^{Cip1}$ was higher in iMSCs compared to JPCs, however statistically not significant. Significant differences in $P16^{INK4a}$ and $P21^{Cip1}$ expression was detected in iPSCs compared to JPCs ($p < 0.05$) and iMSCs ($p < 0.001$).

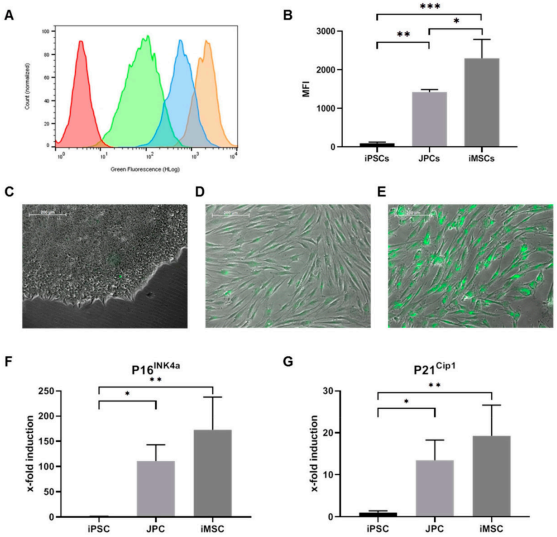

Figure 6. Cellular senescence of JPCs, iPSCs, and iMSCs. Determination of SA-β-galactosidase activity using a fluorescent SA-β-gal assay kit. (**A**) Representative histogram of SA-β-gal activity detected in iPSCs (green), JPCs (blue), iMSCs (orange) and an unstained control (red) by flow cytometry and (**B**) median fluorescence index (MFI) values displayed as mean values ± SD, compared by one-way ANOVA. Fluorescent SA-β-gal activity detected by fluorescence microscopy in (**C**) iPSCs, (**D**) JPCs and (**E**) iMSCs (10× magnification, scale bar = 200 µm). Expression of senescence marker genes (**F**) $P16^{INK4a}$ and (**G**) $P21^{Cip1}$ is displayed as induction values relative to the expression of iPSCs (control) and compared by one-way ANOVA ($n = 3$, * $p < 0.05$, ** $p < 0.01$, *** $p < 0.001$).

3. Discussion

The use of iPSCs to produce clinically relevant cells for regenerative medicine is a promising perspective. Still, there are many hurdles to overcome until such cells can enter the clinical practice. To approach this aim, we established a protocol for the generation of footprint-free iPSCs and iMSCs under xeno-free conditions [13]. In the present study, we compared the resulting iMSCs with the originating isogenic JPCs concerning their three-lineage differentiation potential and investigated a potential rejuvenation of iMSCs, which has previously been observed in iPSC-derived cells [10,17].

Our results showed a high multipotent differentiation potential of iMSCs, demonstrating the clinical relevance of these cells for applications in regenerative medicine. Qualitative evaluation of the tri-lineage differentiation of iMSCs indicated a higher stem cell potential of iMSCs compared to JPCs, which was supported by significantly higher induction of the chondrogenic marker gene *SOX9* and the osteogenic marker gene *ALP* in iMSCs compared to the originating JPCs.

In addition, an increased telomere length was found in iPSCs and iMSCs. Telomere elongation was shown to be a consequence of reprogramming caused by telomerase activation in iPSCs [18]. The two-fold higher telomere length detected in iMSCs compared to JPCs indicated a higher proliferative capacity of these cells, as telomere elongation had been demonstrated to enable cells to overcome replicative senescence [19].

To examine possible rejuvenation in the generated iMSCs, growth rates, mitochondrial activities, and SA-β-gal activities were investigated. Surprisingly, iMSCs showed lower proliferation rates and mitochondrial activities compared to JPCs. In addition, iMSCs expressed higher levels of the senescence marker genes $P16^{INK4a}$ and $P21^{Cip1}$, as well as higher SA-β-gal activities, clearly displaying an early senescence phenotype. However, as telomeres were elongated in iMSCs compared to JPCs, replicative senescence can be excluded as a possible reason for this phenotype.

Similar to our findings, Feng et al. observed early senescence in iPSC-derived hemangioblast cells and assumed an influence of retroviral vector insertion and reactivation of reprogramming genes during iPSC differentiation [20]. This theory was refuted by a study from Gokoh et al. demonstrating that the avoidance of stressful conditions, and a more efficient protocol using additional cytokines for hemangioblast differentiation, could overcome these issues [21]. We also hypothesize that cellular stress caused by the differentiation process could induce senescence in iMSCs. This assumption is supported by the observation of massive cell death after single-cell plating of iPSCs, and later transfer to uncoated cell culture dishes, during iMSC differentiation. A mechanism possibly underlying this senescence phenotype could be the stress-induced production of reactive oxygen species and subsequent activation of the $P16^{INK4a}$ pathway, caused by the disruption of iPSC colonies, similar to tissue damage-induced senescence [22,23]. Further, we discovered that higher iMSC yields could be achieved by using iPSCs that had not been passaged for 10 or more days, which was possibly priming iPSC differentiation by high cell densities. Therefore, we consider iMSC differentiation by this protocol a highly selective process that favors cells that are already differentiated or in which differentiation has been primed prior to separation.

Devito et al. also observed senescent cells during iMSC differentiation when using a similar method with single-cell plating and incubation of separated iPSCs in MSC medium containing hPL [24]. Interestingly, they did not observe senescent cells when using a protocol in which iPSCs were first incubated with the TGF-β signaling inhibitor SB-431542 to induce differentiation for 20 days, before separation and selection of iMSCs in MSC medium [24].

Thus, we assume that iMSC generation by single-cell plating of iPSCs and subsequent incubation in serum containing MSC media, as performed in this study and as suggested by several recent publications [25,26], is not sufficiently effective and needs to be further optimized to allow the generation of high-quality iMSCs for clinical applications. We are convinced that this can be achieved by improving efficiency and reducing cellular stress during iMSC differentiation, for example by introducing differentiation stimulating factors like SB-431542, and by avoiding separation of undifferentiated iPSCs.

Furthermore, iMSCs are promising since they show less sensitivity to INF-γ stimulation as described in the literature [27]. Our generated iMSCs reveal also a clear insensitivity to IFN-γ-mediated HLA-DR expression compared to the JPCs, as shown in the Supplementary Figure S1. In further studies, immunomodulatory functions of generated iMSCs would be of interest in order to assess their clinical applicability. Among others, Rap-1, as a novel modulator of NF-κB activity and as a key regulator of paracrine activities of MSCs [28], should be investigated.

4. Materials and Methods

4.1. Cell Culture

JPCs derived from three donors were included in this study in accordance with the local ethical committee (approval number 074/2016BO2) and after obtaining written informed consent. Jaw periosteal tissue was extracted during routine surgery and JPCs were isolated and expanded as previously reported [13]. JPCs and iMSCs were grown in hPL5-medium (DMEM/F12 (Gibco) + 5% human platelet lysate (hPL, ZKT Tübingen GmbH), 100 U/mL penicillin-streptomycin (Pen-Strep, Lonza, Basel, Switzerland), 2.5 µg/mL amphotericin B (Biochrom, Berlin, Germany)).

iPSCs were maintained in Essential 8 medium (E8, Thermo Fisher Scientific Inc., Waltham, MA, USA) with daily medium changes and passaged every 4–6 days using 10 µM Y27632 ROCK inhibitor (Selleck Chemicals LLC, Houston, TX, USA).

4.2. Generation of Integration-Free iPSCs from JPCs Using srRNA

JPCs were reprogrammed to iPSCs as previously published [13]. Briefly, JPCs were incubated in hPL5 medium containing 0.2 µg/mL recombinant B18R protein (eBioscience, San Diego, CA, USA) prior to transfection with a self-replicating VEE-OKSM-GFP RNA. From day 1–5 transfected cells were incubated with hPL5 + 25% B18R conditioned medium (BcM) + 1 µg/mL puromycin (Invivogen, Toulouse, France) to select transfected cells. Total of 250 µM histone deacetylase inhibitor sodium butyrate (NaB, Selleck Chemicals LLC, Houston, TX, USA) was added to the medium to enhance reprogramming efficiency. At day 7, the medium was changed to E8 medium (Essential 8, Thermo Fisher Scientific Inc., Waltham, USA) + 25% BcM. Single iPSC colonies were picked and transferred into VTN-coated wells containing E8 medium + 10 µM Y27632 ROCK inhibitor (Selleck Chemicals LLC, Houston, TX, USA) and maintained in E8 medium with daily medium changes. Passaging was performed every 4–6 days.

4.3. Differentiation of iPSCs to iMSCs

Very low concentrations of iPSCs (≤ 10% confluency) were seeded into VTN-coated 12-well plates and cultivated in E8 medium without passaging for 10 days to stimulate spontaneous differentiation. After this period, the cells were detached using Accutase and transferred into VTN-coated 6-well plates containing E8 medium and 10 µM ROCK inhibitor Y27632 (passage 0). The next day, the medium was changed to hPL5 + 150 µM L-ascorbic acid 2-phosphate (Sigma-Aldrich, St. Louis, MO, USA) and replaced every other day. After reaching 80% confluency, cells were passaged (split ratio 1:3) using Accutase. ROCK inhibitor was added to the medium for 24 h after passaging. For following cell passaging TrypLE Express was used and no further ROCK inhibitor was added. Cells were passaged until the morphology of the cells had changed to a spindle-shaped MSC-like appearance (3–5 passages). Cells exhibiting MSC morphology were expanded in hPL5 prior to further experiments.

4.4. Tri-Lineage Differentiation of iMSCs

4.4.1. Osteogenic Differentiation

To stimulate osteogenic differentiation, iMSCs were cultivated in osteogenic medium (DMEM/F12 + 10% hPL, Pen-Strep, amphotericin B, 0.1 mM L-ascorbic acid 2-phosphate (Sigma-Aldrich, St. Louis, MO,

USA), β-glycerophosphate (AppliChem, Darmstadt, Germany), 4 µM dexamethasone (Sigma-Aldrich, St. Louis, MO, USA)) with medium changes every other day. After 15–25 days, cells were fixed with 4% formalin and monolayers were stained with 1 mL of Alizarin red solution (40 mM, pH 4.2) for 20 min. Unbound dye was washed off with dest. water and images were taken using an inverted microscope (Leica, Wetzlar, Germany).

4.4.2. Adipogenic Differentiation

For adipogenic differentiation, 5×10^4 cells/well were seeded into 12-well plates and incubated with adipogenic medium (AM) containing (DMEM/F12 + 10% hPL, Pen-Strep, amphotericin B, 0.2 mM indomathacin (Sigma-Aldrich, St. Louis, MO, USA), 0.5 mM 3-isobutylxanthin (Sigma-Aldrich, St. Louis, MO, USA), 1 µM dexamethasone (Sigma-Aldrich, St. Louis, MO, USA)) 10 µg/mL insulin (Sigma-Aldrich, St. Louis, MO, USA).

RNA isolation for gene expression analysis was performed at day 10. After 10–15 days, cells were fixed with 4% formalin and stained with 0.5 mL of a 3 µg/mL oil red O solution (Sigma-Aldrich, St. Louis, MO, USA) containing 60% isopropanol for 15 min. Unbound dye was washed off with dest. water and images were taken using an inverted microscope (Leica, Wetzlar, Germany).

4.4.3. Chondrogenic Differentiation

For chondrogenic differentiation, cells were harvested and resuspended in control medium (CO, hPL5) and chondrogenic medium (CM) containing DMEM high glucose (4,5 g/L) + pyruvate (1 mM) (Thermo Fisher Scientific Inc., Waltham, USA), 1 % ITS+ Premix (Corning Inc., New York, USA), 100 U/mL Pen-Strep (Lonza, Basel, Switzerland), 2.5 µg/mL amphotericin B (Biochrom, Berlin, Germany), 0.1 µM L-ascorbic acid 2-phosphate (Sigma-Aldrich, St. Louis, MO, USA), 0.1 µM dexamethasone (Sigma-Aldrich, St. Louis, MO, USA), and 10 ng/mL TGF-β1 (PeproTech, Hamburg, Germany) at a concentration of 1.25×10^6 cells/mL. Total of 0.2 mL/well of the cell suspension (0.25×10^6 cells) was added into a low adherence V-bottom polypropylene 96-well plate and centrifuged for 5 min at 350× *g* to form pellets. The medium was changed every other day. On day 20, pellets were harvested for gene expression analysis. After 25 days, pellets were fixed with 4% formalin, embedded in paraffin, and cut with a microtome. Slices were stained using a 0.04 % toluidine blue staining solution.

4.5. Mitochondrial Activity Assay

To compare the mitochondrial activities of iMSCs and JPCs, the EZ4U kit (Biomedica, Vienna, Austria) was used. Proliferation measurements were performed on five consecutive days in intervals of 24 h, following the manufacturer's instructions. Briefly, 1.33×10^3 cells/well were seeded into 96-well plates containing 0.2 mL hPL5 on day 0. After the respective incubation times (1–5 days), the medium was replaced by 200 µL medium + 20 µL of pNPP-substrate, and the mixture was incubated for 4 h at 37 °C. Subsequently, absorption was measured at a wavelength of 450/620 nm using an ELx800 ELISA Reader (Bio-Tek, Winooski, VT, USA). KC4 software was used for data evaluation.

4.6. Growth Kinetics

2.5×10^4 cells were seeded into 12-well plates containing hPL5 in triplicates and harvested for cell counting in an interval of 24 h on five consecutive days. After trypsinization, cells of three wells were pooled, centrifuged, and resuspended in PBS. To identify the dead cells, cell suspensions were incubated with 10 µg/mL propidium iodide (Sigma-Aldrich, St. Louis, MO, USA) for 1 min before cell counting. Subsequently, cell concentrations were measured using the Guava EasyCyte 6HT-2L flow cytometry instrument (Merck Millipore, Billerica, MA, USA).

4.7. Senescence Assay

To assess the cellular senescence, beta-galactosidase activity was detected using the Senescence Assay Kit (Abcam, Cambridge, UK) following the manufacturer's instructions. Briefly, 2.5×10^4 cells were seeded in triplicates into 12-well plates containing hPL5. After 48 h, fresh hPL5 medium containing 3 µL/mL of senescence dye was added to the cells and incubated for 1–2 h. After incubation, fluorescence microscopic images were taken using an Axio Observer.Z1 microscope and AxioVision 4.8.2 software (Carl Zeiss, Oberkochen, Germany). Subsequently, cells were detached, pooled, and resuspended in wash buffer (included in the kit) and flow cytometry measurements were performed using the Guava EasyCyte 6HT-2L flow cytometry instrument (Merck Millipore, Billerica, MA, USA).

4.8. Telomere Length Measurement

The telomere length of JPCs, JPC-derived iPSCs, and iMSCs was analyzed using absolute human length quantification qRT-PCR Assay Kit (ScienCell, Carlsbad, CA, USA) according to the manufacturer's instructions. Therefore, genomic DNA was isolated using QIAamp DNA Mini Kit (Qiagen, Hilden, Germany). qRT-PCR reactions were performed in CFX Connect Real-Time PCR Detection System (Bio-Rad) using IQ™ SYBR®Green Supermix (Bio-Rad) and 10 ng gDNA. A genomic DNA sample with known telomere length served as reference for target sample quantification and a single copy reference was used for data normalization.

4.9. Gene Expression Analysis of JPCs and iMSCs

RNA isolation from JPCs and iMSCs was performed using the NucleoSpin RNA kit (Macherey-Nagel, Düren, Germany) following the manufacturer's instructions. RNA concentration was measured using a Qubit 3.0 fluorometer and the corresponding RNA BR Assay Kit (Thermo Fisher Scientific Inc., Waltham, MA, USA). Total of 0.5 µg of RNA was used for first-strand cDNA synthesis using the SuperScript Vilo Kit (Thermo Fisher Scientific Inc., Waltham, MA, USA). The quantification of mRNA expression levels was performed using the real-time LightCycler System (Roche Diagnostics, Mannheim, Germany). For the PCR reactions, commercial PPARγ, LPL, Leptin, COL2A1, COL10A1, SOX9, COMP, ALP, RUNX2, OCN, COL1A1 primer kits (Search LC, Heidelberg, Germany), and DNA Master SYBR Green I (Roche, Basel, Switzerland) were used. The amplification was performed with a touchdown PCR protocol of 40 cycles (annealing temperature between 68–58 °C), following the manufacturer's instructions. Copy numbers of each sample were calculated on the basis of a standard curve (standard included in the primer kits), and normalized to the housekeeping gene glyceraldehyde-3-phosphate dehydrogenase (*GAPDH*). X-fold induction values were calculated by the quotient of the sample and the corresponding control (iPSCs).

4.10. Statistical Analysis

For the evaluation of differentiation marker gene expression, cell growth and mitochondrial activity data, means ± standard deviations were calculated and compared by two-way ANOVA (p adjusted using Sidak's multiple comparison test) using GraphPad Prism 8.1.0 software. Mean ± standard deviations of senescence marker gene expression was compared by one-way ANOVA (p adjusted using Tukey's multiple comparison test). To analyze the telomere lengths and SA-β-Gal expression (MFI), means ± SD were calculated and compared by one-way ANOVA (p adjusted using Tukey's multiple comparison test). A p-value ≤ 0.05 was considered significant.

5. Conclusions

This study showed a high potential of footprint- and xeno-free generated iMSCs to differentiate into bone, cartilage, and fat in vitro, demonstrating the clinical relevance of this cell type. However, the quality of the resulting cells was not satisfactory because of the observation of early senescence.

Revised protocols should focus on raising differentiation efficiency and avoiding cellular stress to increase iMSC quality.

Supplementary Materials: Supplementary materials can be found at http://www.mdpi.com/1422-0067/21/2/587/s1. Figure S1: HLA-I and HLA-II expression of JPCs and iMSCs

Author Contributions: Methodology, validation, investigation, data curation, writing-original draft preparation, F.U.; methodology, writing—review and editing, M.W.; conceptualization, funding acquisition, project administration, supervision, writing—review and editing, D.A. and M.A.-A.; resources, writing—review and editing, H.-P.W. and S.R. All authors have read and agreed to the published version of the manuscript.

Funding: This research was funded by German Research Foundation, grant number AL 1486/6-1/AV 133/7-1.

Conflicts of Interest: The authors declare no conflict of interest.

Abbreviations

AM	adipogenic medium
ANOVA	analysis of variance
BcM	B18R-conditioned medium
CM	chondrogenic medium
CO	control
FBS	fetal bovine serum
GAGs	glycosaminoglycans
GFP	green fluorescent protein
hPL	human platelet lysate
iMSC	iPSC-derived mesenchymal stem/stromal like cell
iPSC	induced pluripotent stem cell
JPC	jaw periosteal cell
kb	kilo basepairs
MFI	median fluorescence index
mRNA	messenger RNA
MSC	mesenchymal stem/stromal cell
NaB	sodium butyrate
OB	osteoblast medium
OSKM	OKT4, SOX2, KLF4, cMYC
PBS	phosphate buffered saline
PCR	polymerase chain reaction
Puro	puromycin
qRT-PCR	quantitative real-time polymerase chain reaction
ROCK	rho-associated protein kinase
SA-β-gal	senescence-associated beta-galactosidase
SD	standard deviation
SEM	standard error of mean
srRNA	self-replicating ribonucleic acid

References

1. Čamernik, K.; Barlič, A.; Drobnic, M.; Marc, J.; Jeras, M.; Zupan, J. Mesenchymal Stem Cells in the Musculoskeletal System: From Animal Models to Human Tissue Regeneration? *Stem Cell Rev. Rep.* **2018**, *14*, 346–369. [CrossRef] [PubMed]
2. Fitzsimmons, R.E.B.; Mazurek, M.S.; Soos, A.; Simmons, C.A. Mesenchymal Stromal/Stem Cells in Regenerative Medicine and Tissue Engineering. *Stem Cells Int.* **2018**, *2018*, 1–16. [CrossRef] [PubMed]
3. Gebler, A.; Zabel, O.; Seliger, B. The immunomodulatory capacity of mesenchymal stem cells. *Trends Mol. Med.* **2012**, *18*, 128–134. [CrossRef]
4. Zachar, L.; Bačenková, D.; Rosocha, J. Activation, homing, and role of the mesenchymal stem cells in the inflammatory environment. *J. Inflamm. Res.* **2016**, *9*, 231–240. [CrossRef] [PubMed]

5. Wagner, W.; Ho, A.D. Mesenchymal Stem Cell Preparations—Comparing Apples and Oranges. *Stem Cell Rev. Rep.* **2007**, *3*, 239–248. [CrossRef]
6. Baker, N.; Boyette, L.B.; Tuan, R.S. Characterization of bone marrow-derived mesenchymal stem cells in aging. *Bone* **2015**, *70*, 37–47. [CrossRef]
7. Yu, J.; Thomson, J.A. Induced Pluripotent Stem Cells. In *Principles of Tissue Engineering*; Lanza, R., Langer, R., Vacanti, J., Eds.; Academic Press: Boston, MA, USA, 2014; pp. 581–594.
8. Jung, Y.; Bauer, G.; Nolta, J.A. Concise review: Induced pluripotent stem cell-derived mesenchymal stem cells: Progress toward safe clinical products. *Stem Cells* **2012**, *30*, 42–47. [CrossRef]
9. Ng, J.; Hynes, K.; White, G.; Sivanathan, K.N.; VanDyke, K.; Bartold, P.M.; Gronthos, S. Immunomodulatory Properties of Induced Pluripotent Stem Cell-Derived Mesenchymal Cells. *J. Cell. Biochem.* **2016**, *117*, 2844–2853. [CrossRef]
10. Lapasset, L.; Milhavet, O.; Prieur, A.; Besnard, E.; Babled, A.; Aït-Hamou, N.; Leschik, J.; Pellestor, F.; Ramirez, J.-M.; De Vos, J.; et al. Rejuvenating senescent and centenarian human cells by reprogramming through the pluripotent state. *Genes Dev.* **2011**, *25*, 2248–2253. [CrossRef]
11. Spitzhorn, L.-S.; Megges, M.; Wruck, W.; Rahman, S.; Otte, J.; Degistirici, Ö.; Meisel, R.; Sorg, R.V.; Oreffo, R.O.C.; Adjaye, J. Human iPSC-derived MSCs (iMSCs) from aged individuals acquire a rejuvenation signature. *Stem Cell Res. Ther.* **2019**, *10*, 100. [CrossRef]
12. Turinetto, V.; Vitale, E.; Giachino, C. Senescence in Human Mesenchymal Stem Cells: Functional Changes and Implications in Stem Cell-Based Therapy. *Int. J. Mol. Sci.* **2016**, *17*, 1164. [CrossRef] [PubMed]
13. Umrath, F.; Steinle, H.; Weber, M.; Wendel, H.-P.; Reinert, S.; Alexander, D.; Avci-Adali, M. Generation of iPSCs from Jaw Periosteal Cells Using Self-Replicating RNA. *Int. J. Mol. Sci.* **2019**, *20*, 1648. [CrossRef] [PubMed]
14. Alexander, D.; Hoffmann, J.; Munz, A.; Friedrich, B.; Geis-Gerstorfer, J.; Reinert, S. Analysis of OPLA scaffolds for bone engineering constructs using human jaw periosteal cells. *J. Mater. Sci. Mater. Med.* **2008**, *19*, 965–974. [CrossRef] [PubMed]
15. Ferretti, C.; Mattioli-Belmonte, M. Periosteum derived stem cells for regenerative medicine proposals: Boosting current knowledge. *World J. Stem Cells* **2014**, *6*, 266–277. [CrossRef]
16. Roberts, S.J.; Van Gastel, N.; Carmeliet, G.; Luyten, F.P. Uncovering the periosteum for skeletal regeneration: The stem cell that lies beneath. *Bone* **2015**, *70*, 10–18. [CrossRef] [PubMed]
17. Frobel, J.; Hemeda, H.; Lenz, M.; Abagnale, G.; Joussen, S.; Denecke, B.; Saric, T.; Zenke, M.; Wagner, W. Epigenetic rejuvenation of mesenchymal stromal cells derived from induced pluripotent stem cells. *Stem Cell Rep.* **2014**, *3*, 414–422. [CrossRef]
18. Marión, R.M.; Strati, K.; Li, H.; Tejera, A.; Schoeftner, S.; Ortega, S.; Serrano, M.; Blasco, M.A. Telomeres Acquire Embryonic Stem Cell Characteristics in Induced Pluripotent Stem Cells. *Cell Stem Cell* **2009**, *4*, 141–154. [CrossRef]
19. Bodnar, A.G.; Ouellette, M.; Frolkis, M.; Holt, S.E.; Chiu, C.P.; Morin, G.B.; Harley, C.B.; Shay, J.W.; Lichtsteiner, S.; Wright, W.E. Extension of Life-Span by Introduction of Telomerase into Normal Human Cells. *Science* **1998**, *279*, 349–352. [CrossRef]
20. Feng, Q.; Klimanskaya, I.; Gomes, I.; Kim, H.; Chung, Y.; Honig, G.R.; Kim, K.-S.; Lanza, R.; Lu, S.-J. Hemangioblastic Derivatives from Human Induced Pluripotent Stem Cells Exhibit Limited Expansion and Early Senescence. *Stem Cells* **2010**, *28*, 704–712. [CrossRef]
21. Gokoh, M.; Nishio, M.; Nakamura, N.; Matsuyama, S.; Nakahara, M.; Suzuki, S.; Mitsumoto, M.; Akutsu, H.; Umezawa, A.; Yasuda, K.; et al. Early Senescence Is Not an Inevitable Fate of Human-Induced Pluripotent Stem-Derived Cells. *Cell. Reprogramming* **2011**, *13*, 361–370. [CrossRef]
22. McHugh, D.; Gil, J. Senescence and aging: Causes, consequences, and therapeutic avenues. *J. Cell Boil.* **2017**, *217*, 65–77. [CrossRef] [PubMed]
23. Jun, J.-I.; Lau, L.F. The matricellular protein CCN1 induces fibroblast senescence and restricts fibrosis in cutaneous wound healing. *Nat. Cell Biol.* **2010**, *12*, 676–685. [CrossRef] [PubMed]
24. DeVito, L.; Klontzas, M.E.; Cvoro, A.; Galleu, A.; Simon, M.; Hobbs, C.; Dazzi, F.; Mantalaris, A.; Khalaf, Y.; Ilic, D. Comparison of human isogeneic Wharton's jelly MSCs and iPSC-derived MSCs reveals differentiation-dependent metabolic responses to IFNG stimulation. *Cell Death Dis.* **2019**, *10*, 277. [CrossRef] [PubMed]

25. Luzzani, C.D.; Miriuka, S.G. Pluripotent Stem Cells as a Robust Source of Mesenchymal Stem Cells. *Stem Cell Rev. Rep.* **2017**, *13*, 68–78.
26. Nejadnik, H.; Diecke, S.; Lenkov, O.D.; Chapelin, F.; Donig, J.; Tong, X.; Derugin, N.; Chan, R.C.F.; Gaur, A.; Yang, F.; et al. Improved approach for chondrogenic differentiation of human induced pluripotent stem cells. *Stem Cell Rev. Rep.* **2015**, *11*, 242–253. [CrossRef]
27. Sun, Y.-Q.; Zhang, Y.; Li, X.; Deng, M.-X.; Gao, W.-X.; Yao, Y.; Chiu, S.-M.; Liang, X.; Gao, F.; Chan, C.W.; et al. Insensitivity of Human iPS Cells-Derived Mesenchymal Stem Cells to Interferon-γ-induced HLA Expression Potentiates Repair Efficiency of Hind Limb Ischemia in Immune Humanized NOD Scid Gamma Mice. *Stem Cells* **2015**, *33*, 3452–3467. [CrossRef]
28. Zhang, Y.; Chiu, S.; Liang, X.; Gao, F.; Zhang, Z.; Liao, S.; Liang, Y.; Chai, Y.-H.; Low, D.J.H.; Tse, H.-F.; et al. Rap1-mediated nuclear factor-kappaB (NF-κB) activity regulates the paracrine capacity of mesenchymal stem cells in heart repair following infarction. *Cell Death Discov.* **2015**, *1*, 15007. [CrossRef]